Capacity and Error Probability Analysis for Space Time Block Codes and Pulse Position Amplitude Modulation Ultra Wideband Communication Systems

by

Hao Zhang
B.Sc., Shanghai Jiaotong University, 1994
MBA, New York Institute of Technology, 2001

A Dissertation Submitted in Partial Fulfillment of the
Requirements for the Degree of
DOCTORAL OF PHILOSOPHY
in the Department of Electrical and Computer Engineering

Capacity and Error Probability Analysis for
Space Time Block Codes and Pulse Position Amplitude Modulation Ultra Wideband Communication Systems

Supervisor: Dr. Aaron Gulliver

Abstract

The capacity and error probability of space-time block codes (STBC) are derived for PAM/PSK/QAM modulation in different fading channels. The approach is based on an equivalent scalar AWGN (additive white Gaussian noise) channel with a channel gain proportional to the Frobenius norm of the matrix channel for the STBC. Rayleigh, Ricean and Nakagami fading channels are considered. Both independent and correlated fading channels are investigated. The analysis has further extended to a Direct Sequence Code Division Multiple Access (DS-CDMA) multiuser system employing STBC.

A new modulation scheme called pulse amplitude position modulation (PPAM) for Ultra-Wideband (UWB) communication systems is proposed, which combines pulse position modulation (PPM) and pulse amplitude modulation (PAM) to provide good system performance and low computational complexity. The capacity and error probability are presented.

Table of Contents

List of Tables

List of Figures

Acknowledgements

This work has been made possible by the generous support from many people. First of all, I would like to express my thanks to my supervisor Dr. T. Aaron Gulliver for his invaluable advice and encouragement throughout my doctoral studies. His insight, kindness, and genuine concern for his students made working with him a memorable experience. I also would like to thank my committee members for their time and their technical and spiritual support during the course of this study. I also would like to thank Dr. Vijay Bhargava, Dr. Afzal Suleman, and Ms. Vicky Smith for their kindly support during my transfer from M.A.Sc to Ph.D program. I sincerely appreciate the extra time and effort they had spent in providing me valuable guidance and suggestions. I am also very grateful to my dear fellow graduate students in communication group, namely Wei Li, Caner Budakoglu, Richard Chen, Yihai Zhang, Ubolthip Sethakaset, William Chow, and in DSP group, namely Paramesh Ramachandran, Deepali Arora, and Brad Riel, for their invaluable discussion, assistance and support. I am also grateful to all my other friends and colleagues at ECE. Your compassion has made the journey of my research a wonderful memory.

To my dear wife Na Zhang, as it is her conditionless care and love that made this work possible.

Thank my beloved family who helped and encouraged me to finish my Ph.D. successfully.

List of Notations

AWGN	Additive White Gaussian Noise
BEP	Bit Error Probability
CDMA	Code Division Multiple Access
DS	Direct Sequence
MAI	Multiple Access Interference
MGF	Moment Generating Function
MIMO	Multiple Input
MRC	Maximum Ratio Combining
OFDM	Orthogonal Frequency Division Multiplexing
OOK	On Off Keying
OSTBC	Orthogonal Space Time Block Code
PAM	Pulse Amplitude Modulation
PDF	Probability Density Function
PPAM	Pulse Position Amplitude Modulation
PPM	Pulse Position Modulation
PSK	Phase Shift Keying
QAM	Quadrature Amplitude Modulation
SEP	Symbol Error Probability
SISO	Single Input Single Output
SNR	Signal to Noise Ratio
STBC	Space-Time Block Code
STTC	Space-Time Trellis Code
TH	Time Hopping
UWB	Ultra-WideBand

Chapter 1

Introduction

High data rate wireless communication has been one of the major drivers for the development in communications in last decade. The great popularity of cellular phones, radio paging, wireless Local Area Network (LAN), mobile computing device and other personal communication services (PCS) demonstrates the rising demand for wireless communication, and has inspired many proposals for high-speed data services up to 2 Mb/s for diversified applications. The third-generation (3G) mobile communications standards [1] were designed to provide a wide range of user service, spanning from voice to high-rate data services, supporting rates of at least 144 kb/s in vehicular, 384 kb/s in outdoor-to-indoor, and 2 Mb/s in indoor as well as picocellular applications [1].

Research challenges for high data rate wireless communications include the development of efficient coding and modulation schemes, smart signal processing techniques to improve the quality of service and spectral efficiency of the wireless system, and better techniques for sharing the limited spectrum among different high capacity users. Remarkable technologies have been proposed to deal with these challenges, such as multiple antenna systems, space time processing, orthogonal frequency division multiplexing (OFDM), ultra-wideband radio, beamforming, and so

on.

In this work, we focus on the capacity and error probability analysis for space time block coded (STBC) and ultra-wideband (UWB) communication systems. The information capacity of wireless communication systems increases dramatically by employing multiple receive and transmit antennas [2][3]. To take advantage of both spatial diversity and time or frequency diversity, space time block coding (STBC) [4][5][6] is generated considering the joint design of coding, modulation, and transmit and receive diversity with multiple antennas. The spatial-temporal structure of these codes can be exploited to increase the capacity of wireless systems with a very simple receiver structure. As an emerging wireless technology for communications, ultra-wideband (UWB) radio uses a wide swath of spectrum to transmit low-powered, ultra-short radio pulses through the air, and is capable of transmitting data at several hundred Mbit/s typically over short distances under restricted power limits [7]. These systems are therefore considered suitable for high-data-rate applications, such as streaming media, and for use in battery-powered wireless data devices.

In this chapter, a brief overview of space time block codes (STBC) and ultra wideband (UWB) communication are given in Sections 1.1 and 1.2, as well as related work in each field, respectively. The outline of the thesis is given in Section 1.3. Finally Section 1.4 summarizes the contributions of this work.

1.1 Overview of space time block codes

1.1.1 Multiple antenna systems

The characteristics of a wireless channel present a fundamental technical challenge for reliable communications subject to time-varying impairments such as noise,

interference, and multipath [8]-[12]. In an effort to conquer fading to support high rate data transmission over such a channel, several diversity techniques were naturally introduced to improve the performance of wireless communication system. Space diversity, i.e. multiple antenna system, has received significant attention recently after extensive research on time diversity and frequency diversity [13]-[15]. [2] and [3] showed the enormous capacity promised by multiple antenna systems in a fading environment, which greatly inspired the search for optimum techniques and coding algorithms for multiple input multiple output (MIMO) channels. The classic approach is to use multiple receive antennas or polarization diversity reception and employ maximum ratio combining (MRC) [16]-[19] of the received signals to improve performance. However, receive diversity techniques have typically been applied at the base stations since applying receive diversity at the mobile stations increases their computational complexity which may not be allowed by the limited power. Limitations on the power and size of the mobile terminals requires serious design consideration when employing sophisticated power consuming signal processing techniques for reliable communications and efficient spectral utilization. Though continuing advances in very large scale integration (VLSI) system, application-specific integrated circuit (ASIC) technology for low power devices, and system on chip (SOC) provide a partial solution, involving less signal processing burden on mobile terminals than fixed base stations with relatively larger power supply makes good engineering sense.

Different transmit diversity techniques have then been proposed earlier in order to introduce diversity gain for mobile stations by upgrading base stations. For example, [20][21] presented a switch diversity scheme with information feedback, [22]-[24] presented a diversity scheme invoking feedforward or training information, and [25][26] proposed a blind diversity scheme. Recently, space time trellis coding (STTC) [27]-[33] was proposed by jointly designing the channel coding, modulation and

transmit diversity. Performance criteria for designing STTC codes were derived in [27] for a flat fading channel. STTC perform extremely well, however, the computational complexity is also significant. When the number of antennas is fixed, the decoding complexity of STTC increases exponentially as a function of the diversity level and transmission rate [29]. In addressing the issue of complexity, a remarkable scheme, called OSTBC, was proposed by [34] using two transmit antennas and generalized in [35] to an arbitrary number of antenna to provide full diversity gain with extremely low computational complexity. Despite the associated performance penalty comparing with STTC, OSTBC is still very appealing in terms of its simplicity and performance. Further study in [36][37] has shown that OSTBC concatenated with channel codes outperform STTC with comparable complexity.

1.1.2 Space Time Block Codes

In this section, we present the principles of OSTBC following the seminal contributions in [34]-[37]. Consider a wireless system with N transmit antennas and M receive antennas. The channel is assumed to be quasi-static with flat fading, which means that the channel is constant within one frame period, but varies independently between frames. Furthermore, perfect channel state information is assumed available at the receiver, but the channel is unknown at the transmitter. Let T represent the number of time slots used to transmit S symbols. Hence, a general form for the transmission matrix of a OSTBC is

$$G=\begin{pmatrix} g_{11} & g_{21} & \cdots & g_{N1} \\ g_{12} & g_{22} & \cdots & g_{N2} \\ . & . & \cdots & . \\ . & . & \cdots & . \\ g_{1T} & g_{2T} & \cdots & g_{NT} \end{pmatrix}, \tag{1.1}$$

where g_{ij} represents a linear combination of the signal constellation components and their conjugates, and are transmitted simultaneously from the i_{th} transmit antennas in the j_{th} time slot for $i = 1 \ldots N$ and $j = 1 \ldots T$. Since there are S symbols transmitted over T time slots, the code rate of the OSTBC is given by

$$R = S/T . \tag{1.2}$$

At a particular time nT, the received signal corresponding to the n_{th} input block spanning T time slots is

$$\mathbf{Y}_{nT} = \mathbf{H}\mathbf{G}^{T} + \mathbf{W}_{nT}, \tag{1.3}$$

where $\mathbf{Y}_{nT}$ is an $M \times T$ matrix, $\mathbf{H}$ is an $M \times N$ fading channel coefficient matrix with i.i.d. (independent, identically distributed) entries modeled as circular complex Gaussian random variables, $\mathbf{G}^{T}$ is the transpose of $\mathbf{G}$ with size $N \times T$, and $\mathbf{W}_{nT}$ is an $M \times T$ receiver noise matrix with i.i.d. entries modeled as circular complex Gaussian random variables with zero mean and variance $N_o/2$ in each dimension. At the receiver end, a combining technique [34]-[36] similar to MRC can be applied to obtain full diversity gain.

A. Two Transmit Antennas OSTBC

As mentioned above, the simplest form of OSTBC, which is a two transmit antenna based scheme associated with N=2, was proposed by [34]. The associated transmission matrix is

$$\mathbf{G}_2 = \begin{pmatrix} x_1 & x_2 \\ -x_2^* & x_1^* \end{pmatrix}. \tag{1.4}$$

It is shown in the transmission matrix $\mathbf{G}_2$ that there are N=2 transmit antennas, S=2 input symbols, namely x_1, x_2, and the code spans T=2 time slots. x_1^* and x_2^* are the conjugates of symbols x_1 and x_2, respectively. Since S=T=2, the code rate given by (1.4)

is unity. The associated encoding and transmission process in shown in Table 1.

Table 1.1 Encoding and transmission process for the OSTBC $\mathbf{G}_2$

Time Slot	Transmit Antenna	
T	Tx_1	Tx_2
1	x_1	x_2
2	$-x_2^*$	x_1^*

At any particular time instant T, two signals are simultaneously transmitted from transmit antennas Tx_1 and Tx_2. For example, in time slot 1, signal x_1 and x_2 are transmitted simultaneously from the transmit antennas Tx_1 and Tx_2, respectively. In the next time slot, signal $-x_2^*$ and x_1^* are transmitted simultaneously from transmit antennas Tx_1 *and* Tx_2, respectively.

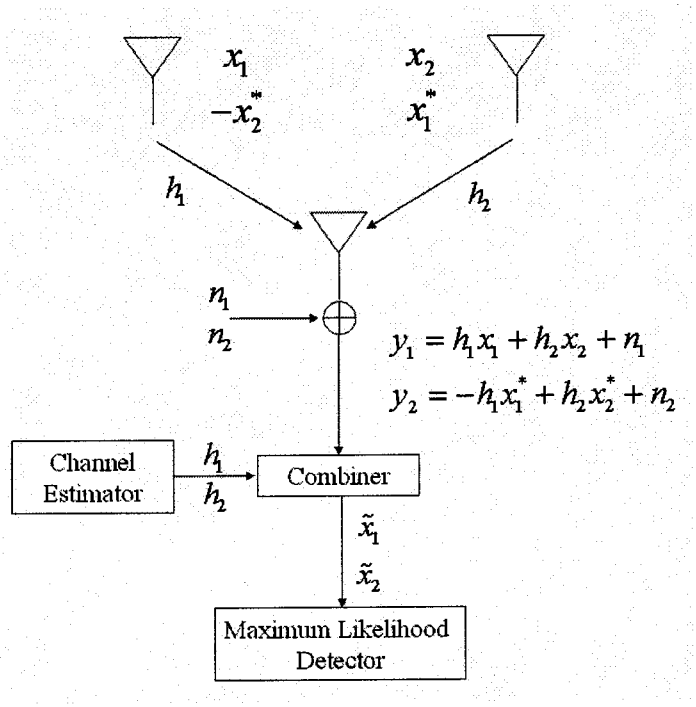

Fig.1.1 Baseband representation of OSTBC $\mathbf{G}_2$ of (1.4) with one receive antenna

Fig.1.1 shows the baseband representation of OSTBC G_2 of (1.4) with one receive antenna. As mentioned earlier, the channel is assumed to be flat fading, i.e. the complex fading envelop h_1 and h_2 are assumed to be constant across the corresponding two consecutive time slots. Independent additive white Gaussian noise (AWGN) samples are added by the receiver in each time slot. The received signals over flat fading channels can be expressed as

$$y_1 = h_1 x_1 + h_2 x_2 + n_1 \tag{1.5}$$

$$y_2 = -h_1 x_1^* + h_2 x_2^* + n_2 \tag{1.6}$$

where y_1 is the first received signal and y_2 is the second. Note that the received signal y_1 consists of the transmitted signals x_1 and x_2, while y_2 consists of their conjugates. In order to decode the transmitted signals, we have to extract the signals x_1 and x_2 from the received signals y_1 and y_2. With perfect channel state information available at the receiver, the received signals are combined as follows to decode x_1 and x_2

$$\begin{aligned} \tilde{x}_1 &= h_1^* y_1 + h_2 y_2^* \\ &= \left(|h_1|^2 + |h_2|^2\right) x_1 + h_1^* n_1 + h_2 n_2^* \end{aligned} \tag{1.7}$$

$$\begin{aligned} \tilde{x}_2 &= h_2^* y_1 - h_1 y_2^* \\ &= \left(|h_1|^2 + |h_2|^2\right) x_2 + h_2^* n_1 - h_1 n_2^* \end{aligned} \tag{1.8}$$

It is easy to see from (1.7) and (1.8) that x_1 and x_2 have been separated from y_1 and y_2 by simple multiplications and additions due to the orthogonality of OSTBC [35]. Both signals $\tilde{x}_1$ and $\tilde{x}_2$ are then passed to the maximum likelihood detector as shown in Fig.1.1 to determine the most likely transmitted symbols x_1 and x_2. Note that the OSTBC combiner has a form similar to MRC for receive diversity.

Similarly, for OSTBC G2 with 2 receive antennas, the received signals can be combined to generate $\tilde{x}_1$ and $\tilde{x}_2$ as follows

$$\tilde{x}_1 = \left(|h_{11}|^2 + |h_{12}|^2 + |h_{21}|^2 + |h_{22}|^2\right)x_1 + h_{11}^* n_{11} + h_{12} n_{12}^* + h_{21}^* n_{21} + h_{22} n_{22}^* \tag{1.9}$$

$$\tilde{x}_2 = \left(|h_{11}|^2 + |h_{12}|^2 + |h_{21}|^2 + |h_{22}|^2\right)x_1 + h_{12}^* n_{11} - h_{11} n_{12}^* + h_{22}^* n_{21} - h_{21} n_{22}^* . \tag{1.10}$$

In the generalized form with M receive antennas, we have

$$\tilde{x}_1 = \sum_{i=1}^{M}\left[\left(|h_{i1}|^2 + |h_{i2}|^2\right)x_1 + h_{i1}^* n_{i1} + h_{i2} n_{i2}^*\right] \tag{1.11}$$

$$\tilde{x}_2 = \sum_{i=1}^{M}\left[\left(|h_{i1}|^2 + |h_{i2}|^2\right)x_2 + h_{i2}^* n_{i1} - h_{i1} n_{i2}^*\right]. \tag{1.12}$$

It can be easily observed that OSTBC $\mathbf{G}_2$ with M receive antennas has the same diversity order as MRC with $2M$-order receive diversity.

B. Other OSTBCs

It is shown in [35] based on the theory of orthogonal designs that full rate OSTBCs exist for any number of transmit antennas using an arbitrary real constellation such as PAM. For an arbitrary complex constellation such as PSK/QAM, half rate OSTBCs exist for any number of transmit antennas, while full rate OSTBCs only exist for 2 transmit antennas. In another word, $\mathbf{G}_2$ is the only full rate complex OSTBC. As specific cases for three and four transmit antennas, rate ½ and 3/4 OSTBCs are given in [35], and are denoted as $\mathbf{G}_3$, $\mathbf{G}_4$, and $\mathbf{H}_3$, $\mathbf{H}_4$, respectively, and are given by

$$\mathbf{G}_3 = \begin{pmatrix} x_1 & x_2 & x_3 \\ -x_2 & x_1 & -x_4 \\ -x_3 & x_4 & x_1 \\ -x_4 & -x_3 & x_2 \\ \overline{x}_1 & \overline{x}_2 & \overline{x}_3 \\ -\overline{x}_2 & \overline{x}_1 & -\overline{x}_4 \\ -\overline{x}_3 & \overline{x}_4 & \overline{x}_1 \\ -\overline{x}_4 & -\overline{x}_3 & \overline{x}_2 \end{pmatrix}, \tag{1.13}$$

$$\mathbf{G}_4 = \begin{pmatrix} x_1 & x_2 & x_3 & x_4 \\ -x_2 & x_1 & -x_4 & x_3 \\ -x_3 & x_4 & x_1 & -x_2 \\ -x_4 & -x_3 & x_2 & x_1 \\ \overline{x}_1 & \overline{x}_2 & \overline{x}_3 & \overline{x}_4 \\ -\overline{x}_2 & \overline{x}_1 & -\overline{x}_4 & \overline{x}_3 \\ -\overline{x}_3 & \overline{x}_4 & \overline{x}_1 & -\overline{x}_2 \\ -\overline{x}_4 & -\overline{x}_3 & \overline{x}_2 & \overline{x}_1 \end{pmatrix}, \tag{1.14}$$

$$\mathbf{H}_3 = \begin{pmatrix} x_1 & x_2 & \frac{x_3}{\sqrt{2}} \\ -\overline{x}_2 & \overline{x}_1 & \frac{x_3}{\sqrt{2}} \\ \frac{\overline{x}_3}{\sqrt{2}} & \frac{\overline{x}_3}{\sqrt{2}} & \frac{(-x_1 - \overline{x}_1 + x_2 - \overline{x}_2)}{2} \\ \frac{\overline{x}_3}{\sqrt{2}} & -\frac{\overline{x}_3}{\sqrt{2}} & \frac{(x_2 + \overline{x}_2 + x_1 - \overline{x}_1)}{2} \end{pmatrix}, \tag{1.15}$$

and

$$\mathbf{H}_4 = \begin{pmatrix} x_1 & x_2 & \frac{x_3}{\sqrt{2}} & \frac{x_3}{\sqrt{2}} \\ -\overline{x}_2 & \overline{x}_1 & \frac{x_3}{\sqrt{2}} & -\frac{x_3}{\sqrt{2}} \\ \frac{\overline{x}_3}{\sqrt{2}} & \frac{\overline{x}_3}{\sqrt{2}} & \frac{(-x_1 - \overline{x}_1 + x_2 - \overline{x}_2)}{2} & \frac{(-x_2 - \overline{x}_2 + x_1 - \overline{x}_1)}{2} \\ \frac{\overline{x}_3}{\sqrt{2}} & -\frac{\overline{x}_3}{\sqrt{2}} & \frac{(x_2 + \overline{x}_2 + x_1 - \overline{x}_1)}{2} & \frac{(-x_1 - \overline{x}_1 - x_2 + \overline{x}_2)}{2} \end{pmatrix}. \tag{1.16}$$

[38]-[40] present two simpler rate 3/4 OSTBCs, namely

$$H_3 = \begin{pmatrix} x_1 & x_2 & x_3 \\ -x_2^* & x_1^* & 0 \\ x_3^* & 0 & -x_1^* \\ 0 & x_3^* & -x_2^* \end{pmatrix} \tag{1.17}$$

for three transmit antennas and

$$H_4 = \begin{pmatrix} x_1 & x_2 & x_3 & 0 \\ -x_2^* & x_1^* & 0 & x_3 \\ x_3^* & 0 & -x_1^* & x_2 \\ 0 & x_3^* & -x_2^* & -x_1 \end{pmatrix} \tag{1.18}$$

for four transmit antennas. [41] presents two generalized complex orthogonal space–time block codes

$$G_5 = \begin{bmatrix} x_1 & x_2 & x_3 & 0 & x_4 \\ -x_2^* & x_1^* & 0 & x_3 & x_5 \\ x_3^* & 0 & -x_1^* & x_2 & x_6 \\ 0 & x_3^* & -x_2^* & -x_1 & x_7 \\ x_4^* & 0 & 0 & -x_7^* & -x_1^* \\ 0 & x_4^* & 0 & x_6^* & -x_2^* \\ 0 & 0 & x_4^* & x_5^* & -x_3^* \\ 0 & -x_5^* & x_6^* & 0 & x_1 \\ x_5^* & 0 & x_7^* & 0 & x_2 \\ -x_6^* & -x_7^* & 0 & 0 & x_3 \\ x_7 & -x_6 & -x_5 & x_4 & 0 \end{bmatrix} \tag{1.19}$$

of rate 7/11 for five transmit antennas and

$$G_6 = \begin{bmatrix}
x_1 & x_2 & x_3 & 0 & x_4 & x_8 \\
-x_2^* & x_1^* & 0 & x_3 & x_5 & x_9 \\
x_3^* & 0 & -x_1^* & x_2 & x_6 & x_{10} \\
0 & x_3^* & -x_2^* & -x_1 & x_7 & x_{11} \\
x_4^* & 0 & 0 & -x_7^* & -x_1^* & x_{12} \\
0 & x_4^* & 0 & x_6^* & -x_2^* & x_{13} \\
0 & 0 & x_4^* & x_5^* & -x_3^* & x_{14} \\
0 & x_5^* & -x_6^* & 0 & -x_1 & x_{15} \\
x_5^* & 0 & x_7^* & 0 & x_2 & x_{16} \\
x_6^* & x_7^* & 0 & 0 & -x_3 & x_{17} \\
x_7 & -x_6 & -x_5 & x_4 & 0 & x_{18} \\
x_8^* & 0 & 0 & -x_{11}^* & -x_{15}^* & -x_1^* \\
0 & x_8^* & 0 & x_{10}^* & x_{16}^* & -x_2^* \\
0 & 0 & x_8^* & x_9^* & -x_{17}^* & -x_3^* \\
0 & 0 & 0 & x_{18}^* & x_8^* & -x_4^* \\
0 & 0 & -x_{18}^* & 0 & x_9^* & -x_5^* \\
0 & -x_{18}^* & 0 & 0 & x_{10}^* & -x_6^* \\
x_{18}^* & 0 & 0 & 0 & x_{11}^* & -x_7^* \\
0 & -x_9^* & x_{10}^* & 0 & x_{12}^* & x_1 \\
x_9^* & 0 & x_{11}^* & 0 & x_{13}^* & x_2 \\
-x_{10}^* & -x_{11}^* & 0 & 0 & x_{14}^* & x_3 \\
-x_{12}^* & -x_{13}^* & -x_{14}^* & 0 & 0 & x_4 \\
-x_{16}^* & -x_{15}^* & 0 & -x_{14}^* & 0 & x_5 \\
-x_{17}^* & 0 & x_{15}^* & -x_{13}^* & 0 & x_6 \\
0 & -x_{17}^* & -x_{16}^* & x_{12}^* & 0 & x_7 \\
0 & x_{14} & -x_{13} & -x_{15} & x_{11} & 0 \\
x_{14} & 0 & -x_{12} & -x_{16} & x_{10} & 0 \\
-x_{13} & x_{12} & 0 & x_{17} & x_9 & 0 \\
x_{15} & -x_{16} & x_{17} & 0 & x_8 & 0 \\
-x_{11} & x_{10} & x_9 & -x_8 & x_{18} & 0
\end{bmatrix} . \tag{1.20}$$

of rate 3/5 for six transmit antennas.

In Table 1.2, we summarize the parameters associated with all OSTBC codes given in [35]-[41]. The decoding algorithms and the corresponding performances of these OSTBCs were given in [36].

Table 1.2 Different OSTBCs

STBC	Code Rate R	No. of Tx Antennas N	No. of Input Symbols S	Code Span T
G2	1/2	2	2	2
G3	1/2	3	4	8
G4	1/2	4	4	8
H3	3/4	3	3	4
H4	3/4	4	3	4
G5	7/11	5	7	11
G6	3/5	6	18	30

1.1.3 Related Work on Space Time Block Codes

As OSTBC is a remarkable technique which can provide full diversity gain with very low computational complexity, it is helpful to learn more about the characteristics of OSTBC from the perspective of capacity and error probability.

A loss in capacity, characterized by the code rate and the number of receive antennas, is shown in [42][43] for an arbitrary channel. Following the analysis in [36][42][43], a characterization based on an equivalent scalar AWGN (additive White Gaussian Noise) channel multiplied by a coefficient, which is a function of the Frobenius norm of the channel matrix with multiple antennas, was given in [42] for full rate OSTBC. The

Shannon and outage capacity for the equivalent scalar AWGN channel were also given. The Shannon capacity $C = W\log_2(1+SNR)$, where SNR is the signal-to-nose ratio and W is the channel bandwidth, predicts the channel capacity C for an AWGN channel with continuous-valued inputs and outputs. However, a channel employing OSTBC with PAM/PSK/QAM modulation has discrete-valued inputs and continuous-valued outputs, which imposes an additional constraint on the capacity calculation. In this work, we generalize the effective channel representation in [42] for all rate orthogonal OSTBCs, including the rate 1/2 OSTBCs, the rate 3/4 OSTBCs $\mathbf{H}_3$ and $\mathbf{H}_4$, and other codes given previously. A new capacity calculation taking into account the constraint of discrete-valued inputs is presented here, as well as the capacity loss incurred by employing OSTBC.

In [44], an analysis of the bit error probability (BEP) of $\mathbf{G}_2$ for q-ary PSK was presented for Rayleigh fading channels using the PDF of the phase of the received signal from [45]. However, the BEP for q-PSK (q>4) is very complex following this approach. In [46], a union bound on the symbol error probability for OSTBC was presented. A general form for the exact pairwise error probability of space-time codes was obtained in [47] based on the moment generating function (MGF) of the Gaussian tail function. [48] derived the exact expression for the pairwise error probability in a flat Rayleigh fading channel in terms of the message symbol distance between two message vectors for QPSK, 16-QAM, 64 QAM, and 256-QAM. In [49], a unified approach for calculating error rates of linearly-modulated signals over generalized fading channels was presented. However, all of the results in [46]-[49] are either given in open form which has to be evaluated via numerical integration or only as a performance bound. Closed form expression of error probability for OSTBC over flat fading channels still remains an open problem. [50] derived the performance criteria for space-time coded wireless

communication systems taking into account both spatial and temporal channel correlation. Performance analysis for correlated fading channels with diversity reception were studied in [51][52]. [53] derived expressions for the cumulative distribution function of the uncoded symbol error rate for OSTBC $\mathbf{G}_2$ over correlated Rayleigh and Ricean fading channels. In addition, [53] introduce a quantitative measure to compare the diversity gain offered by two channels at a given outage rate. In [54], OSTBC was applied to a CDMA downlink, and a novel decoding algorithm as well as a performance bound were presented. In this work, we analyze the error probability of OSTBCs for PAM/PSK/QAM modulation from an *SNR* perspective based upon the equivalent scalar channel induced by the OSTBC. Using the PDF of the *SNR*, closed-form symbol error probabilities are given for various combinations of modulation and fading channels. Furthermore, these results are extended to a multiuser DS-CDMA system employing OSTBC. Expressions for the capacity and error probability of the system are derived and analyzed. Capacity and error probability of OSTBC over correlated fading channels are also investigated in this work. Closed form expressions of error probability for PAM/PSK/QAM with Rayleigh fading channels are also derived.

1.2 Overview of Ultra Wideband Communications

1.2.1 Motivation of Ultra Wideband Modulation

High data rate multiple access wireless communication over a short range in a multipath indoor wireless channel is a technical challenge [55]. The channel is impaired by deep fading produced by dense multipath signals arriving at the receiver with different time delays that can be as small as fractions of a nanosecond [56]. For

reliable communication over such a channel, large transmit power and/or diversity techniques [45] are required. Signals with bandwidth on the order of a GHz to allow a Rake receiver [45] to be operable in this environment can be employed to achieve frequency diversity [14].

The easiest way to generate GHz UWB communication signals is to use subnanosecond pulses, which typically spread the power from DC to several GHz depending on the pulse shape and the required bandwidth. The technology for transmitting and receiving such UWB pulses while controlling their relative position in the time dimension with great accuracy, so called pulse position modulation (PPM), is now available [57][58]. UWB modulation uses impulse signals that consist of trains of time-shifted subnanosecond or amplitude modulated pulses, so called pulse amplitude modulation (PAM). If data is transmitted using PPM/PAM, multiple pulses are transmitted for a single symbol, and time-hopping (TH) spread spectrum (SS) is applied to achieve multiple access capability. The TH PPM/PAM combination results in non-constant envelope "carrier-less" UWB modulated waveforms that can received by correlation receiver, making a relatively simple and low-cost transceiver viable [59].

It can be shown that an UWB system is comparable to a CDMA system operating with the same bandwidth. However, the use of subnanosecond pulses automatically gives an effective processing gain of about 50 dB with a data transmission rate of about 9.6 Kb/s, which brings advantage to UWB over current 2G/3G CDMA system [60]. Meanwhile an UWB system can also accommodate a large number of users. These large processing gains are necessary for UWB equipment to be operable license-free, and be able to coexist with current running narrow band systems without significant mutual interference.

Compared with a fast frequency hopping receiver operating with the same processing

gain, UWB has an edge in uncoded error-probability because of its coherence. Compared with infrared technology, UWB has the advantage of easy penetration of the buildings which facilitates wireless communication. Finally, compared with millimeter wave communications for the same short-range communication environment, UWB is potentially cheaper and simpler.

1.2.2 PPM/PAM UWB Communication System

Typically PAM, PPM or On/Off Keying (OOK) modulation is employed for UWB communications. PPM modulation uses the precise collocation of the impulses in time to convey information, while PAM and OOK use amplitude for this purpose. UWB systems with PAM and PPM modulation have been extensively investigated. In [7][59]-[62] a time-hopping multiple-access scheme for UWB systems with PPM was considered. A PPM UWB system over an AWGN channel was considered from the capacity perspective (subject to FCC part 15 rules) in [63][64]. The performance of a PAM UWB system with a Rake receiver was investigated in [65]-[67] for an indoor wireless channel with multipath interference. An all digital multiple access scheme based upon PAM and TDM was proposed in [66]. The construction of equal energy N-orthogonal Time-Shift-Modulated codes was described in [68]. In [69], the effective capacity of a pulse-position hopping CDMA system with OOK modulation was analyzed. Although M-ary PPM has better performance than M-ary PAM for $M>2$ in an UWB environment, it requires more accurate timing synchronization and has a higher computational complexity, particularly for large M. In general, with a correlation receiver, M-ary PPM requires M correlators, while M-ary PAM only requires one.

A typical time hopping format for the signal of the kth user in an UWB system is given by [70]

$$s^{(k)}(t) = \sum_{j=-\infty}^{\infty} A^{(k)}_{d_{\lfloor j/N_s \rfloor}} q\left(t - jT_f - c_j^{(k)} T_c - \delta_{d^{(k)}_{\lfloor j/N_s \rfloor}}\right), \tag{1.21}$$

where $A^{(k)}_{d_{\lfloor j/N_s \rfloor}}$ is the signal amplitude, *q(t)* represents the transmitted impulse waveform that nominally begins at time zero, and the quantities associated with *(k)* are transmitter dependent. T_f is the frame time, which is typically a hundred to a thousand times the impulse width resulting in a signal with very low duty cycle. Each frame is divided into N_h time slots with duration T_c. The pulse shift pattern $c_j^{(k)}$, $0 <= c_j^{(k)} <= N_h$, (also called time-hopping sequence), is pseudorandom with period T_c. This provides an additional shift in order to avoid catastrophic collisions due to multiple access interference. The sequence *d* is the data stream generated by the *k*th source after channel coding, and $\delta_{d^{(k)}_{\lfloor j/N_s \rfloor}}$ is the additional modulation time shift utilized for PPM determined by the input data *d*. If $N_s > 1$, a repetition code is introduced, i.e. N_s pulses are used for the transmission of the same information symbol. For PPM, $A^{(k)} = 1$, while $\delta = 0$ for PAM.

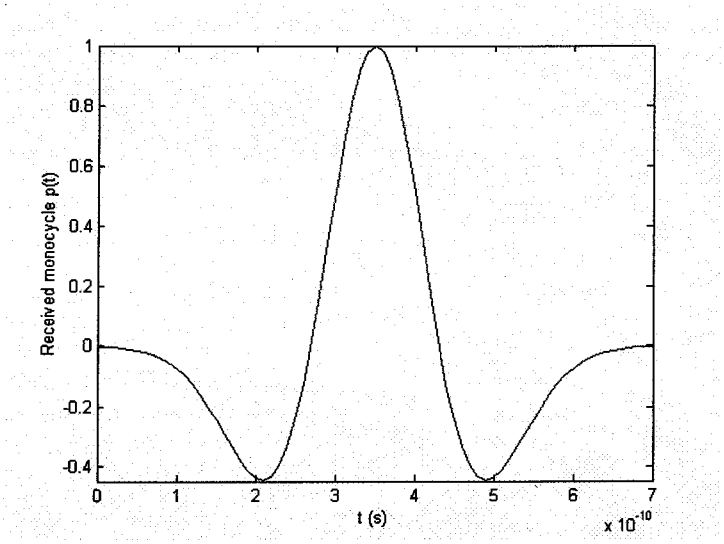

Fig.1.2 A Typical idealized received monocycle p(t) at the receiver as a function of time in subnanoseconds. $p(t+3.5)=\left[1-4\pi\left(t/\tau_m\right)^2\right]\exp\left[-2\pi\left(t/\tau_m\right)^2\right]$ with τ_m=0.2877.

Even an ideal channel and antenna system modifies the shape of the transmitted monocycle *p(t)* at the output of receiver. A typical idealized model of the received pulse shape is shown in Fig. 1.2 as second derivative Gaussian pulse. To facilitate analysis, we always assume that the true transformed pulse shape is known at the receiver and can be used to determine the correlation receiver structure. Therefore, the received signal can be modeled as the derivative of the transmitted pulses assuming propagation in free space [1]

$$\begin{aligned} r(t) &= \sum_{k=1}^{K}\left(s^{(k)}\left(t-\tau_k\right)\right)' + w(t) \\ &= \sum_{k=1}^{K}\sum_{j=-\infty}^{\infty} A^{(k)}_{d_{\lfloor j/N_s \rfloor}}\, p\left(t - jT_f - c_j^{(k)}T_c - \delta_{d^{(k)}_{\lfloor j/N_s \rfloor}}\right) + w(t) \end{aligned}, \qquad (1.22)$$

where *w(t)* is AWGN noise with power density $N_o/2$, τ_k is the propagation delay for the *k*th user and *p(t)* is the received pulse waveform. If only one user is present, the optimal receiver is an *N*-ary correlation receiver followed by a detector. When more

than one link is active in the multiple-access system, the optimal receiver is a complex structure that takes advantage of all receiver knowledge regarding the characteristics of the multiple-access interference (MAI) [70]. However, for simplicity, an N-ary correlation receiver is typically used even when there is more than one active user. Fig. 1.3 shows the structure of the correlation receiver of a PPM UWB system for user 1, where $h_i^{(k)}(t-\tau_i)$ is the basis function of the i_{th} correlator for user k. Note that for an N-ary PPM UWB system, N cross-correlators are required for demodulation.

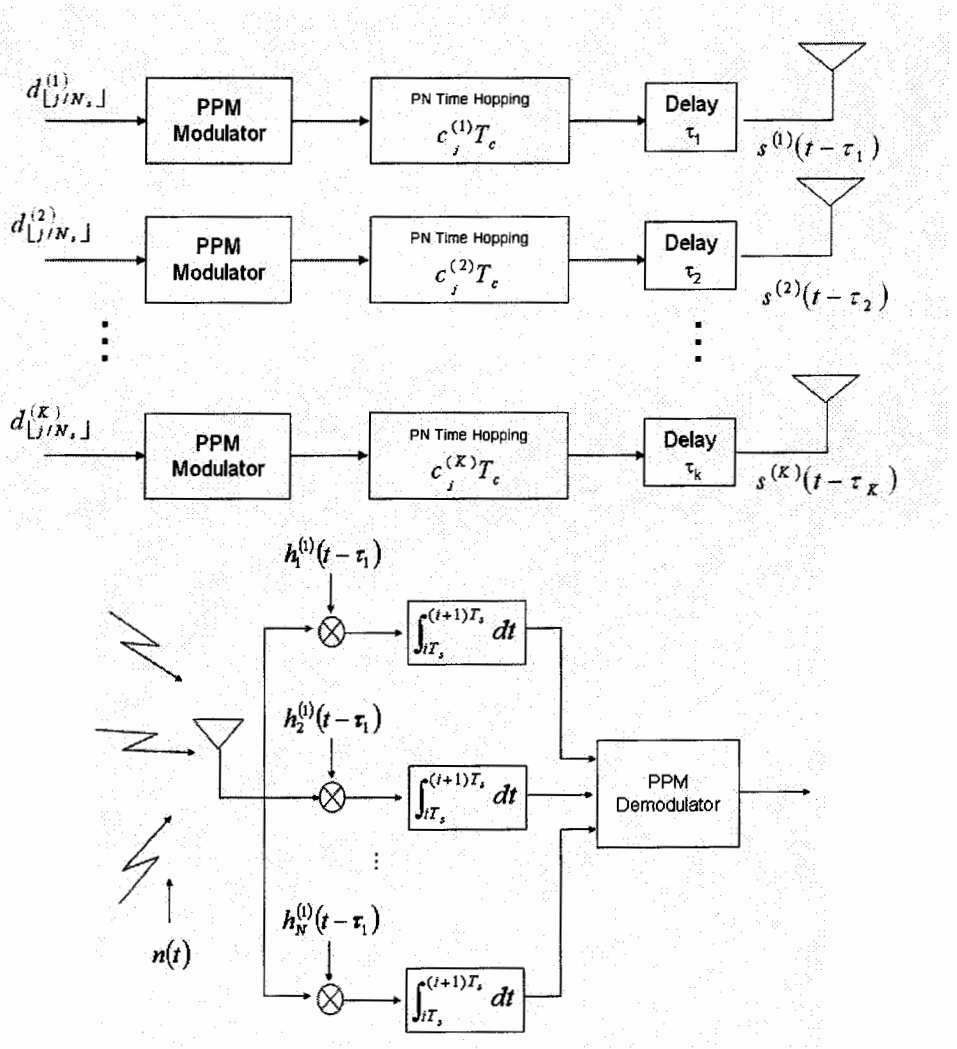

Fig.1.3 System model of a time-hopping multiple-access PPM UWB system

1.2.3 Related Works on UWB Communication System

The same attributes that make UWB technologically attractive [59][61] also create the communication design challenges [71][72] which yield a rich source of research problems. Among these are UWB channel propagation measurements [75][76], channel modeling, including multipath angle of arrival characterization [73][74][77][78][79], PPM signal selection and signal design [80]-[83], channel capacity analysis for PPM TH UWB [63][64][69], TH sequence design, fast TH sequence acquisition and tracking, demodulation and synchronization with limited radiated power, multiple-access performance calculation [59][61][62][65][66][67][70][80][81], PAM signal design, multiple access design, and Rake receiver implementation[65]-[67], as well as network issues. Some possible research subjects will be listed as future work later in the thesis.

1.3 Outline of the Thesis

The first goal of this thesis is to develop a theoretical capacity and error probability analysis of OSTBC over both independent and correlated flat fading channels. A second goal of this thesis is to propose a new modulation scheme, called pulse position amplitude modulation (PPAM), for UWB communication to provide good performance with low complexity. Both the capacity and performance of the proposed PPAM scheme are analyzed for a time-hopping multiple access UWB system over an AWGN channel.

This thesis is organized as follows.

In Chapter 2, OSTBC and UWB systems are studied from an information theoretic point of view. The channel capacity of multiple antenna system over fading channels is reviewed and the Shannon capacity of OSTBC is derived. Channel capacities for PPM and PAM signals over an AWGN channel are reviewed and the channel capacity of PPM/PAM UWB systems are derived subject to FCC Part 15 rules for both single user and time-hopping multiple access systems.

In Chapter 3, we introduce the equivalent scalar AWGN channel model for OSTBC over fading channels for all rate OSTBCs. Based on the effective scalar channel model, the distribution of the effective SNR over different fading channels is derived. The channel capacity of OSTBC with PAM/PSK/QAM is demonstrated and closed-form error probability expressions are presented for OSTBC with PAM/PSK/QAM over Rayleigh, Ricean and Nakagami-m fading channels. Both independent fading and correlated flat fading are investigated. Furthermore, we extend the analysis to a DS-CDMA system, an effective scalar AWGN channel is derived subject to the Gaussian approximation for a DS-CDMA system employing OSTBC over different fading channels. Capacity and error probability analysis are presented.

Chapter 4 proposes a new modulation scheme: PPAM. Capacity and error probability analysis are conducted over an AWGN channel for both single user and time-hopping multiple access PPAM UWB system. Exact error probabilities for orthogonal PPAM

UWB are derived and performance bounds are provided.

Finally, we draw some conclusions and suggest future work in Chapter 5.

1.4 Contributions of This Work

The work presented here makes a number of novel contributions to the field. The major contributions are summarized below.

1. A generalized equivalent scalar channel model for OSTBC including all rate OSTBCs which facilitates the analysis of OSTBC by transforming the MIMO OSTBC channel into a Single Input Single Out (SISO) AWGN channel.
2. With the generalized equivalent scalar channel, we present the capacity of OSTBC over flat fading channels, including Rayleigh, Ricean or Nakagami-m, with q-ary real or complex signal constellation
3. With the generalized equivalent scalar channel, we present closed-form expressions for the error probability of OSTBC with q-ary PAM/PSK/QAM over flat Rayleigh, Ricean and Nakagami-m fading channels.
4. Using a Gaussian approximation, we derive the equivalent scalar channel of a DS-CDMA systems employing OSTBCs, and present the channel capacity and closed form error probability over flat Rayleigh, Ricean, and Nakagami-m fading channels.

5. With the generalized equivalent scalar channel, capacity and error probability of OSTBCs over correlated fading channels are derived to show the impact of correlation.
6. A new modulation scheme, called pulse position amplitude modulation (PPAM), is proposed for UWB systems.
7. The capacity for PPAM UWB over an AWGN channel for both single user and time-hopping multiple access systems is presented subjected to FCC Part 15 rules.
8. Exact error probabilities for orthogonal PPAM UWB are derived.
9. Simple performance upper bounds are derived for a PPAM UWB system.

Chapter 2

Information Theory Considerations of Multiple Antenna and UWB Systems

The next frontier in the development of wireless communications is the conversion from current voice-based/lower rate data services to future high data rate applications such as rich content wireless internet. For example, sending video rather than voice requires the data rate to increase by two or three orders of magnitude. Increasing the transmit power is simple but costly, and restricted by radio regulations. Continued advances in VLSI and ASIC digital processing techniques will be a key factor in this conversion. A more economical solution is to exploit spatial diversity and channel coding through multiple antennas at the transmitter and receiver. Traditionally, spatial processing has been designed separately from channel coding, e.g., equalizer and combiner at receiver. Motivated by the fact that an integrated design might have advantages over the conventional individual approach, a step in this direction is the

integration of spatial and temporal processing into what is now commonly referred to as space-time processing [24][84][85]. It has been recognized that a joint approach offers more benefits than temporal and spatial processing applied separately [86]. Another means of increasing the data rate is to increase the channel bandwidth, which is forbidden by the current expensive and crowded frequency spectrum with conventional wireless technology. However, the emergence of UWB communications has rekindled this idea with its ultra-wide bandwidth and extra-low power which can safely coexist with current existing wireless systems.

In this chapter, theoretical capacities will be studied for both multiple antenna and UWB systems. Starting from a review of channel capacity with multilevel/phase modulation over AWGN and fading channels, the capacity of MIMO fading channel with q-ary modulation are presented. Then the capacity of an UWB system with PPM and PAM are investigated subject to FCC part 15 rules. Finally, a summary of the chapter is given.

2.1 Channel Capacity with Multilevel/phase Modulation

2.1.1 Shannon Capacity

In general, the channel capacity is a function of the channel realization, transmitted

signal power and noise. Assuming quasi-static and frequency-nonselective conditions for a SISO channel, the famous standard formula for the Shannon capacity [45] expressed in bps/Hz, i.e. normalized with respect to the bandwidth, is

$$C = \log_2(1 + SNR) \tag{2.1}$$

where SNR is the receive signal to noise ratio, defined by E_b/N_0, where E_b is the energy per bit.

2.1.2 MIMO Capacity over Fading Channels

For a MIMO channel represented by the $M \times N$ channel matrix $\mathbf{H}$ where N and M are the number of the transmit and receive antennas, respectively, the capacity of the multiple antenna system over a fading channel expressed in bits/s/Hz, i.e. normalized with respect to bandwidth, is given in [2][3] as

$$C = \mathbf{E}\left[\log_2 \det\left(\mathbf{I} + \frac{E_s}{NN_0}\mathbf{H}\mathbf{H}^{\dagger}\right)\right] \quad \text{bits/s/Hz} \tag{2.2}$$

where E[.] is the expected value operator, $\mathbf{I}$ is the identity matrix with dimension M, $\dagger$ is the operation of matrix transpose and conjugate. The overall transmit power is fixed and independent of the number of transmit antennas, N, so that a constant power is distributed among the transmit antenna elements. This facilitates the capacity comparison and allows us to demonstrate the impact of varying the number of transmit antennas. We define the outage capacity value C_{out} such that $C > C_{out}$ with a specified probability threshold. Fig 2.1 illustrates the 99% outage capacity of (2.2) with two transmit antennas and multiple receive antennas. For large M, such as M = 10, every 6 dB increase in SNR achieves 2 more bps/Hz. The outage capacity demonstrates that

high spectral efficiencies are possible for fading channels even though it is traditionally viewed as an impairment for high rate data transmission.

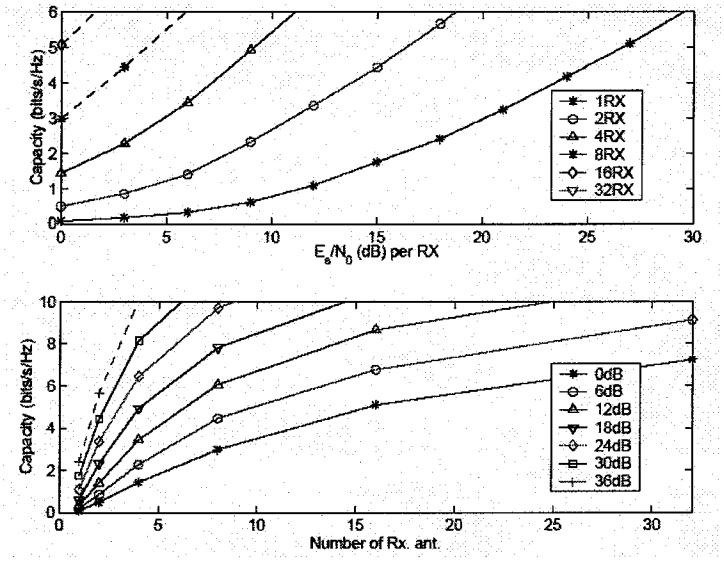

Fig.2.1 99% outage capacity of two transmit antennas and multiple receive antennas.

2.1.3 Channel Capacity of Multilevel/phase Modulation Channels

The Shannon capacity predicts the channel capacity C for an AWGN channel with continuous-valued inputs and outputs. However, a channel employing multilevel/phase modulation, for example PAM, PSK or QAM modulation, has discrete-valued inputs and continuous-valued outputs, which imposes an additional constraint on the capacity calculation. We consider the modulation channels with discrete-input and continuous-output, which was given in [45] as

$$C = \max_{P(x_i)} \sum_{k=0}^{q-1} \int_{-\infty}^{\infty} p(y|x_k) P(x_k) \log_2 \frac{p(y|x_k)}{p(y)} dy \tag{2.3}$$

where

$$p(y) = \sum_{i=0}^{q-1} p(y|x_i) P(x_i), \tag{2.4}$$

x_k is the discrete-valued input, and y is the continuous-valued output, modeled as

$$y(t) = x(t) + w(t) \tag{2.5}$$

where $w(t)$ is an additive white Gaussian noise process, and t is the time sequence.

Assuming an equal a priori probability real or complex signal constellation, i.e. $P(x_i) = \frac{1}{q}$, the channel capacity of an AWGN channel with q-ary modulation is then [87]

$$\begin{aligned} C &= \log_2(q) - \frac{1}{q}\sum_{k=0}^{q-1} \mathbf{E}_{y|x_k}\left\{\log_2 \frac{\sum_{i=0}^{q-1} p(y|x_i)}{p(y|x_k)}\right\} \\ &= \log_2(q) - \frac{1}{q}\sum_{k=0}^{q-1} \mathbf{E}_{y|x_k}\left\{\log_2 \sum_{i=0}^{q-1} \exp\left[-\frac{|x_k + w - x_i|^2 - |w|^2}{2\sigma^2}\right]\right\} \end{aligned}, \tag{2.6}$$

where E[.] is the expected value operator, w is the complex white Gaussian noise, modeled as a Gaussian distributed random variable with zero mean and variance σ^2 in each real dimension. (2.6) can be evaluated by Monte Carlo simulation. Note that (2.6) is a universal formula applied to q-ary PAM/PSK/QAM. Fig. 2.2 demonstrates the channel capacity of q-ary PSK over an AWGN channel, and Fig. 2.3 demonstrates the channel capacity of q-ary PAM over an AWGN channel.

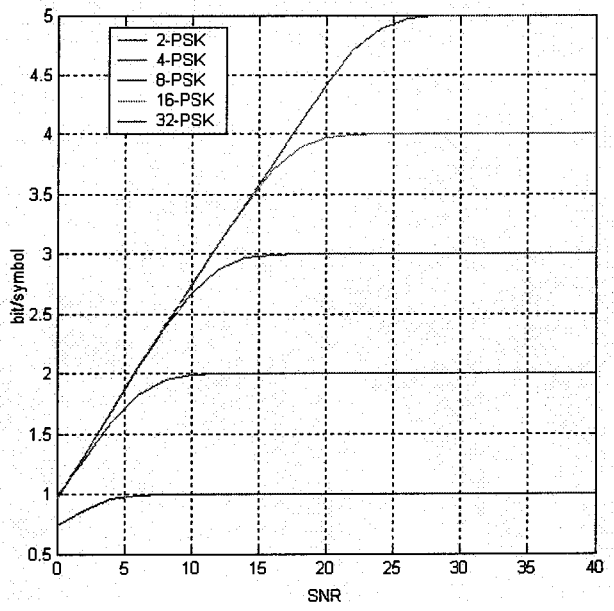

Fig.2.2 Channel Capacity of bandlimited AWGN channels with q-ary PSK modulation.

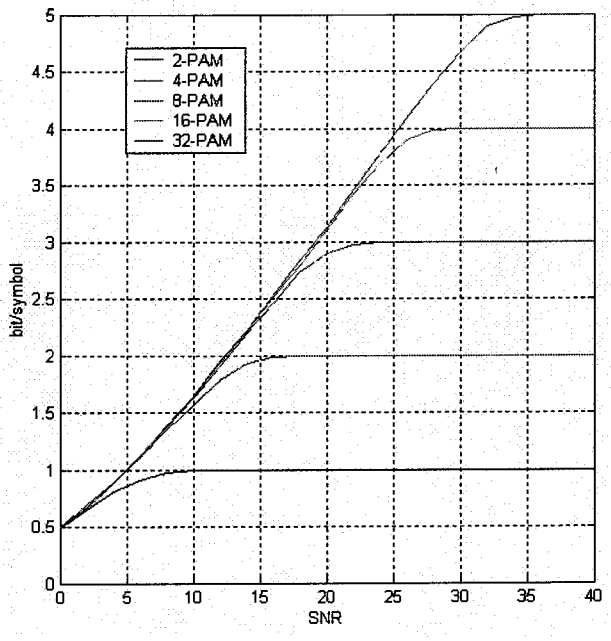

Fig.2.3 Channel Capacity of bandlimited AWGN channels with q-ary PAM modulation.

On wireless channels, channel capacity is typically degraded by fading phenomena which arise from multipath propagation. We model the complex process received at the

output of a noisy flat-fading wireless channel as

$$y(t) = h(t)x(t) + w(t) \tag{2.7}$$

where $h(t)$ is a generally time-correlated ergodic fading complex sequence independent of $x(t)$ and $w(t)$, and $w(t)$ is a complex zero mean AWGN sequence with variance $N_0/2$ in each dimension. Assuming coherent detection at the receiver, the effect of fading is reduced to the multiplication of the transmitted symbol x by the real nonnegative

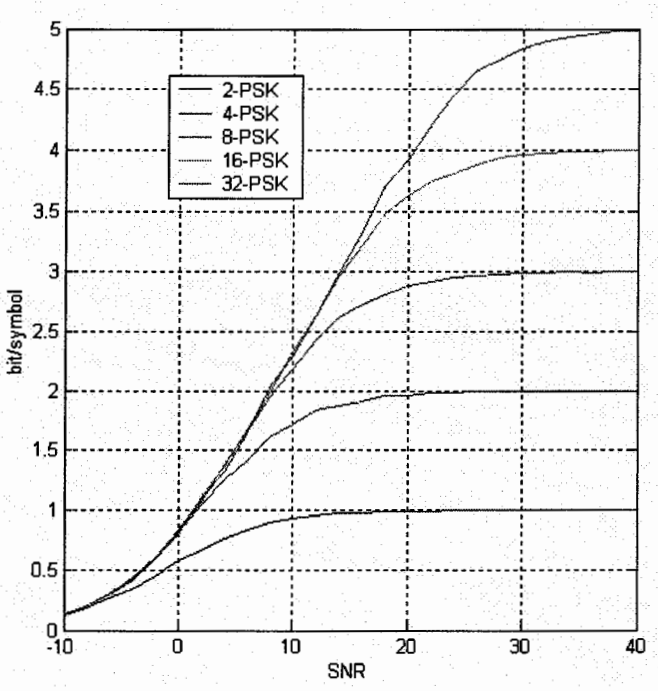

Fig.2.4 Channel Capacity of q-ary PSK over Rayleigh fading channel.

random variable $h = |h(t)|$, which represents the envelope of the complex fading coefficient $h(t)$. Therefore, without loss of generality, we can rewrite (2.7) for the observations in the following equivalent baud-rate sampled form

$$y(n)=h(n)x(n)+w(n). \tag{2.8}$$

With perfect channel state information available at the receiver, it is known [89][90] that the capacity of the channel in (2.8) can be directly obtained by averaging the corresponding conditional capacity $\tilde{C}(h)$ with respect to the probability density function (pdf) of the fading gain g. By doing so, we obtain the following expression for the channel capacity of fading channels for an equiprobable signal constellation

$$C_f=\int_0^{\infty}\tilde{C}(h)p(h)dh, \tag{2.9}$$

where

$$\tilde{C}(h)=\log_2(q)-\frac{1}{q}\sum_{k=0}^{q-1}\mathbf{E}_{y|x_k}\left\{\log_2\sum_{i=0}^{q-1}\exp\left[-\frac{|y-hx_k|^2-|y-hx_i|^2}{N_0}\right]\right\}. \tag{2.10}$$

Monte Carlo simulation can then be applied to evaluate (2.9). Fig. 2.4 shows the channel capacity for a Rayleigh fading channel with q-ary PSK. Compared with Fig. 2.2, the fading degrades the channel capacity significantly for low SNR.

2.1.4 Channel Capacity of Multilevel/phase Modulation Channels for Multiple Antenna System

Considering a narrow-band system with N transmit antennas and M receive antennas. Let's assume N coded streams $\{x_i(n)\}$, $1 \le i \le N$, which take values from a q-ary real/complex signal constellation $Ax \equiv \{\alpha_1,\ldots,\alpha_q\}$ simultaneously transmitted from the M transmit antennas. The channel is assumed to be flat fading, and the fading gain $h_{ji}(n)$ from transmit antenna i to receive antenna j at the n_{th} sample slot is modeled as

a zero mean complex random variable with variance 0.5 per real dimension. Therefore the received signal $y_j(n)$ at receive antenna j and time n is modeled as

$$y_j(n)=\sum_{i=1}^{N} h_{ji}(n)x_i(n)+w_j(n), \quad 1\le j\le M \tag{2.11}$$

where the noise sequences $w_j(n)$ are mutually independent zero mean stationary white Gaussian complex processes with variance $N_0/2$ per real dimension. The capacity of the MIMO channel conditioned on the channel fading gain matrix **H** is given by [91]

$$C^{*}_{M,N}=\int \tilde{C}^{*}_{M,N}(?)p(?)d? \tag{2.12}$$

where

$$\tilde{C}^{*}_{M,N}(\mathbf{H})=N\log_2 q-\left(\frac{1}{q}\right)^{N}\left(\frac{1}{\pi N_0}\right)^{M}\sum_{\mathbf{x}\in(Ax)^N}\int_{\mathbf{y}\in C^M}\exp\left(-\|\mathbf{y}-\mathbf{Hx}\|^2/N_0\right) \times\log_2\left[\sum_{\mathbf{x}'\in(Ax)^N}\exp\left(\|\mathbf{y}-\mathbf{Hx}\|^2-\|\mathbf{y}-\mathbf{Hx}'\|^2\right)/N_0\right]d\mathbf{y}\Bigg), \tag{2.13}$$

N and M are the number of transmit and receive antenna, respectively, $Ax\equiv\{\alpha_1,\ldots,\alpha_q\}$ is the q-ary complex signal constellation, $(Ax)^N$ indicates the set given by the N-fold Cartesian product of Ax by itself, the coded vector $\mathbf{x}\equiv[x_1\cdots x_N]\in(Ax)^N$ is an q^N-variate random variable with outcomes taking values on the expanded signal constellation $(Ax)^N$, $\mathbf{y}\equiv[y_1\cdots y_M]^T$ is the M-dimensional output vector of receive antennas. Considering a system with two transmit antennas and one receive antenna as an example and 4-PSK, we have

$$\tilde{C}^{*}_{1,2}(\mathbf{H})=4-\frac{1}{16}\sum_{k=0}^{3}\sum_{p=1}^{3}\mathbf{E}_{y|x_k x_p}\left[\log_2\left[\sum_{i=0}^{3}\sum_{q=1}^{3}\exp\left(\|y-h_{11}x_k-h_{12}x_p\|^2-\|y-h_{11}x_i-h_{12}x_q\|^2\right)/N_0\right]\right]. \tag{2.14}$$

2.2 Channel Capacity of UWB over AWGN

The UWB technology is very attractive for wireless communication to make available a large amount of spectrum to a variety of users without significant interference between them. With the bandwidth restrictions effectively removed, UWB promises a very high data rate over short or medium ranges subject to the power restriction. In this section, we consider the channel capacity of UWB systems in terms of bits/channel use. The major objective is to develop an understanding of the role of various parameters on the capacity of UWB communications.

2.2.1 Channel Capacity of Pulse Position Modulated Channels

The capacity of q-PPM is the same as that of a q dimensional orthogonal signal set, and of q-ary frequency shift keying (FSK). Assuming a equiprobable signal constellation, we have

$$p(\mathbf{y}|x_i)=\left(\frac{1}{2\pi\sigma^2}\right)^{\frac{q}{2}}\exp\left[-\frac{\left(y_i-\sqrt{E_s}\right)^2}{2\sigma^2}\right]\prod_{\substack{j=1\\ j\neq i}}^{q}\exp\left(-\frac{y_j^2}{2\sigma^2}\right), \tag{2.15}$$

where E_s is the energy of the PPM signal. The channel capacity of q-ary orthogonal modulation given by (2.3) can then be reduced to [92]

$$C_{PPM}=\log_2(q)-\mathbf{E}\left[\log_2\sum_{i=0}^{q-1}\exp\left[\sqrt{\frac{2E_s}{N_0}}(v_i-v_1)\right]\right], \tag{2.16}$$

where v_1 is a Gaussian variable with zero mean and variance one, v_i is also Gaussian

distributed with mean $\sqrt{2E_s/N_0}$ and unit variance for $i \neq 1$. Fig. 2.5 illustrates the channel capacity of q-PPM over AWGN channel.

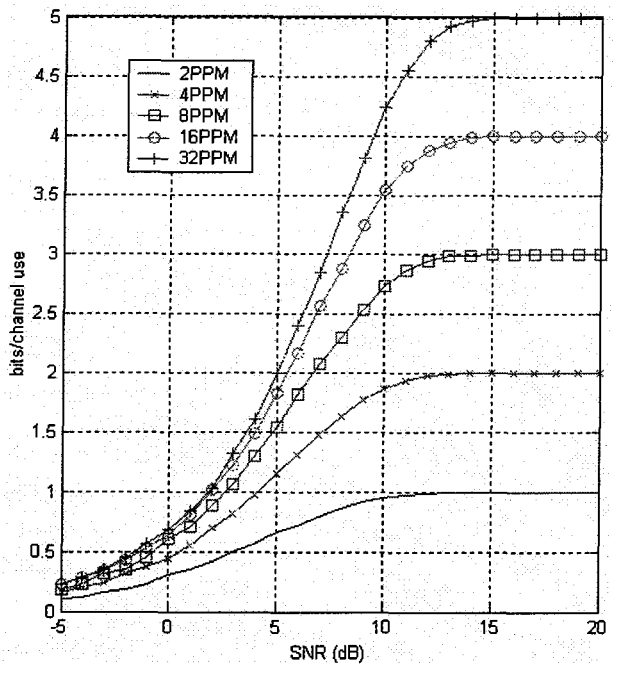

Fig.2.5 Channel Capacity of PPM over AWGN channel.

2.2.2 Channel Capacity of PPM UWB

PPM is a typical modulation for UWB communication which controls the precise location of the signal in time to convey information. The capacity of PPM over an AWGN channel derived above serves as the starting point to which the UWB-specific constraints are introduced. The most important constraint for a practical UWB system is the power spectrum density limitation to avoid the possible interference to other communication system operating within the frequency spectrum of the UWB system. On Feb 14, 2002, FCC issued regulations related to UWB, by which the transmit power

of an UWB system is required to be regulated under FCC Part 15 rules, i.e. emissions above 900 MHz shall not exceed field strength levels of E = 500 microvolts/meter/MHz measured at a distance of 3 meters from the transmitter.

To assess the communication distance assuming compliance with FCC part 15 rules, we takes a common link budget model [45]

$$P_r(d)(dBm) = P_t(dBm) + G_t(dB) + G_r(dB) - PL(dB), \qquad (2.17)$$

where P_t is the transmit UWB power, P_r is the received power at distance d, G_t and G_r are antenna gain for the transmit and receive antennas, respectively, both assumed to be odB for simplicity. The path loss PL depends on the propagation model, but there is no commonly accepted model for UWB so far. It is shown in [74] that the received signal strength approximately follows a d^{-4} dependency with distance d in an environment with dense multipath, while follows d^{-2} dependency in short range such as several meters, i.e. dominate by the line of sight (LOS) path. The general path loss model for UWB is

$$PL(dB) = 10\log\frac{(4\pi d)^n}{\lambda}, \qquad (2.18)$$

where n is the power attenuation exponent and λ is the wavelength corresponding to the center frequency f_c. With the approximate relationship between E and P_t given by [45]

$$P_t = \frac{4\pi d^2 E^2}{120\pi G_t}, \tag{2.19}$$

we can obtain the power constraint on transmit power for an UWB system with a 1 GHz bandwidth as

$$P_t \leq \text{-11 dBm.} \tag{2.20}$$

A certain minimum SNR is required at the receiver to properly detect and decode the received signal. Considering thermal noise as the primary source of interference, the following relationship is obtained

$$\frac{SNR}{G} \leq -11dBm - N_{thermal} - F - 10\log\frac{(4\pi d)^n}{\lambda}, \tag{2.21}$$

where $G = N_s T_f W_p$ is the equivalent processing gain resulting from the low duty cycle, W_p is the bandwidth of the UWB impulse related to the pulse duration T_p, F is the noise figure set to 5 dB, $N_{thermal}$ is the thermal noise floor, calculated as the product of the Boltzman's constant, room temperature (typically 300K), noise figure and bandwidth, and n is the path loss exponent. It is easily shown that the maximum reliable communication distance is determined primarily by the signal to noise ratio *SNR*. The spectral efficiency in bits/s/Hz for PPM UWB can be obtained from (2.16) as

$$\bar{C}_{PPM} = \frac{C_{PPM}}{N_s T_f W_p} = \frac{C_{PPM}}{G} \text{ [bits/s/Hz].} \tag{2.22}$$

Fig. 2.6 shows the relationship between spectral efficiency and communication distance

with G=100 and n=2. The same relationship is shown in Fig. 2.7 with n=4.

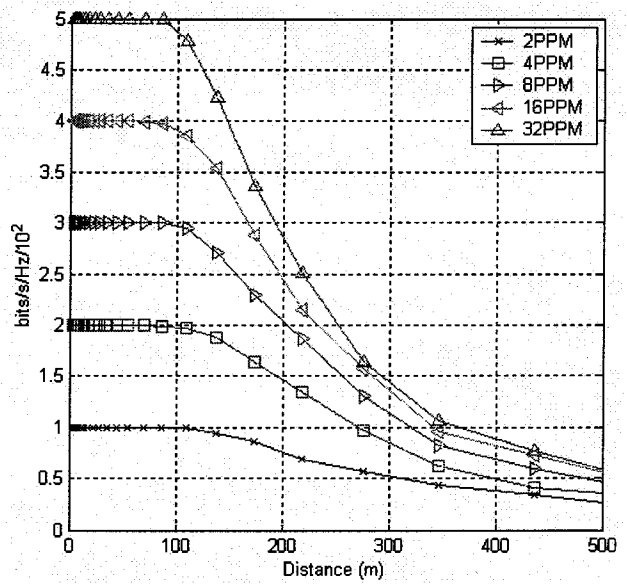

Fig.2.6 PPM UWB spectral efficiency versus communication distance for n=2 and G=100.

With a power attenuation exponent n=2 and processing gain G=100, a spectral efficiency of 5×10^{-2} bits/s/Hz can be obtained within a distance of 100m for 32-PPM. For a 1 GHz channel, the range of communication is 75m for a data rate up to 50 Mbits/s and about 325m for a data rate of 10 Mbits/s. However, for n=4, the maximum communication distance for a data rate of 50 Mbits/s is less than 10m for 32-PPM.

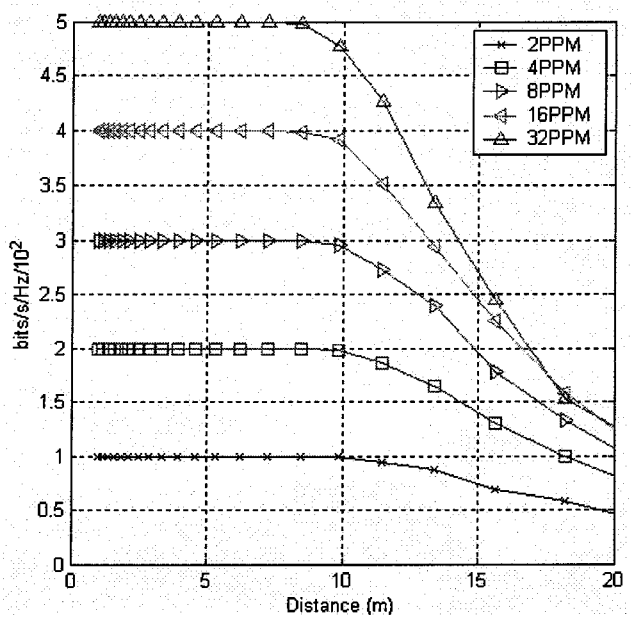

Fig.2.7 PPM UWB spectral efficiency versus communication distance for n=4 and G=100.

2.2.3 Channel Capacity of PAM UWB

Following the same analysis, we find the spectral efficiency in bits/s/Hz of PAM UWB is

$$\bar{C}_{PAM} = \frac{C_{PAM}}{N_s T_f W_p} = \frac{C_{PAM}}{G} \tag{2.23}$$

where C_{PAM} can be obtained from (2.6). Applying the same power constraint as in (2.20), and the same link budget model as in (2.17), the same relationship (2.21) can be obtained for PAM UWB. Again the maximum reliable communication distance is determined primarily by the signal to noise ratio *SNR*. The relationship between the channel spectral efficiency and communication range for PAM UWB is shown in Fig. 2.9. It is shown that 32-PAM can achieve 5×10^{-2} bits/s/Hz spectral efficiency within a

range less than 5m. For a 1 GHz channel, 32-PAM UWB can provide 20 Mbits/s data transmission within a distance of 90 meters. Compared with 32-PPM UWB, 32-PAM obviously is not an attractive choice. However, as shown in the figure, the maximum distance for a data rate of 10 Mbits/s with 2-PAM is 150 meters, which is farther than the 100 meters with 2-PPM.

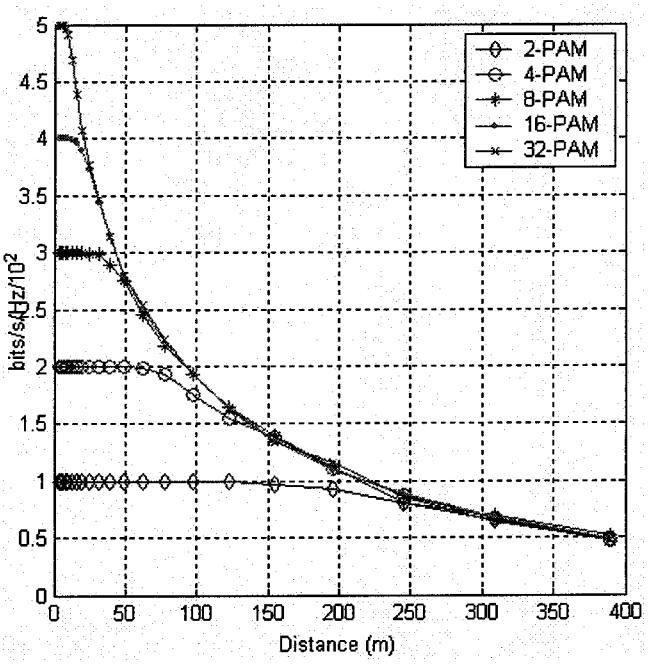

Fig.2.8 PAM UWB spectral efficiency versus communication distance for n=2 and G=100.

2.3 Summary

In this chapter, the channel capacity of multiple antenna systems with multilevel/phase modulated signal constellations was first considered over fading channels. Spectral efficiency of an UWB system was demonstrated assuming compliance with FCC Part 15

rules for both PAM and PPM signals. The relationship between the maximum communication range and reliable data rate was shown. The results presented here will serve as the starting point for the capacity analysis in the following chapters.

Chapter 3

Capacity and Error Probability of OSTBC over Fading Channels

In this chapter, the capacity and error probability of orthogonal space-time block codes (OSTBC) are considered for PAM/PSK/QAM modulation in fading channels. We first introduce an equivalent scalar AWGN channel with a channel gain proportional to the Frobenius norm of the matrix channel applied for all rate OSTBCs, which practically transforms the MIMO OSTBC channel into a SISO AWGN channel utilizing the inherited orthogonality of its coding scheme. We then approach the capacity and error probability based on the equivalent scalar AWGN channel with conventional method as shown in [45]. Capacity and probability of error expressions are derived for PSK/PAM/QAM modulation with OSTBC considering flat Rayleigh, Ricean and Nakagami fading channels. As an application, these results are extended to obtain the capacity and probability of error for a multiuser direct sequence code division multiple access (DS-CDMA) system employing OSTBC. Furthermore, capacity and error

probability of OSTBC over correlated fading channels are also investigated. Some elegant results are obtained. Finally, a summary is given to conclude the chapter.

3.1 The Effective Scaled AWGN Channel

In [42], the equivalent scaled AWGN channel induced by the OSTBC for complex constellations was given as

$$\mathbf{y}_{nT} = \|\mathbf{H}\|_F^2 \mathbf{x}_{nT} + \mathbf{w}_{nT}, \tag{3.1}$$

assuming a full code rate, where y_{nT} is the $S \times 1$ complex matrix after OSTBC decoding from the received matrix Y_{nT}, x_{nT} is the $S \times 1$ complex input matrix with each entry having energy E_s/N, E_s is the maximum total transmitted energy on the N transmit antennas per symbol time, and w_{nT} is complex Gaussian noise with zero mean and variance $\|\mathrm{H}\|_F^2 N_0/2$ in each real dimension. $\|\mathrm{H}\|_F^2 = \sum_{i=1}^{N}\sum_{j=1}^{M}\|h_{ij}\|^2$ is the squared Frobenius norm of $\mathbf{H}$, h_{ij} is the channel gain from the i_{th} transmit antenna to the j_{th} receive antenna and these gains are considered independent. A flat fading channel is assumed, i.e. h_{ij} is a constant over a timeslot T. Taking into account the code rate, the equivalent AWGN scaled channel with a space-time block code is

$$\mathbf{y}_{nT} = \frac{1}{R}\|\mathbf{H}\|_F^2 \mathbf{x}_{nT} + \mathbf{w}_{nT}, \tag{3.2}$$

where $\mathbf{w}_{nT}$ is complex Gaussian noise with zero mean and variance $\frac{1}{R}\|\mathbf{H}\|_F^2 N_0/2$ in

each real dimension. Therefore, the effective instantaneous SNR, denoted as γ_s, at the receiver is

$$\gamma_s = \frac{E_s}{NRN_0}\|\mathbf{H}\|_F^2 . \tag{3.3}$$

Let $h = \frac{1}{R}\|\mathbf{H}\|_F^2 = \sum_{i=1}^{N}\sum_{j=1}^{M}\frac{1}{R}\|h_{ij}\|^2$, then the OSTBC channel model of (3.2) can be simplified to

$$\mathbf{y}_{nT} = h\mathbf{x}_{nT} + \mathbf{w}_{nT}, \tag{3.4}$$

and γ_s can be written as

$$\gamma_s = \frac{E_s}{NN_0}h . \tag{3.5}$$

3.2 Distribution of the Equivalent Channel Coefficients and SNR for Fading Channels

As shown in (3.4), h is the equivalent channel coefficient for the effective scalar AWGN channel. In this section, we will find the probability density function of this equivalent channel coefficient h and the effective instantaneous *SNR* for various fading channels.

3.2.1 Rayleigh Fading

With Rayleigh fading, h_{ij} can be modeled as a complex Gaussian variable with zero mean and variance σ^2 in each dimension. The PDF of h is then a central chi-square

distribution with *2MN* degrees of freedom

$$p_{rayleigh}(h) = \frac{R^{MN}}{\left(2\sigma^2\right)^{MN}\Gamma(MN)} h^{MN-1} e^{-hR/2\sigma^2}, h \geq 0. \tag{3.6}$$

Consequently, the instantaneous *SNR* per symbol γ_s is also chi-square distributed. Using a change of variables, the PDF of γ_s is given by

$$p_{rayleigh}(\gamma_s) = \frac{1}{\bar{\gamma}_c^{\,MN}\Gamma(MN)} \gamma_s^{MN-1} e^{-\gamma_s/\bar{\gamma}_c}, \gamma_s \geq 0, \tag{3.7}$$

where $\bar{\gamma}_c$ is the average SNR per channel, which is assumed to be identical for all channels, i.e.

$$\bar{\gamma}_c = \frac{E_s}{NRN_0} \mathrm{E}\left[\left\|h_{ij}\right\|^2\right] = \frac{2\sigma^2 E_s}{NRN_0}. \tag{3.8}$$

It can easily be shown that the instantaneous *SNR* per bit γ_b has the same PDF except that $\bar{\gamma}_c = \frac{E_s}{NRN_0 \log_2 q}$ for a q-ary signal constellation.

3.2.2 Ricean Fading

For Ricean fading, h_{ij} can be modeled as a complex Gaussian variable with means m_I and m_Q for the real and imaginary parts, respectively, and variance σ^2 in each dimension. In this case, $\|\mathbf{H}\|_F^2$ has a noncentral chi-square distribution with *2MN* degrees of freedom. The PDF of *h* is given by

$$p_{ricean}(h) = \frac{R}{2\sigma^2}\left(\frac{Rh}{s^2}\right)^{(MN-1)/2} e^{-(s^2+Rh)/2\sigma^2} I_{MN-1}\left(\sqrt{Rh}\frac{s}{\sigma^2}\right), h \geq 0, \tag{3.9}$$

where $s^2 = MN(m_I^2 + m_Q^2)$ is the noncentrality parameter, $I_\alpha(x)$ is the αth-order modified Bessel function of the first kind, which can be represented by the infinite series

$$I_n(x) = \sum_{k=0}^{\infty} \frac{(x/2)^{n+2k}}{k!\Gamma(n+k+1)}. \tag{3.10}$$

The Ricean parameter is defined as $\beta = \frac{m_I^2 + m_Q^2}{2\sigma^2}$, (3.9) can then be written as

$$p_{ricean}(h) = \sum_{i=0}^{\infty} \frac{(MN\beta)^i e^{-MN\beta} R^{MN+i}}{\Gamma(i+1)\Gamma(MN+i)(2\sigma^2)^{MN+i}} h^{MN+i-1} e^{-\frac{Rh}{2\sigma^2}}, h \geq 0. \tag{3.11}$$

Using a change of variables, the PDF of the instantaneous *SNR* per symbol γ_s is

$$p_{ricean}(\gamma_s) = \sum_{i=0}^{\infty} \frac{(MN\beta)^i e^{-MN\beta} \gamma_s^{MN+i-1} e^{-\frac{\gamma_s}{\bar{\gamma}_c}}}{\Gamma(i+1)\Gamma(MN+i)\bar{\gamma}_c^{MN+i}}, \gamma_s \geq 0, \tag{3.12}$$

where $\bar{\gamma}_c$ is the average SNR per channel, which is assumed to be identical for all channels, as given in (3.8).

As for Rayleigh fading, the instantaneous *SNR* per bit γ_b has the same PDF except that $\bar{\gamma}_c = \frac{E_s}{NRN_0 \log_2 q}$ for a q-ary signal constellation.

3.2.3 Nakagami-m Fading

For Nakagami-*m* fading with integer *m*, $\|h_{ij}\|$, the amplitude of the channel coefficient h_{ij}, has a Nakagami-m distribution with variance Ω in each dimension. The random

variable $y = \frac{1}{R}\|h_{ij}\|^2$ then has PDF [45]

$$p(y) = \frac{R^m}{(2\sigma^2)^m \Gamma(m)} y^{m-1} e^{-Ry/2\sigma^2}, \tag{3.13}$$

where $\sigma^2 = \frac{\Omega}{m}$.

Observing that the PDF for Nakagami fading has the same form as the PDF for Rayleigh fading, but with degree *2m* in (3.7), a single Nakagami-*m* fading channel is equivalent to an m diversity system for a Rayleigh fading channel. It is then straightforward to show that results for OSTBCs over Nakagami fading channels can be obtained by considering Rayleigh fading channels with the channel diversity order increased from *MN* to *mMN*. Consequently, the PDF of the instantaneous *SNR* per symbol γ_s can be obtained directly from (3.7) as

$$p_{Nakagami,m}(\gamma_s) = \frac{1}{\bar{\gamma}_c^{\,mMN} \Gamma(mMN)} \gamma_s^{\,mMN-1} e^{-\gamma_s/\bar{\gamma}_c}, \tag{3.14}$$

where $\bar{\gamma}_c$ is the average SNR per channel, which is assumed to be identical for all channels, as given in (3.8).

Again as for Rayleigh fading, the instantaneous *SNR* per bit γ_b has the same PDF except that $\bar{\gamma}_c = \frac{E_s}{NRN_0 \log_2 q}$ for a q-ary signal constellation.

3.3 Capacity of OSTBC over Fading Channels

3.3.1 Shannon Capacity

From chapter 2, the full open-loop capacity of a MIMO channel is given in (2.2) according to [2][3]. Invoking the effective scalar AWGN channel for OSTBC in (3.2), the MIMO OSTBC channel is transformed to a SISO scaled AWGN channel. Thus the Shannon capacity of OSTBC over a fading channel with continuous-valued inputs and continuous-valued outputs for complex signals is given by (2.1) as

$$\begin{aligned}\overline{C} &= \mathrm{E}\left[R\log_2\left(1+\frac{E_s}{RNN_0}\|\mathrm{H}\|_F^2\right)\right] \text{ bits/s/Hz.} \\ &= \mathrm{E}\left[R\log_2(1+\gamma_s)\right]\end{aligned} \tag{3.15}$$

Given the PDF of γ_s, the capacity of the equivalent OSTBC channel can be obtained from

$$\overline{C} = R\int_0^\infty \log_2(1+\gamma_s)p(\gamma_s)d\gamma_s, \tag{3.16}$$

where $p(\gamma_s)$ is given in Section 3.2 for Rayleigh, Ricean, and Nakagami-*m* fading.

As the capacity depends on the instantaneous SNR which is random distributed, it is treated as a random variable. Consequently, the channel capacity at a given outage probability p, C_p, can be defined as a measure of the capacity, i.e. the channel could offer a random capacity greater than C_p with a probability p. Note that it is not necessary for the channel to be uncorrelated.

3.3.2 Channel Capacity with Multilevel/Phase Modulation

Both (2.2) and (3.16) were obtained assuming continuous-valued inputs. Here we

consider modulation channels with discrete-valued multilevel/phase inputs and continuous-valued outputs. Assuming maximum likelihood (ML) soft decoding with perfect channel state information at the receiver, the capacity C^*_{STBC} of the OSTBC channel (3.2) can be obtained by averaging the corresponding conditional capacity $\tilde{C}^*(\mathrm{H})$ with respect to the joint PDF of the channel matrix **H**. By doing so, the following expression for the capacity C^*_{STBC} of the fading channel is obtained

$$C^*_{STBC} = \mathbf{E}\left[\tilde{C}^*(\mathrm{H})\right] = \int \tilde{C}^*(\mathrm{H}) p(\mathrm{H}) d\mathrm{H} \quad \text{bits/s/Hz}, \tag{3.17}$$

with

$$\begin{aligned}\tilde{C}^*(\mathrm{H}) = R\Bigg(& \log_2 q - \frac{1}{q}\sum_{j=1}^{q} \frac{1}{\pi(\frac{1}{R}\|\mathrm{H}\|_F^2 N_0)} \int_{y\in C} \exp\left(-\left\| y - \frac{1}{R}\|\mathrm{H}\|_F^2 \alpha_j \right\|^2 \Big/ (\frac{1}{R}\|\mathrm{H}\|_F^2 N_0) \right) \\ & \times \log_2 \left[\sum_{s=1}^{q} \exp\left(\left\| y - \frac{1}{R}\|\mathrm{H}\|_F^2 \alpha_j \right\|^2 - \left\| y - \frac{1}{R}\|\mathrm{H}\|_F^2 \alpha_s \right\|^2 \right) \Big/ (\frac{1}{R}\|\mathrm{H}\|_F^2 N_0)) \right] dy \Bigg)\end{aligned} \tag{3.18}$$

bits/s/Hz,

where α_j, j=1...q, is a real signal in the q-ary real constellation (PAM) or a complex signal in the q-ary complex signal (PSK/QAM) constellation, and $p(\mathrm{H})$ is the joint PDF of the $M \times N$ random elements of the channel matrix **H** for the fading channel. Applying the channel model (3.4), (3.17) can be simplified to a one dimension integral containing the PDF of h

$$C^*_{STBC,R} = \mathbf{E}\left[\tilde{C}^*(h)\right] = \int \tilde{C}^*(h) p(h) dh, \tag{3.19}$$

where

$$\begin{aligned}\tilde{C}^*(h) = R\Bigg(& \log_2 q - \frac{1}{q}\sum_{j=1}^{q} \frac{1}{\pi h N_0} \int_{y\in C} \exp\left(-\left\| y - h\alpha_j \right\|^2 / hN_0 \right) \\ & \times \log_2 \left[\sum_{s=1}^{q} \exp\left(\left(\left\| y - h\alpha_j \right\|^2 - \left\| y - h\alpha_s \right\|^2 \right) / hN_0 \right) \right] dy \Bigg)\end{aligned} \tag{3.20}$$

Note that (3.19) applies to both real signal constellations such as PAM, and complex signal constellations such as PSK/QAM.

3.3.3 Capacity Comparison

It is shown in [42] that the difference between (3.15) and (2.2) is the capacity loss incurred by using a OSTBC in a MIMO fading channel with continue-valued inputs. The capacity of a MIMO fading channel with q-ary PAM/PSK/QAM is given in (2.12) according to [91] as

$$C_{M,N}^{*} = \int \tilde{C}_{M,N}^{*}(?)p(?)d? \ , \tag{3.21}$$

where

$$\tilde{C}_{M,N}^{*}(\mathbf{H}) = N\log_2 q - \left(\frac{1}{q}\right)^N \left(\frac{1}{\pi N_0}\right)^M \sum_{\mathbf{x}\in(Ax)^N} \int_{\mathbf{y}\in C} \exp\left(-\|\mathbf{y} - \mathbf{Hx}\|^2 / N_0\right) \times \log_2 \left[\sum_{\mathbf{x}'\in(Ax)^N} \exp\left(\|\mathbf{y}-\mathbf{Hx}\|^2 - \|\mathbf{y}-\mathbf{Hx}'\|^2\right)/N_0\right] d\mathbf{y} \Bigg), \tag{3.22}$$

N and M are the number of transmit and receive antenna, respectively, $Ax \equiv \{\alpha_1,\ldots,\alpha_q\}$ is the q-ary complex signal constellation, $(Ax)^N$ indicates the set give by the N-fold Cartesian product of Ax by itself, the coded vector $\mathbf{x} \equiv [x_1 \cdots x_N] \in (Ax)^N$ is an q^N-variate random variable with outcomes taking values on the expanded signal constellation $(Ax)^N$, $\mathbf{y} \equiv [y_1 \cdots y_M]^T$ is the M-dimensional output vector of the receive antennas.

It can easily be shown that the second terms in (3.20) and (3.22) vanish as the SNR increases, which implies that the capacity of a MIMO fading channel approaches $N\log_2 q$ bits/s/Hz, while the capacity with OSTBC approaches only $R\log_2 q$ bits/s/Hz for large SNR. While the capacity loss incurred by using OSTBC of $(N-R)\log_2 q$ bits/s/Hz is fairly significant, it will be shown that the SNR threshold for reliable data

transmission is reduced because of the diversity gain of OSTBC.

3.3.4 Numerical Results

The OSTBC Shannon capacity C_p for an outage capacity of p =98% is obtained from the cumulative distribution functions computed by Monte Carlo simulation. The OSTBC Shannon capacity with N=2,4, and 8 transmit antennas and M = 1,2, 4 and 8 receive antennas are considered for Rayleigh and Ricean quasi-static flat fading, with the channel assumed to be uncorrelated.

Fig. 3.1, Fig. 3.2, and Fig. 3.3 illustrate the 98% outage capacity for $\mathbf{G}_2$, $\mathbf{G}_4$, and $\mathbf{H}_4$ OSTBCs over a Rayleigh fading channels. The full open-loop capacity [2] (the channel is only known by receiver) is also included for reference. Note that the capacities of OSTBCs are significantly lower than those for theoretic Shannon limits, specially for large N and M. However $\mathbf{G}_2$ code with one receive antenna is the only scenario that OSTBC can achieve 100% of the Shannon capacity.

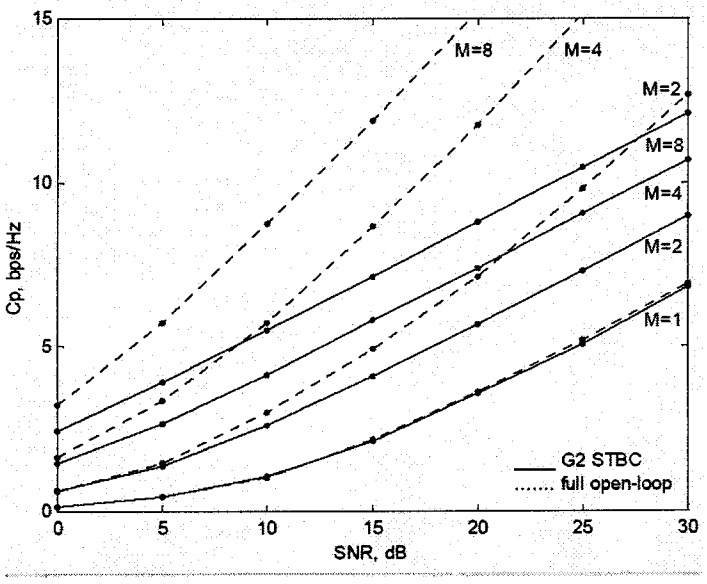

Fig.3.1 98% outage capacity of OSTBC $\mathbf{G}_2$ versus SNR with multiple receive antennas.

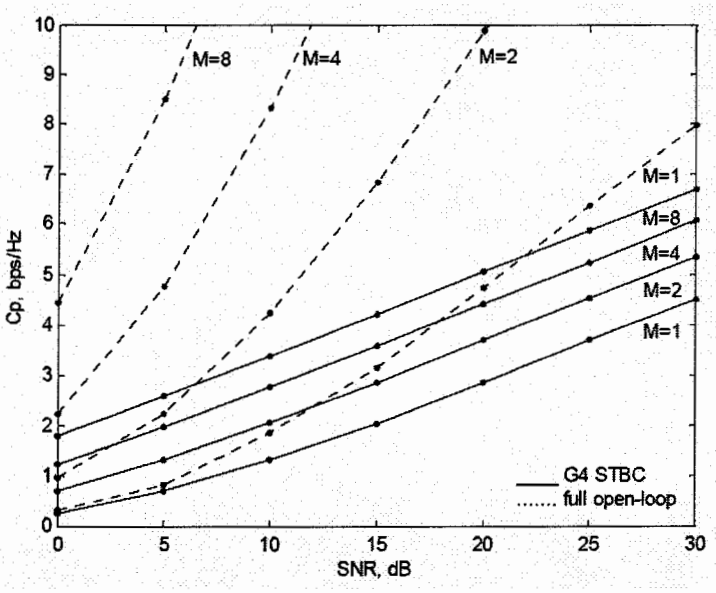

Fig.3.2 98% outage capacity of OSTBC $\mathbf{G}_4$ versus SNR with multiple receive antennas.

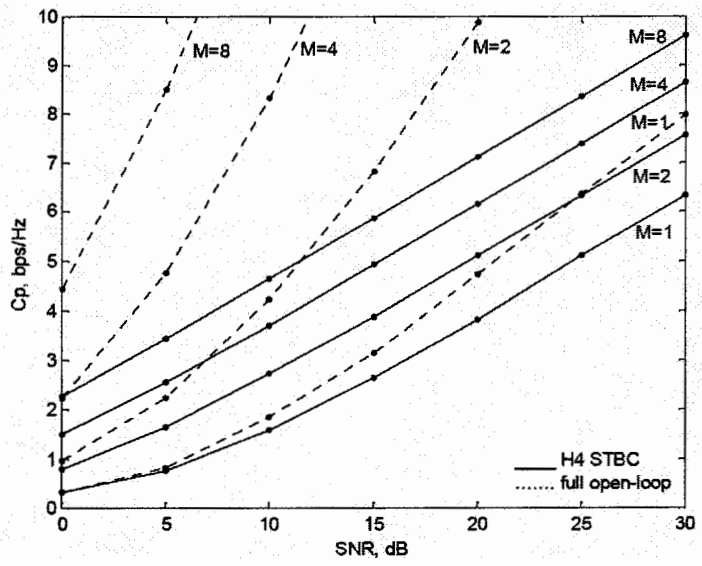

Fig.3.3 98% outage capacity of OSTBC $\mathbf{H}_4$ versus SNR with multiple receive antennas.

Fig. 3.4 shows the 98% outage capacity for some OSTBCs achieved over correlated Rayleigh fading channels versus the correlation coefficient between two antenna elements at the base station. The signal to noise ratio is set to 18 dB. It is shown that the achieved capacity significantly decreases due to the channel correlation effect when the number of receive antenna

decreases.

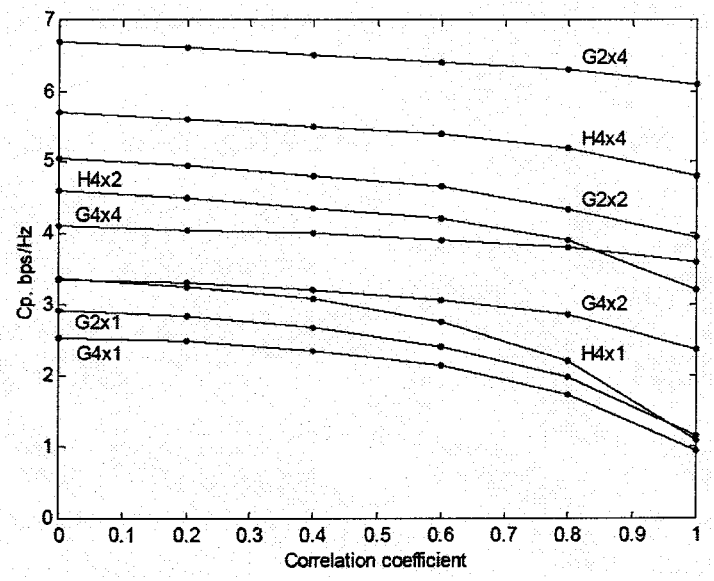

Fig.3.4 98% outage capacity of several OSTBCs versus correlation coefficient with multiple receive antennas.

Fig.3.5 and Fig. 3.6 show the 98% outage capacity of several OSTBCs in a Ricean fading channel, for M=2 and 4, respectively. The channel matrix for Ricean fading can be modeled [93] as

$$\mathbf{H} = \mathbf{H}_{sp} + \mathbf{H}_{sc}, \tag{3.23}$$

where $\mathbf{H}_{sp}$ is the specular component (LOS), which is modeled as a constant and $\mathbf{H}_{sc}$ is the scattering component modeled as a Gaussian random variable with zero mean and unit variance. The SNR for both figures was set to 18 dB. Noted that the OSTBC capacity slightly increases with the Ricean parameter (when the LOS component is dominant and the channel tends to be Gaussian). On the other hand, the Shannon capacity with a OSTBC decrease dramatically when the Ricean parameter increases. Note that both the full open-loop and G2 × 4 converges to 8 bps/Hz for large Rice

parameter, which results the channel approach Gaussian, i.e. the rank of the channel matrix **H** is one.

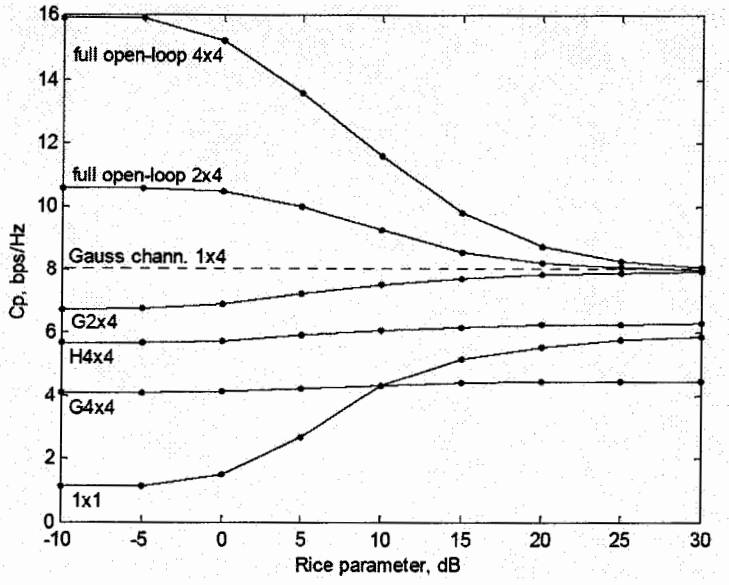

Fig.3.5 98% outage capacity of some OSTBCs versus Rice parameter β – I.

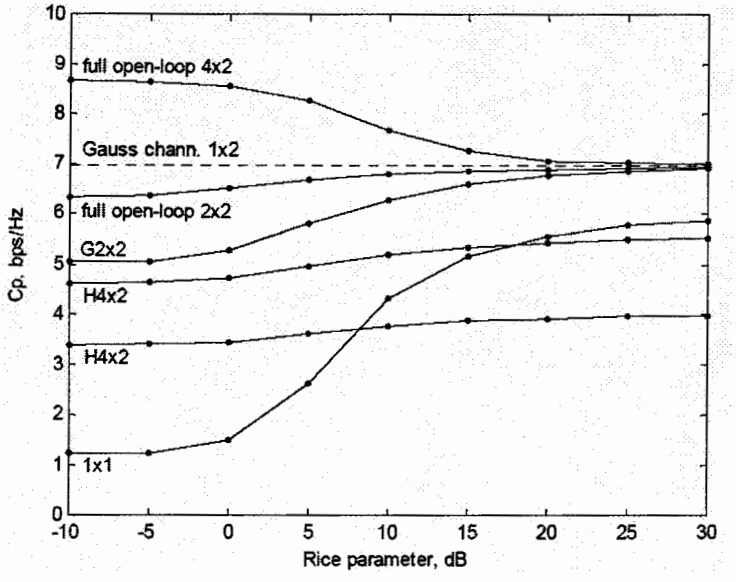

Fig.3.6 98% outage capacity of several OSTBCs versus Ricean parameter β– II.

Fig. 3.7 shows the capacity using OSTBC $\mathbf{G_2}$ over a Ricean fading channel with 1, 2, and

4 receive antennas for BPSK, QPSK and 8-PSK. The Ricean parameter is ß=100. This figure shows that the achievable capacity with OSTBC $\mathbf{G_2}$ does not increase as the number of receive antennas increases. However, the SNR threshold required to achieve full channel capacity improves as the number of receive antennas increases. The channel capacity with a single antenna over a Ricean fading channel for PSK is included for reference.

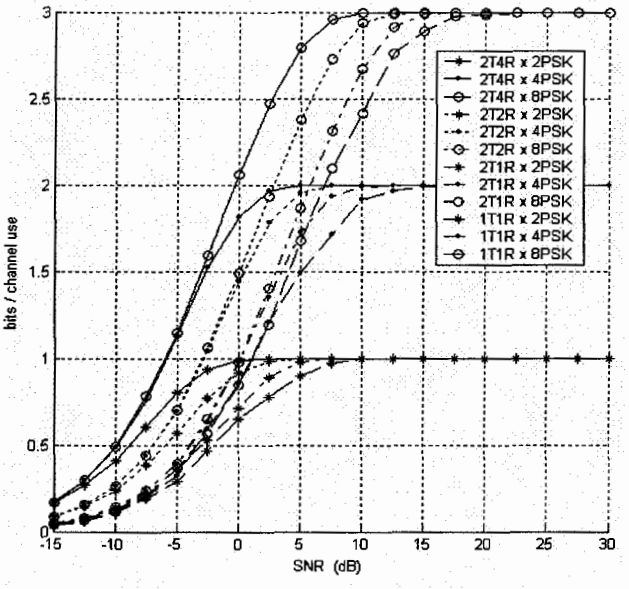

Fig.3.7 Capacity of OSTBC $\mathbf{G_2}$ in a Ricean fading channel, with Ricean parameter ß=100.

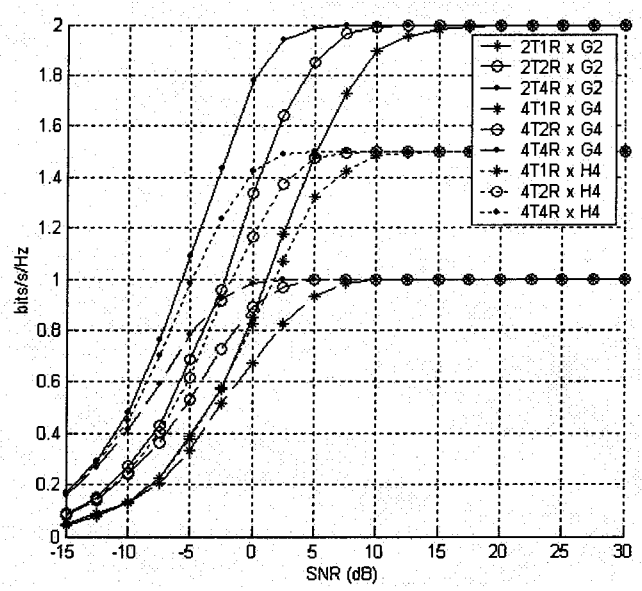

Fig.3.8 Capacity of 4-PSK with space-time block codes and Rayleigh fading.

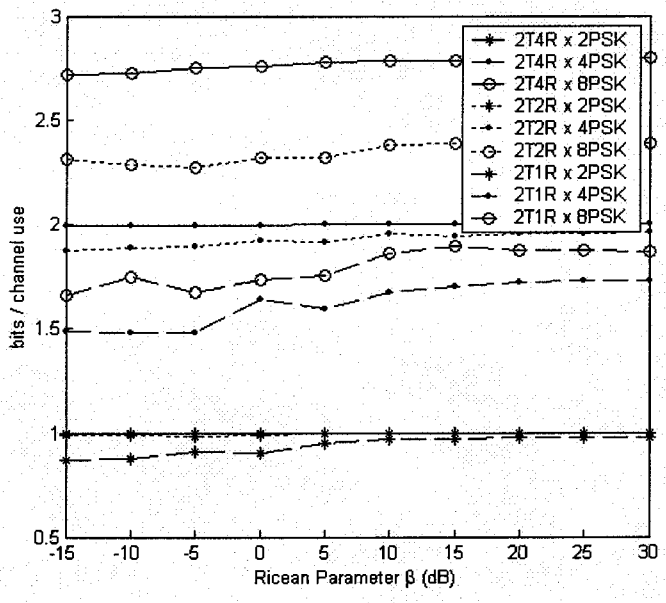

Fig.3.9 Capacity with OSTBC $\mathbf{G}_2$ versus the Ricean parameter ß, SNR=5 dB.

The capacity using several OSTBCs over a Rayleigh fading channel is given in Fig. 3.8. This shows that $\mathbf{G}_2$ is the optimal code from a capacity perspective, and $\mathbf{H}_4$ is more efficient than $\mathbf{G}_4$. Comparing Fig. 3.7 with Fig. 3.8 for the 4-PSK case, the system

achieves capacity at a lower SNR over a Ricean fading channel with ß=100 than over a Rayleigh fading channel. Fig. 3.9 shows the relationship between the Ricean parameter ß and capacity with $\mathbf{G_2}$. Note that the capacity is insensitive to the Ricean parameter when ß > 15 dB.

3.4 Error Probability of OSTBC over Uncorrelated Fading Channels

3.4.1 Error Probability with Rayleigh Fading

Let $P_q(\gamma_s)$ denote the error probability of a q-ary signal constellation with OSTBC in an AWGN channel. The error probability of OSTBC with Rayleigh fading can be obtained by averaging $P_q(\gamma_s)$ over the PDF of γ_s

$$P_{STBC,q} = \int_0^\infty P_q(\gamma_s) p_{rayleigh}(\gamma_s) d\gamma_s . \tag{3.24}$$

Note that $P_q(\gamma_s)$ could be symbol error probability (SEP) or bit error probability (BEP).

3.4.1.1 Probability of Error for PAM

Since full rate OSTBCs exist for any number of transmit antennas using a real PAM constellation [5], R=1 for q-ary PAM. The average SEP for PAM over AWGN is [45, Eq. 5.2-45]

$$P_q(\gamma_s) = 2\left(1-\frac{1}{q}\right)\mathbf{Q}\left(\sqrt{\frac{6}{q^2-1}\gamma_s}\right), \tag{3.25}$$

where **Q**(.) is the Gaussian tail function. Substituting (3.7) and (3.25) into (3.24), the average SEP of PAM with OSTBC is

$$P_{STBC,PAM,q} = \int_0^\infty 2\left(1-\frac{1}{q}\right)\mathbf{Q}\left(\sqrt{\frac{6}{q^2-1}\gamma_s}\right)\frac{1}{\bar{\gamma}_c^{\,MN}\Gamma(MN)}\gamma_s^{\,MN-1}e^{-\gamma_s/\bar{\gamma}_c}d\gamma_s. \qquad (3.26)$$

To evaluate the integral in (3.26), the following integral function can be employed

$$f(L) = \int_0^\infty Q\left(\sqrt{ax}\right)x^{L-1}e^{-x/u}dx = \frac{1}{2}u^L\Gamma(L)\left[1-\sum_{k=0}^{L-1}\mu\left(\frac{1-\mu^2}{4}\right)^k\binom{2k}{k}\right], \qquad (3.27)$$

where $\mu = \sqrt{\frac{au}{2+au}}$. The proof is given in Appendix I.

The closed-form symbol error probability for PAM with OSTBC is then

$$P_{STBC,PAM,q} = \left(1-\frac{1}{q}\right)\left[1-\sum_{k=0}^{MN-1}\mu\left(\frac{1-\mu^2}{4}\right)^k\binom{2k}{k}\right], \qquad (3.28)$$

where $\mu = \sqrt{\frac{3\bar{\gamma}_c}{q^2-1+3\bar{\gamma}_c}}$.

3.4.1.2 Probability of Error for PSK

Based on the equivalent scalar AWGN channel model presented in Section 3.1, the error probability for q-ary PSK with OSTBC is equivalent to the analysis in [13] [45] for adaptive reception of multiphase signals in Rayleigh fading but with *MN* branch diversity. This approach was also employed in [44]. Following the same steps as in [13], the symbol error probability is

$$P_{STBC,q}=\frac{(-1)^{MN-1}(1-\mu^2)^{MN}}{\pi\Gamma(MN)}\left(\frac{\partial^{MN-1}}{\partial s^{MN-1}}\left\{\frac{1}{s-\mu^2}\left[\frac{\pi}{M}(M-1)-\frac{\mu\sin(\pi/M)}{\sqrt{s-\mu^2\cos^2(\pi/M)}}\cot^{-1}\frac{-\mu\cos(\pi/M)}{\sqrt{s-\mu^2\cos^2(\pi/M)}}\right]\right\}\right)_{s=1},$$

(3.29)

where $\mu=\sqrt{\frac{\bar{\gamma}_c}{1+\bar{\gamma}_c}}$ and the notation $\frac{\partial^{MN-1}}{\partial s^{MN-1}}f(s,\mu)\big|_{s=1}$ denotes the (MN-1)th partial derivative of the function $f(s,\mu)$ evaluated at s = 1. Note that coherent detection with perfect channel state information at the receiver is assumed in (3.29).

Following the approach in [13][45], performing the differentiation indicated in (3.29) and evaluating the resulting function at s = 1 for q = 2 and 4, we obtain the following closed-form bit error probabilities for BPSK and QPSK

$$P_{STBC,2}=\frac{1}{2}\left[1-\mu\sum_{k=0}^{MN-1}\binom{2k}{k}\left(\frac{1-\mu^2}{4}\right)^k\right], \tag{3.30}$$

and

$$P_{STBC,4}=\frac{1}{2}\left[1-\frac{\mu}{\sqrt{2-\mu^2}}\sum_{k=0}^{MN-1}\binom{2k}{k}\left(\frac{1+\mu^2}{4-2\mu^2}\right)^k\right], \tag{3.31}$$

respectively. Note that Gray coding was assumed in the bit error probability calculation for QPSK.

The same procedure can be applied to calculate the SEP for q-ary PSK with q = 8, 16, 32, etc., however the expressions are not as simple as in (3.30) and (3.31). In the reminder of this section, we employ (3.24) in order to derive a simpler expression for the error probability.

It is well known [45] that the BEP of BPSK and QPSK over an AWGN channel are

$$P_{qb}(\gamma_s) = \mathbf{Q}\left(\sqrt{2\gamma_s}\right), \tag{3.32}$$

and

$$P_{qb}(\gamma_s) = \mathbf{Q}\left(\sqrt{\gamma_s}\right), \tag{3.33}$$

respectively. From [94], the exact symbol error probability of M-ary PSK for AWGN channel is

$$P_{PSK,AWGN,M}(\gamma_s) = 2\mathbf{Q}\left(\sqrt{2\gamma_s}\sin\frac{\pi}{q}\right) - \frac{1}{\pi}\int_{\frac{\pi}{2}-\frac{\pi}{q}}^{\frac{\pi}{2}} e^{-\gamma_s \frac{\sin^2 \pi/q}{\cos^2\theta}} d\theta\,. \tag{3.34}$$

For large SNR and large values of q, the SEP of q-ary PSK in an AWGN channel can be approximated as

$$P_q(\gamma_s) \approx 2\mathbf{Q}\left(\sqrt{2\gamma_s}\sin\frac{\pi}{q}\right), \tag{3.35}$$

and the equivalent BEP is

$$P_{qb} \approx \frac{1}{\log q} P_q\,, \tag{3.36}$$

where Gray coding is assumed. This approximation is good for large values of q, however for q=2 there is factor of 2 difference with the exact probability given in (3.30).

By substituting for $P_q(\gamma_s)$ in (3.35) and using (3.27), (3.24) can be written as

$$P_{STBC,PSK,q} \approx \int_0^\infty 2Q\left(\sqrt{2\gamma_s}\sin\frac{\pi}{q}\right)\frac{1}{\bar{\gamma}_c^{MN}\Gamma(MN)}\gamma_s^{MN-1}e^{-\gamma_s/\bar{\gamma}_c}d\gamma_s$$
$$= 1-\sum_{k=0}^{MN-1}\mu\left(\frac{1-\mu^2}{4}\right)^k\binom{2k}{k} \quad , \tag{3.37}$$

where

$$\mu = \sqrt{\frac{\sin^2\frac{\pi}{q}\bar{\gamma}_c}{1+\sin^2\frac{\pi}{q}\bar{\gamma}_c}}. \tag{3.38}$$

Therefore, the BEP can be approximated as

$$P_{STBC,PSK,qb} \approx \frac{1}{\log q}\left(1-\sum_{k=0}^{MN-1}\mu\left(\frac{1-\mu^2}{4}\right)^k\binom{2k}{k}\right). \tag{3.39}$$

By substituting for $P_q(\gamma_s)$ in (3.32) and (3.33), and using (3.27), the exact bit error probability for BPSK and QPSK can be derived from (3.24) as

$$P_{STBC,PSK,qb} = \frac{1}{2}\left(1-\sum_{k=0}^{MN-1}\mu\left(\frac{1-\mu^2}{4}\right)^k\binom{2k}{k}\right), \tag{3.40}$$

where $\mu = \sqrt{\frac{\bar{\gamma}_c}{1+\bar{\gamma}_c}}$ and $\mu = \sqrt{\frac{\bar{\gamma}_c}{2+\bar{\gamma}_c}}$ for BPSK and QPSK, respectively. It can easily be shown that (3.40) is equivalent to (3.30) and (3.31).

Using (3.39), approximations for the bit error probabilities of BPSK and QPSK can be obtained as

$$P_{STBC,2b} \approx 1-\sum_{k=0}^{MN-1}\mu\left(\frac{1-\mu^2}{4}\right)^k\binom{2k}{k}, \quad \mu = \sqrt{\frac{\bar{\gamma}_c}{1+\bar{\gamma}_c}} \tag{3.41}$$

and

$$P_{STBC,4b} \approx \frac{1}{2}\left(1-\sum_{k=0}^{MN-1}\mu\left(\frac{1-\mu^2}{4}\right)^k\binom{2k}{k}\right), \quad \mu=\sqrt{\frac{\bar{\gamma}_c}{2+\bar{\gamma}_c}} \tag{3.42}$$

respectively. As expected, this approximation is unsuitable for BPSK, but (3.42) gives the exact BEP for QPSK. It is shown later that this approximation is very accurate for q>4 and large SNR.

3.4.1.3 Probability of Error for QAM

Rectangular QAM signal constellations are frequently employed because they are equivalent to two PAM signals on quadrature carriers. For q-ary, $q=2^k$ (k even), rectangular QAM, the symbol error probability is given in [45] as

$$P_q = 1-\left(1-P_{\sqrt{q}}\right)^2, \tag{3.43}$$

where

$$P_{\sqrt{q}} = 2\left(1-\frac{1}{\sqrt{q}}\right)Q\left(\sqrt{\frac{3}{q-1}\gamma_s}\right). \tag{3.44}$$

By substituting for $P_q(\gamma_s)$ in (3.44), (3.24) can be written as

$$P_{STBC,PAM,\sqrt{q}} = \int_0^\infty 2\left(1-\frac{1}{\sqrt{q}}\right)Q\left(\sqrt{\frac{3}{q-1}\gamma_s}\right)\frac{1}{\bar{\gamma}_c{}^{MN}\Gamma(MN)}\gamma_s{}^{MN-1}e^{-\gamma_s/\bar{\gamma}_c}d\gamma_s. \tag{3.45}$$

Using (3.27), the closed-form symbol error probability for rectangular q-ary QAM with OSTBC is then

$$P_{STBC,QAM,q} = 1-\left(1-P_{STBC,PAM,\sqrt{q}}\right)^2, \tag{3.46}$$

where

$$P_{STBC,PAM,\sqrt{q}} = \left(1-\frac{1}{\sqrt{q}}\right)\left[1-\sum_{k=0}^{MN-1}\mu\left(\frac{1-\mu^2}{4}\right)^k\binom{2k}{k}\right], \tag{3.47}$$

and $\mu = \sqrt{\dfrac{3\bar{\gamma}_c}{2q-2+3\bar{\gamma}_c}}$.

3.4.2 Error Probability Over Ricean Fading

Substituting $p_{ricean}(\gamma_s)$ for $p_{rayleigh}(\gamma_s)$ in (3.24), and following the same procedure used previously, the SEP for OSTBC over a Ricean fading channel is

$$P_{STBC,Ricean,q} = \sum_{n=0}^{\infty}\frac{(MN\beta)^n e^{-MN\beta}}{\Gamma(n+1)}\lambda\left[1-\sum_{i=0}^{MN+n-1}\mu\left(\frac{1-\mu^2}{4}\right)^i\binom{2i}{i}\right], \tag{3.48}$$

where

$$\mu = \sqrt{\frac{3\bar{\gamma}_c}{q^2-1+3\bar{\gamma}_c}} \quad \text{and} \quad \lambda = \left(1-\frac{1}{q}\right), \tag{3.49}$$

for q-ary PAM,

$$\mu = \sqrt{\frac{\sin^2\dfrac{\pi}{q}\bar{\gamma}_c}{1+\sin^2\dfrac{\pi}{q}\bar{\gamma}_c}} \quad \text{and with} \quad \lambda = \frac{1}{2} \text{ for } q=2 \text{ and } \lambda = 1 \text{ for } q>2, \tag{3.50}$$

for q-ary PSK, and

$$\mu = \sqrt{\frac{3\bar{\gamma}_c}{2q-2+3\bar{\gamma}_c}} \text{ and } \lambda = \left(1-\frac{1}{\sqrt{q}}\right), \tag{3.51}$$

for $\sqrt{q}$ -ary PAM in q-ary rectangular QAM. The symbol error probability of q-ary rectangular QAM can then be calculated using (3.46).

3.4.3 Error Probability with Nakagami-m Fading

As in Section 3.2.3, the error probability over Nakagami-*m* fading, *m* is an integer, can be obtained from the results in Section 3.4.1 above by increasing the diversity order from *MN* to *mMN*. The SEP for OSTBC over Nakagami-*m* fading channel is then

$$P_{STBC,Nakagami,q}(\gamma_s) = \lambda\left[1-\sum_{k=0}^{mMN-1}\mu\left(\frac{1-\mu^2}{4}\right)^k\binom{2k}{k}\right], \tag{3.52}$$

where, for q-ary PAM

$$\mu = \sqrt{\frac{3\bar{\gamma}_c}{q^2-1+3\bar{\gamma}_c}} \text{ and } \lambda = \left(1-\frac{1}{q}\right); \tag{3.53}$$

for q-ary PSK

$$\mu = \sqrt{\frac{\sin^2\frac{\pi}{q}\bar{\gamma}_c}{1+\sin^2\frac{\pi}{q}\bar{\gamma}_c}} \text{ and with } \lambda = \frac{1}{2} \text{ for } q=2 \text{ and } \lambda = 1 \text{ for } q>2; \tag{3.54}$$

for $\sqrt{q}$ -ary PAM in q-ary rectangle QAM

$$\mu = \sqrt{\frac{3\bar{\gamma}_c}{2q-2+3\bar{\gamma}_c}} \text{ and } \lambda = \left(1-\frac{1}{\sqrt{q}}\right). \tag{3.55}$$

The SEP of q-ary rectangle QAM can then be calculated from (3.46).

3.4.4 Numerical Results

Simulation results are presented to verify the exact and approximate error probabilities given in above sections. In Fig. 3.10, the bit error probability of BPSK with OSTBC $\mathbf{G}_2$ and 1 to 4 receive antennas in Rayleigh fading is shown. These results are identical to those obtained with (3.30). It is shown that more diversity gain can be obtained with more receive antennas. However the incremental gain decreases as the total number of antennas increases.

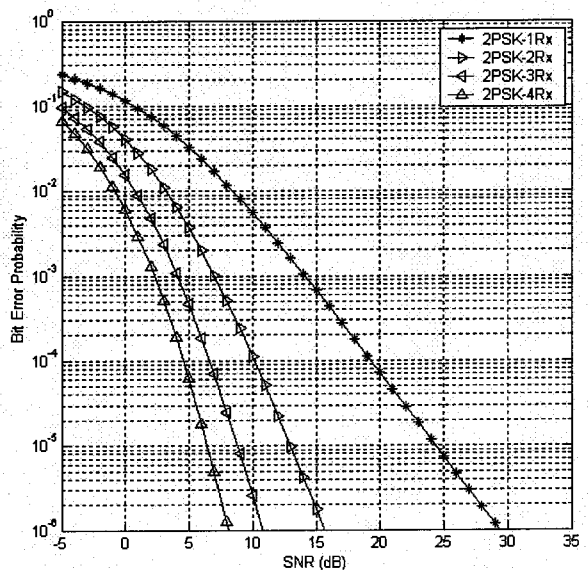

Fig.3.10 BEP of BPSK for OSTBC with two transmit antennas and Rayleigh fading.

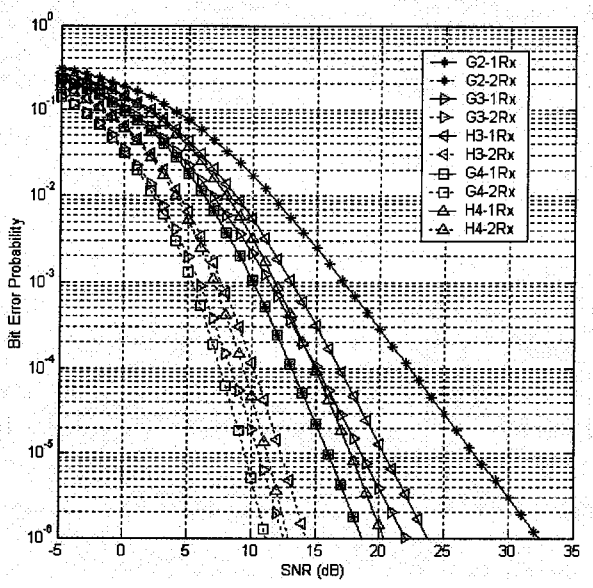

Fig.3.11 BEP of QPSK for OSTBC with one and two receive antennas and Rayleigh fading.

In Fig. 3.11, the bit error probability of QPSK with OSTBCs $\mathbf{G_2}$, $\mathbf{G_3}$, $\mathbf{G_4}$, $\mathbf{H_3}$, and $\mathbf{H_4}$ with one and two receive antennas are presented, and these results are identical to those

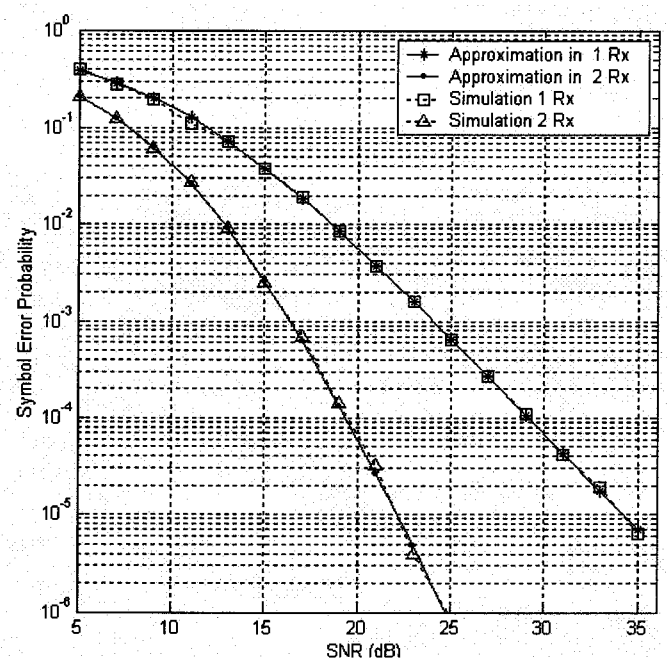

Fig.3.12 SEP of 8-PSK for OSTBC G_2 with one and two receive antennas.

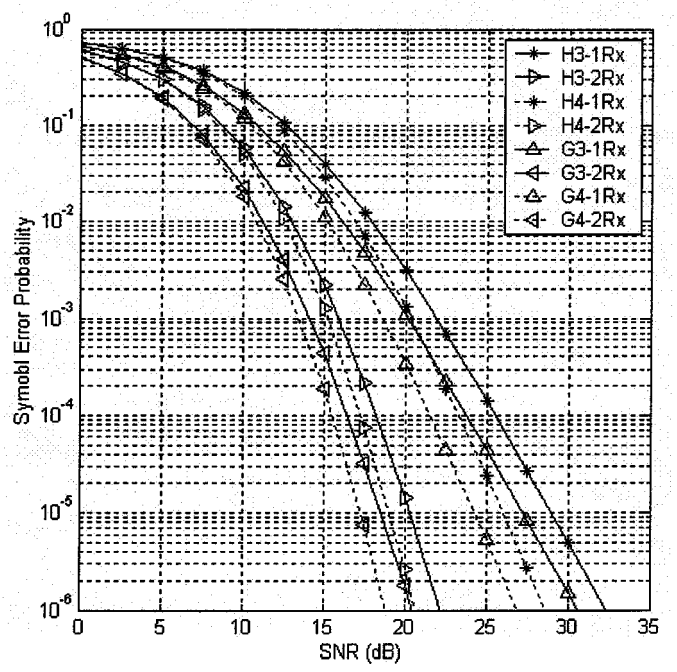

Fig.3.13 SEP of 16-QAM for OSTBC with1 and 2 receive antennas and Rayleigh fading.

obtained using (3.31). Note that $\mathbf{G_4}$ has the best performance compared with other OSTBCs, however, this performance advantage is obtained at the price of code rate. We can further observe that OSTBCs with the same diversity order, i.e. the product of the number of transmit and receive antenna, have the same slop of the performance curve. As a special case, $\mathbf{G_4}$ with one receive antenna and $\mathbf{G_2}$ with two receive antennas have the exact same BEP resulting from the same product of N×R and total channel numbers. Fig. 3.12 shows the comparison between the approximated and simulation symbol error probability for 8-PSK with $\boldsymbol{G_2}$ code. Note that the approximation error is negligible. Fig.3.13 shows the symbol error probability for 16 QAM with one and two receive antennas for different OSTBCs. These results are identical to those obtained with

(3.25).

3.5 Extension to OSTBC DS-CDMA

The growing demand for high-rate data services over wireless channels motivates the design of multiple antenna wireless systems to transmit increased data rates without substantial bandwidth expansion. As a part of the UTRA (Universal Terrestrial Radio Access) FDD (Frequency Division Duplex) standard, OSTBC has been proposed for use in the downlink of Direct Sequence Code Division Multiple Access (DS-CDMA) systems to provide transmit diversity. Significant research has been conducted on OSTBC for DS-CDMA. There is great interest in analyzing the capacity and error probability due to the application of OSTBCs to practical wireless systems like DS-CDMA. In this section, we extend the equivalent SISO channel model obtained in Section 3.1 to a OSTBC DS-CDMA downlink. The capacity and error probability analysis are then presented.

3.5.1 System Model

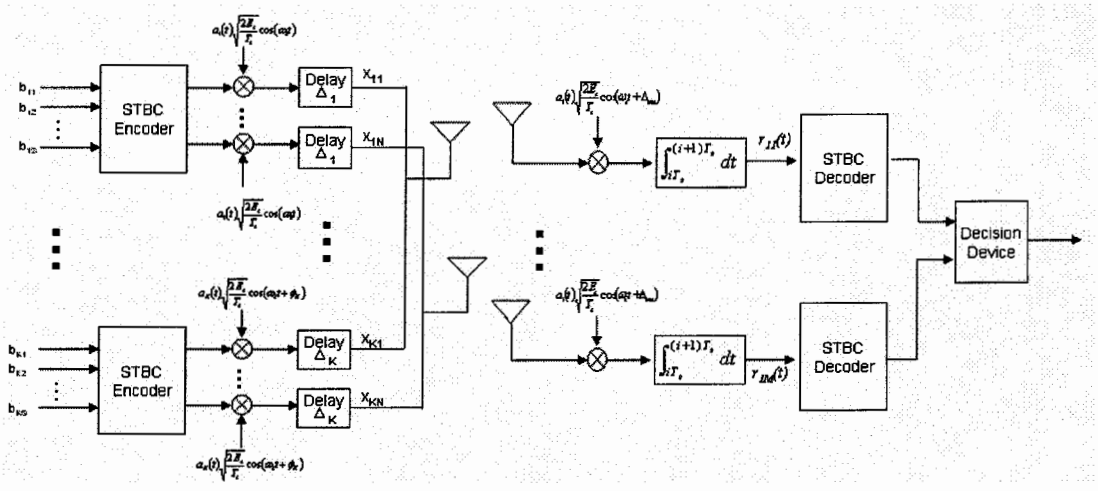

Fig.3.14 System model of OSTBC DS-CDMA.

To facilitate analysis, we generalize the CDMA multiple access interference model from [95][96] to accommodate multiple antennas. The system model is illustrated in Fig. 3.14. In the transmitter, s information symbols for K users are encoded by the respective OSTBC encoders, and then spread by each user's PN code, modulated and transmitted simultaneously from N transmit antennas over T symbol durations. At the receivers, each user has M receive antennas, and the filtered signals are first despread, then sent to OSTBC decoders. The symbol decisions are made based on the M OSTBC decoder outputs. The signal at the jth receive antenna is given by

$$r_j(t)=\sum_{n=1}^{N}\sum_{k=1}^{K}\sqrt{2P_k}\,h_{knj}(t)a_k(t-\tau_{knj})b_{nk}(t-\tau_{knj})\cos\left(\omega_c(t-\tau_{knj})\right)+n(t), \qquad (3.56)$$

where $h_{knj}(t)$ is the channel coefficient from the nth transmit antenna to the jth receive antenna for kth user, $P_k=E_s/T_s$, is the symbol power of the kth user, E_s is the

symbol energy, T_s is the symbol duration, and $a_k(t)$ is the pseudo noise (PN) spreading chip sequence with chip duration T_c, $n(t)$ is zero mean AWGN with power spectral density $N_o/2$ in each real dimension, τ_{knj} is the time delay from the nth transmit antenna to the jth receive antenna, ω_c is the carrier frequency and $b_{nk}(t)$ is the encoded signal transmitted from the nth antenna of user k. Binary modulation is assumed in this model.

3.5.2 Channel Model Analysis

To facilitate the analysis, we assume the first user is the desired one (without loss of generality). The despread signal input to the jth OSTBC decoder for the ith received symbol is

$$\begin{aligned}
\hat{r}_{1j} &= \sum_{q=1}^{N} \int_{(i-1)T_s}^{iT_s} \left[\sqrt{2P_k} \sum_{n=1}^{N} \sum_{k=1}^{K} h_{knj}(t) a_k(t-\tau_{knj}) b_{nk}(t-\tau_{knj}) \cos\left(\omega_c (t-\tau_{knj})\right) + n(t) \right] a_1(t-\tau_{1qj}) \cos\left(\omega_c (t-\tau_{1nj})\right) dt \\
&= \sqrt{\frac{P_1}{2}} T_s \sum_{n=1}^{N} h_{1nj}^{(i)} b_{n1}^{(i)} \\
&+ \int_{(i-1)T_s}^{iT_s} \left[\sqrt{2P_k} \sum_{n=1}^{N} \sum_{\substack{q=1 \\ q \neq n}}^{N} h_{1nj}(t) a_1(t-\tau_{1nj}) b_{n1}(t-\tau_{1nj}) \cos\left(\omega_c (t-\tau_{1nj})\right) \right] a_1(t-\tau_{1qj}) \cos\left(\omega_c (t-\tau_{1nj})\right) dt \\
&+ \int_{(i-1)T_s}^{iT_s} \left[\sqrt{2P_k} \sum_{n=1}^{N} \sum_{k=2}^{K} \sum_{\substack{q=1 \\ q \neq n}}^{N} h_{knj}(t) a_k(t-\tau_{knj}) b_{nk}(t-\tau_{knj}) \cos\left(\omega_c (t-\tau_{knj})\right) \right] a_1(t-\tau_{1qj}) \cos\left(\omega_c (t-\tau_{1nj})\right) dt \\
&+ \sum_{q=1}^{N} \int_{(i-1)T_s}^{iT_s} n(t) a_1(t-\tau_{1qj}) \cos\left(\omega_c (t-\tau_{1nj})\right) dt
\end{aligned} \tag{3.57}$$

Note that only the first part of (3.57) is the desired signal, the remainder consist of the multiple access interference (MAI) produced by the same user from different transmit antennas, the MAI produced by other users, and the AWGN. Using the Gaussian

approximation in [95][96], (3.57) can be written as

$$\hat{r}_{1j} = \sqrt{\frac{P_1}{2}} T_s \sum_{n=1}^{N} h_{1nj} b_{n1} + \eta_{1j}, \tag{3.58}$$

where $\hat{r}_{1j}$ is a Gaussian random variable, and η_{1j} denotes the combination of interferences and noise. The expected value and variance of η_{1j} are

$$E[\eta_{1j}] = 0, \tag{3.59}$$

and

$$\mathbf{Var}[\eta_{1j}] = N(N-1)\frac{T_s^{\,2}}{6G}\sum_{k=1}^{K} P_k + \frac{NN_0T_s}{4}, \tag{3.60}$$

respectively, where G is the processing gain of the CDMA system. Note that (3.58) has the same form as (3.4). After OSTBC decoding is performed on $\hat{r}_{1j}$ given in (3.58), the decision statistic for user 1 over T symbol durations is

$$\hat{\mathbf{r}}_{1T} = \frac{1}{R}\sqrt{\frac{P_1}{2}} T_s \|\mathbf{H}\|_F^2 \mathbf{b}_{1T} + \eta_T, \tag{3.61}$$

where η_{iT} has zero mean and variance $\frac{1}{R}\|\mathbf{H}\|_F^2\left(N(N-1)\frac{T_s^{\,2}}{6G}\sum_{k=1}^{K} P_k + \frac{NN_0T_s}{4}\right)$.

Therefore, the effective instantaneous SNR γ_s at the receiver is

$$\gamma_s = \frac{1}{\frac{N(N-1)K}{3G} + \frac{N}{2E_s/N_0}} \frac{1}{R}\|\mathbf{H}\|_F^2. \tag{3.62}$$

Note that perfect power control is assumed in (3.62), i.e. P_k=P_1.

3.5.3 Capacity Analysis of OSTBC-CDMA

To facilitate the capacity analysis, we first normalize the equivalent channel by $\sqrt{T_s/2}$, then (3.61) can be written in the same form as (3.2)

$$\mathbf{y}_{nT} = \frac{1}{R}\|\mathbf{H}\|_F^2 \mathbf{x}_{nT} + ?_{nT}, \tag{3.63}$$

where $\mathbf{x}_{nT}$ is the input $s \times 1$ complex input matrix with each entry having symbol energy E_s, and $?_{nT}$ has zero mean and variance $\frac{1}{R}\|\mathbf{H}\|_F^2\left(N(N-1)K\frac{E_s}{3G}+\frac{NN_0}{2}\right)$.

The capacity of this OSTBC CDMA system employing a q-ary signal constellation can be obtained directly from (3.17).

3.5.4 Error Probability of OSTBC-CDMA

The average SNR per channel $\bar{\gamma}_c$ is

$$\bar{\gamma}_c = \frac{1}{\frac{N(N-1)K}{3G}+\frac{N}{2E_s/N_0}}\frac{1}{R}\mathrm{E}\left[\|h_{ij}\|^2\right] = \frac{1}{\frac{N(N-1)K}{3G}+\frac{N}{2E_s/N_0}}\frac{1}{R}2\sigma^2, \tag{3.64}$$

and this can be used with the error probability results in Section IV to obtain the performance in fading channels. In particular, the exact BEP of BPSK is given by

$$P_{STBC\_CDMA,Rayleigh,2b} = \frac{1}{2}\left[1-\sum_{k=0}^{MN-1}\mu\left(\frac{1-\mu^2}{4}\right)^k\binom{2k}{k}\right] \tag{3.65}$$

for Rayleigh fading,

$$P_{STBC\_CDMA,Ricean,2b} = \sum_{n=0}^{\infty} \frac{1}{2} \frac{(MN\beta)^n e^{-MN\beta}}{\Gamma(n+1)} \lambda \left[1 - \sum_{i=0}^{MN+n-1} \mu \left(\frac{1-\mu^2}{4} \right)^i \binom{2i}{i} \right] \tag{3.66}$$

for Ricean fading, and

$$P_{STBC,Nakagami,q}(\gamma_s) = \frac{1}{2} \lambda \left[1 - \sum_{k=0}^{mMN-1} \mu \left(\frac{1-\mu^2}{4} \right)^k \binom{2k}{k} \right] \tag{3.67}$$

for Nakagami-*m* fading, where $\mu = \sqrt{\frac{\bar{\gamma}_c}{1+\bar{\gamma}_c}}$, $\bar{\gamma}_c$ is given above in (3.64) and λ is defined as same as single user case. Note that there are two factors in $\bar{\gamma}_c$ which determine the BEP of the system, $\frac{N(N-1)K}{3G}$ and $\frac{N}{2E_s/N_0}$. The first term corresponds to the MAI from other users and the self-interference from different transmit antennas. The second term corresponds to the system noise (AWGN). Note that for large SNR, $\bar{\gamma}_c$ will be dominated by the MAI, i.e., the number of users limits the performance, as expected.

3.5.5 Numerical Results

In Fig. 3.15, the capacity of DS-CDMA with several OSTBCs is shown for BPSK modulation over a Rayleigh fading channel. It is shown that with given number of users and process gain, the system may not be able to achieve full channel capacity even with sufficient SNR due to the dominant MAI component. In this case, increasing the number of antennas will increase the system achievable capacity. Note that the capacity increases significantly as the number of receive antennas increases for the given

number of users and processing gain as expected. However, it should be noted that if the system already

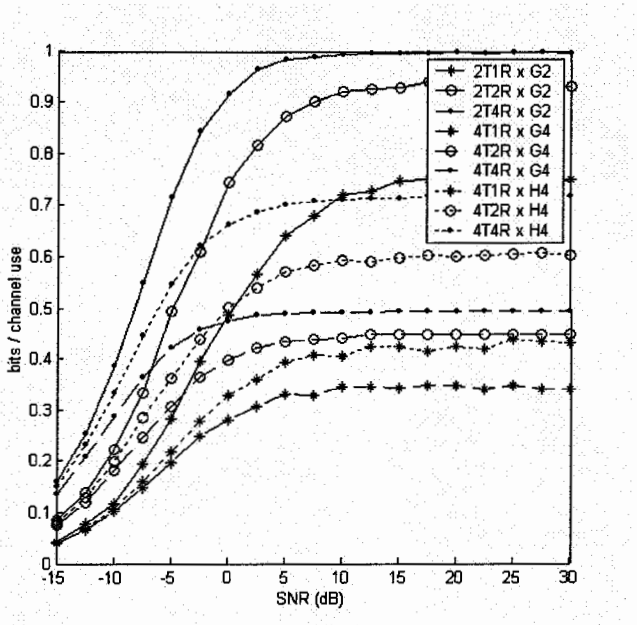

Fig.3.15 Capacity of DS-CDMA with BPSK, OSTBC and Rayleigh fading, G=32, K=30.

can achieve full channel capacity with certain number of antennas, users, and process gain, further increasing the number of antennas will not increase the system capacity anymore.

Fig. 3.16 shows the relationship between the system capacity and the number of users given the processing gain and SNR over Rayleigh fading. Note that the capacity decreases rapidly as the number of users increases with 1 and 2 receive antennas. However, with 4 receive antennas, increasing the number of users has much less effect on capacity.

The BEP of OSTBC $\mathbf{G_2}$ with DS-CDMA and BPSK is given in Fig. 3.17 for 1, 2, 3 and 4

receive antennas. The processing gain is 64 and the number of user is 20. This shows that significant performance gains can be obtained with multiple receive antennas.

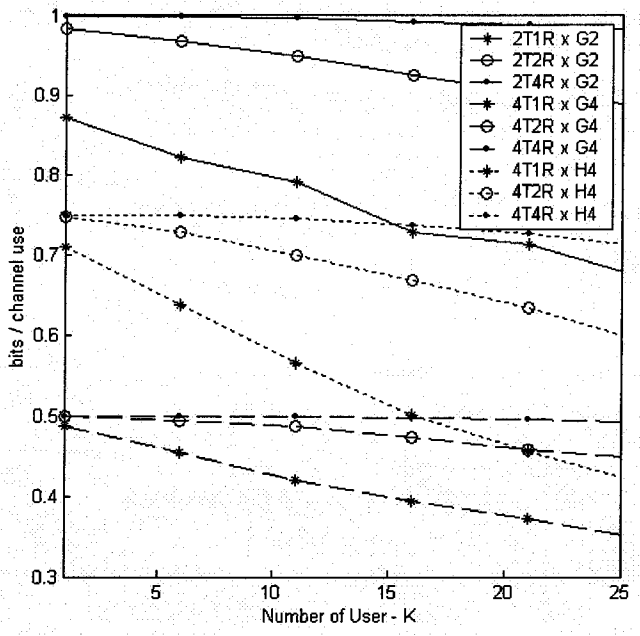

Fig.3.16 Capacity of DS-CDMA with BPSK, OSTBC and Rayleigh fading, G=32, SNR=7 dB.

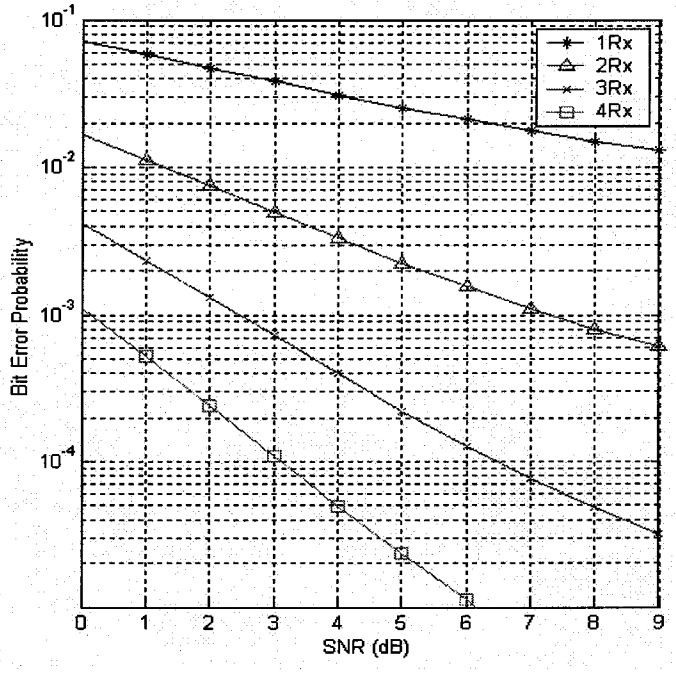

Fig.3.17 Bit error probability of DS-CDMA with BPSK, OSTBC $\mathbf{G}_2$ and Rayleigh fading, G=64,

K=20.

Fig. 3.18 shows the relationship between the BEP and the number of users in the system at a SNR of 7 dB with $\mathbf{G_4}$ and $\mathbf{G_2}$. As the number of users increases, the performance degrades, but with 4 receive antennas the system is capable of accommodating far more users than with 1 receive antenna. As shown in the figure, $\mathbf{G_4}$ provides better performance than $\mathbf{G_2}$, however, this is obtained at the price of a capacity loss as shown in Fig. 3.15.

Note that Rayleigh fading is employed for all DS-CDMA figures.

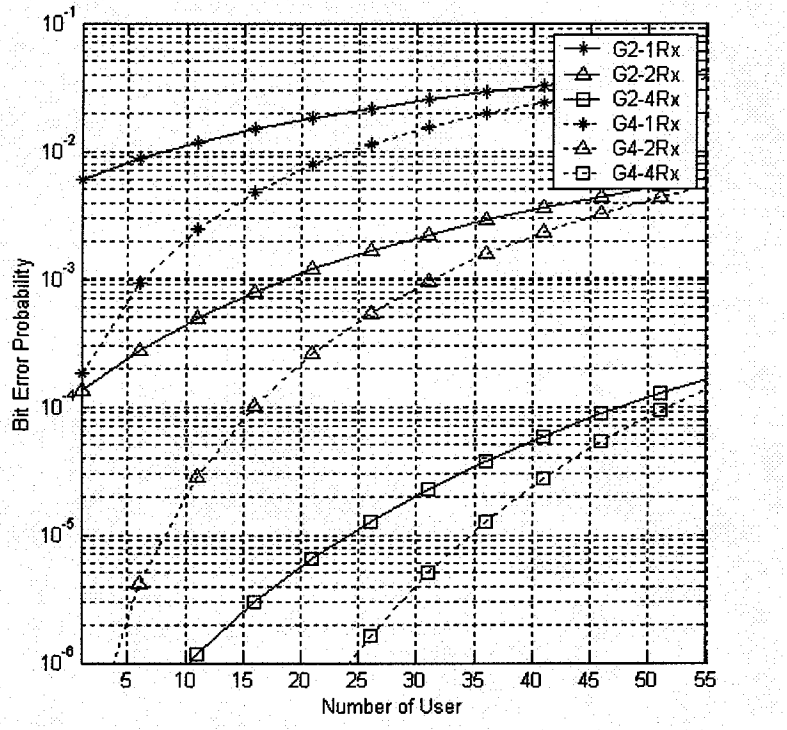

Fig.3.18 Bit error probability versus the number of users for DS-CDMA with BPSK, OSTBC $\mathbf{G_2}$ and $\mathbf{G_4}$ over Rayleigh fading, G=64, SNR=7dB.

3.6 Error Probability of Ricean Fading Channels

As shown in Section 3.4, the error probability for q-ary modulated OSTBC over Ricean fading channel given by (3.48) is a closed-form infinite series expression. However, in this section, we are going to show that the series converges fairly fast and can be evaluated efficiently with control accuracy.

After several simple manipulations, we can write (3.48) as

$$P_{Ricean,M} = \lambda\left[1-\sum_{i=0}^{L-1}\mu\left(\frac{1-\mu^2}{4}\right)^i\binom{2i}{i}\right] - \lambda\sum_{i=0}^{\infty}\mu\left(\frac{1-\mu^2}{4}\right)^{L+i}\binom{2(L+i)}{L+i}\left[1-\sum_{n=0}^{i}\frac{(L\beta)^n e^{-LK}}{\Gamma(n+1)}\right], \quad (3.68)$$

where L is defined as the product of M and N.

As a special case, for Rayleigh fading channel, i.e. ß=0, only first term of (3.68) remains, therefore the closed-form symbol error probability of M-ary linear modulation over Rayleigh fading is obtained as

$$P_{Rayleigh,M} = \lambda\left[1-\sum_{i=0}^{L-1}\mu\left(\frac{1-\mu^2}{4}\right)^i\binom{2i}{i}\right], \quad (3.69)$$

where μ and λ are the same as in (3.68) for different modulation schemes, which corresponding to the results obtained in Section 3.4.1.

Note that each term in the second part of (3.68) is a monotonically decreasing function of i, and is strictly smaller than 1 for all i. Thus truncation to the first N terms will

introduce an error of at most $\lambda\mu\frac{\left(1-\mu^2\right)^{L+N}}{\mu}\left[1-\sum_{n=0}^{N}\frac{(L\beta)^n e^{-LK}}{\Gamma(n+1)}\right]$ in the error probability. The proof is given in Appendix II. Thus the error probability can be evaluated with

Table 3.1 Values of N for the error probability in flat Ricean fading channels with an error less than 10^{-9}, L=1.

N		β=0	β=0 dB	β=5 dB	β=10 dB	β=20 dB
16-QAM	SNR=-10 dB	0	12	20	37	173
	SNR=0 dB	0	12	19	35	171
	SNR=10 dB	0	10	17	33	166
Q-PSK	SNR=-10 dB	0	12	20	36	172
	SNR=0 dB	0	11	18	34	169
	SNR=10 dB	0	7	13	26	153

controlled accuracy. Table 3.1 shows the values of N for different Ricean parameters K and SNR such that for 16QAM and QPSK the approximation error is less than 10^{-9} compared with the exact error probability.

As we stated earlier, the equivalent SISO channel model has many of the same attributes as maximum ratio combining (MRC) multiple channel reception, which enables the direct application of the results obtained here to MRC by interpreting L as the number of receive channel. Exact expressions for bit and symbol error probabilities are derived in [94] for frequency-flat Rayleigh and Ricean fading channels for MRC multiple channel reception, however the results involve several versions of a single integral which have to be evaluated by numerical methods. More recently, [97]

developed a recursive solution for the error probability performance of multichannel M-PSK reception in frequency-selective Ricean fading channels. [98] extends the error rate analysis in [97] to coherent linear modulation systems over flat Ricean fading channels, and specific results for rectangular M-ary QAM constellations are presented. The series representations obtained above have a simpler form than the recursive solution given in [97][98].

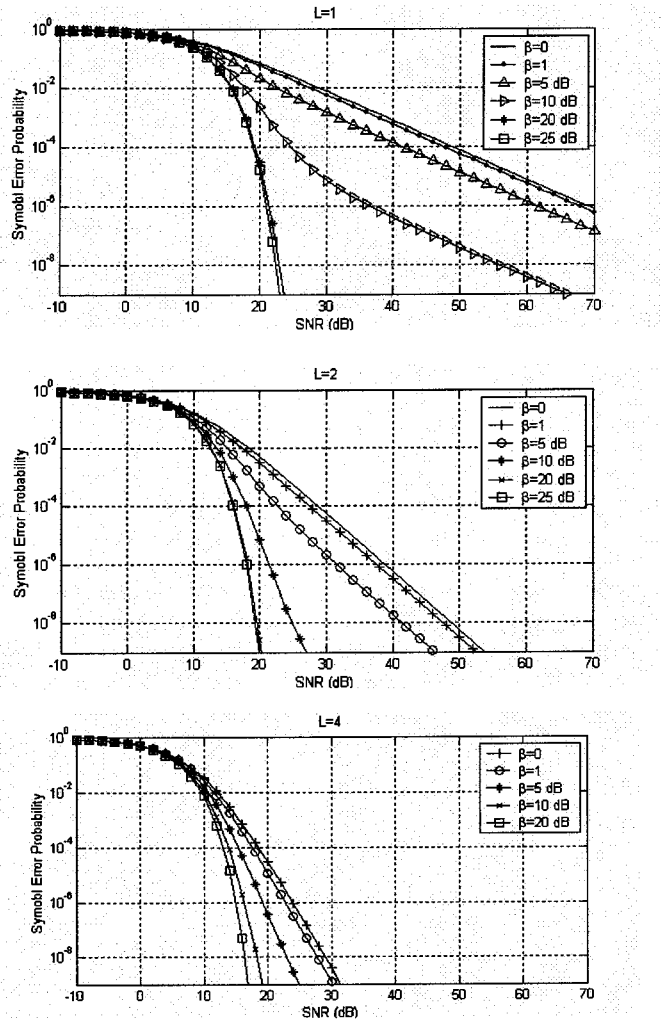

Fig.3.19 SEP of rectangular 16-QAM with different channel diversity orders and values of K over flat Ricean fading channels.

The series expansion can also be truncated to provide a desired level of accuracy. Since the terms in the series can be generated recursively, the computational complexity is also small compared to that required to perform the numerical integration in [94].

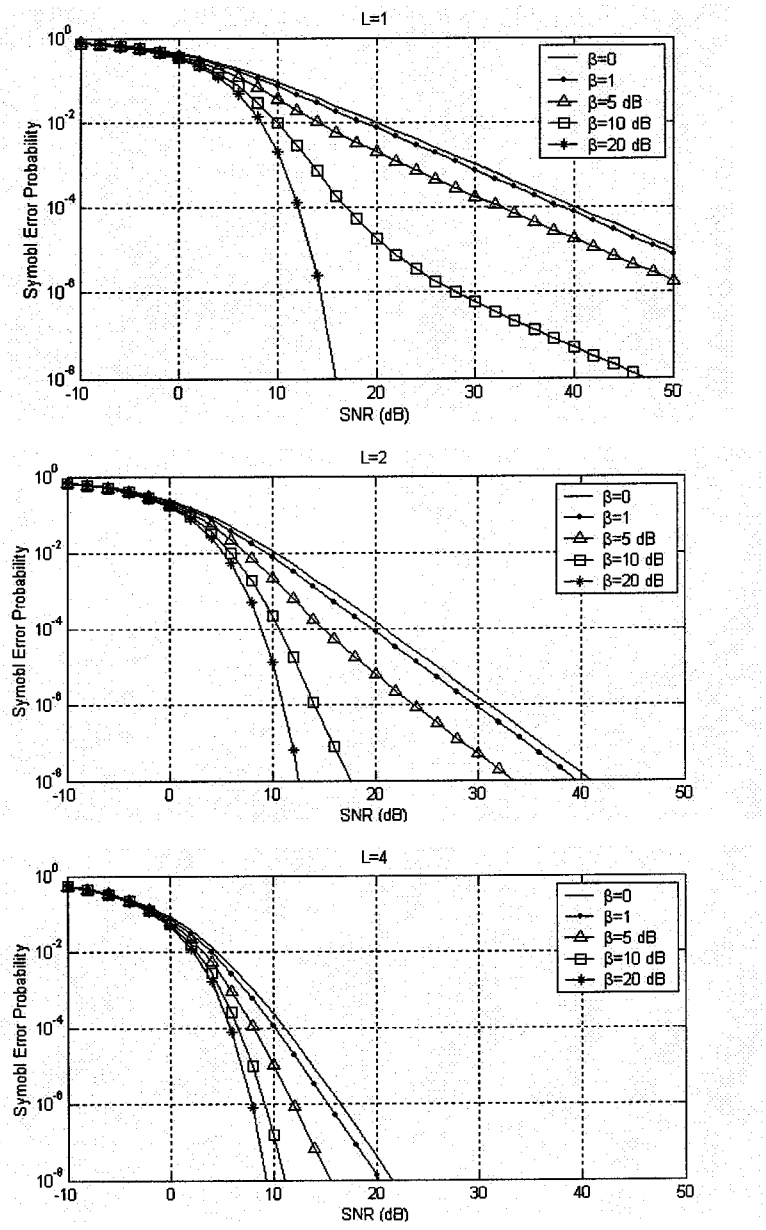

Fig.3.20 SEP of QPSK with different channel diversity orders and values of K over flat Ricean fading channels.

Fig. 3.19 shows the symbol error probability of rectangular 16-QAM over flat Ricean

fading channels with different Ricean parameters K and different orders of channel diversity. Fig. 3.20 shows the symbol error probability of QPSK over flat Ricean fading channel with different Ricean parameters K and different order of channel diversity. As expected, the larger the product of K and L, the larger the performance improvements obtained. Most of the potential diversity gains are obtained with a small number of channels. The figures also show that the performance approaches that of a Gaussian channel as the Ricean parameter increases, as expected. As shown in Fig. 3.19, the difference between K=20dB and 25dB is negligible, i.e. most of the potential performance improvements have been obtained once K = 20 dB.

3.7 Analysis over Correlated Fading Channels

Extensive analysis has been given above assuming uncorrelated MIMO channels. However, independent fading does not always occur in practice. In particular when we are dealing with a size limited mobile station, there may not be sufficient antenna spacing to obtain independent fading in each branch. In addition, the diversity channels in a practical system may have unbalanced average SNRs due to different noise figures or feeding lengths. Therefore, the close-form expressions obtained above may serve as the theoretic limits for a practically system, whose performance is also impacted by the channel correlation coefficients and the unbalanced parameter. In the remainder of this section, we address the issue of the impact of fading correlation on

the capacity and error probability of a MIMO OSTBC system. Starting from the simplest $\mathbf{G}_2$ case with one receive antenna, then extended to arbitrary number of antennas, closed form error probability expressions are obtained for PAM, PSK, and QAM for correlated balanced Rayleigh fading. The impact of correlation on the capacity is also illustrated. A unified approach to the error probability analysis of OSTBC with general branch correlation is presented for Ricean and Nakagami fading channels. However, the expressions are not always in closed form as for correlated balanced Rayleigh fading.

3.7.1 Error Probability of G2 over Unbalanced Correlated Rayleigh Fading Channels

To find the error probability of OSTBC **G2** over unbalanced correlated Rayleigh fading with one receive antenna, all we need to do is to find the pdf of the equivalent output SNR γ_s following the approach given in Section 3.4. For OSTBC **G2**, the pdf of γ_s can be expressed by [99]

$$p(\gamma_s) = \frac{\exp\left(-\frac{\gamma_s}{\Gamma_1}\right) - \exp\left(-\frac{\gamma_s}{\Gamma_2}\right)}{\Gamma_1 - \Gamma_2} \tag{3.70}$$

where

$$\Gamma_1 = \frac{1}{2}\left[\overline{\gamma}_{c1} + \overline{\gamma}_{c2} - \sqrt{\left(\overline{\gamma}_{c1} + \overline{\gamma}_{c2}\right)^2 - 4\overline{\gamma}_{c1}\overline{\gamma}_{c2}\left(1-\rho^2\right)}\right], \tag{3.71}$$

$$\Gamma_2 = \frac{1}{2}\left[\overline{\gamma}_{c1} + \overline{\gamma}_{c2} + \sqrt{\left(\overline{\gamma}_{c1} + \overline{\gamma}_{c2}\right)^2 - 4\overline{\gamma}_{c1}\overline{\gamma}_{c2}\left(1-\rho^2\right)}\right], \quad (3.72)$$

? is the correlation coefficient and $\overline{\gamma}_{c1}$ and $\overline{\gamma}_{c2}$ are the instantaneous SNRs for the two channels, respectively.

Substituting (3.70) into (3.24), and following the same approach as in Section 3.4, we can obtain the error probability expressions as follows

$$P_{STBC,CorrRayleigh,q}(\gamma_s) = \lambda \frac{\Gamma_1}{2(\Gamma_1 - \Gamma_2)}[1-\mu_1] - \lambda \frac{\Gamma_2}{2(\Gamma_1 - \Gamma_2)}[1-\mu_2], \quad (3.73)$$

where, for q-ary PAM,

$$\mu_1 = \sqrt{\frac{3\Gamma_1}{q^2 - 1 + 3\Gamma_1}}, \quad \mu_2 = \sqrt{\frac{3\Gamma_2}{q^2 - 1 + 3\Gamma_2}}, \text{ and } \lambda = \left(1 - \frac{1}{q}\right), \quad (3.74)$$

for q-ary PAM,

$$\mu_1 = \sqrt{\frac{\sin^2\frac{\pi}{q}\Gamma_1}{1+\sin^2\frac{\pi}{q}\Gamma_1}}, \quad \mu_2 = \sqrt{\frac{\sin^2\frac{\pi}{q}\Gamma_2}{1+\sin^2\frac{\pi}{q}\Gamma_2}}, \text{ and with } \lambda = \frac{1}{2} \text{ for } q=2 \text{ and } \lambda = 1 \text{ for } q>2, \quad (3.75)$$

for q-ary PSK, and

$$\mu_1 = \sqrt{\frac{3\Gamma_1}{2q-2+3\Gamma_1}}, \mu_2 = \sqrt{\frac{3\Gamma_2}{2q-2+3\Gamma_2}}, \text{ and } \lambda = \left(1 - \frac{1}{\sqrt{q}}\right), \quad (3.76)$$

for $\sqrt{q}$-ary PAM in q-ary rectangular QAM. The symbol error probability of q-ary rectangular QAM can then be calculated using (3.46).

Assuming we have two balanced fading channels, i.e. $\overline{\gamma}_{c1} = \overline{\gamma}_{c2}$, (3.70) can be simplified as

$$p(\gamma_s) = \frac{\exp\left(-\frac{\gamma_s}{(1+\rho)\overline{\gamma}_c}\right) - \exp\left(-\frac{\gamma_s}{(1-\rho)\overline{\gamma}_c}\right)}{2\rho\overline{\gamma}_c}, \tag{3.77}$$

and the above error probability expressions can be correspondingly simplified.

The application to DS-CDMA OSTBC is straight forward.

3.7.2 A Unified Approach of Error Probability Analysis over Correlated Fading Channels

Consider a OSTBC system with N transmit antennas and M receive antennas over correlated fading channels and assume the characteristic function of γ_s for Nakagami-m fading is given [100][102]

$$\Phi_{\gamma_s}(s) = \frac{1}{\left|I + \frac{1}{m} s D_{\overline{\gamma}_c} M_x\right|^m}, \tag{3.78}$$

where I is the identify matrix with size $MN \times MN$, $D_{\overline{\gamma}_c}$ are the diagonal matrices of size $MN \times MN$, and each diagonal element is the average instantaneous SNR of the corresponding MIMO channel, and M_x is the covariance matrix. The characteristic function of γ_s for Ricean fading is given [102][103] as

$$\Phi_{\gamma_s}(s)=\frac{\exp\left[-sD_{\bar{\gamma}_c}c^T\left(I+sD_{\bar{\gamma}_c}M_x\right)^{-1}c\right]}{\left|I+sD_{\bar{\gamma}_c}M_x\right|} \tag{3.79}$$

where $c=E\left[\mathrm{Re}[H]\right]=\left[c_{1,\cdots},c_{MN}\right]$. Note that the Ricean distributed channel gain is modeled as a complex Gaussian variable with nonzero mean for the real part and zero mean for the imaginary part. Obviously, (3.79) is very difficult to use in the performance analysis because of the existence of **c**.

To facilitate the error probability analysis, we first write the Gaussian tail function in the following form [49]

$$Q\left(\sqrt{ax}\right)=\frac{1}{\pi}\int_0^{\pi/2}\exp\left(-\frac{ax}{2\sin^2\phi}\right)d\phi. \tag{3.80}$$

Then we have

$$\begin{aligned}&\int_0^{\infty}Q\left(\sqrt{a\gamma_s}\right)p(\gamma_s)d\gamma_s\\&=\frac{1}{\pi}\int_0^{\infty}\int_0^{\pi/2}\exp\left(-\frac{a\gamma_s}{2\sin^2\phi}\right)p(\gamma_s)d\phi d\gamma_s.\\&=\frac{1}{\pi}\int_0^{\pi/2}\Phi_{\gamma_s}\left(\frac{a}{2\sin^2\phi}\right)d\phi\end{aligned} \tag{3.81}$$

Applying (3.80) and following the approach in Section 3.4, the error probabilities for Ricean and Nakagami fading channels with q-ary modulation can be obtained as

$$P_{STBC}=\frac{\lambda}{\pi}\int_0^{\pi/2}\Phi_{\gamma_s}\left(\frac{a}{2\sin^2\phi}\right)d\phi, \tag{3.82}$$

where for q-ary PSK $a=2\sin^2\frac{\pi}{q}$ and $\lambda=\frac{1}{2}$ for $q=2$ and $\lambda=1$ for $q>2$, for q-ary PAM, $a=\frac{6}{q^2-1}$ and $\lambda=2\left(1-\frac{1}{q}\right)$, for $\sqrt{q}$ -ary PAM in q-ary rectangular QAM, $a=\frac{3}{q-1}$ and $\lambda=2\left(1-\frac{1}{\sqrt{q}}\right)$, the error probability for q-ary rectangular QAM can then be calculated using (3.46).

(3.78) and (3.79) are obviously difficult to be simplified into closed form expressions, numerical integration is required to evaluate the error probability.

By further assuming balanced fading channels and a constant fading coefficient, i.e. $\overline{\gamma}_{c1}=\cdots=\overline{\gamma}_{c2}=\overline{\gamma}_c$ and $\rho_{ij}=\rho$ for i≠j, the characteristic function for Rayleigh fading can be obtained from either (3.78) by letting m=1 or (3.79) by letting **c**=0. The results from these two approaches coincide each other as

$$\Phi_{\gamma_s}(s)=\frac{1}{\left|I+s\overline{\gamma}_c M_x\right|}. \tag{3.83}$$

Since of the constant correlation, the eigenvalues are given by

$$\lambda_1=\sigma^2\left(1+(MN-1)\rho\right) \text{ and } \lambda_k=\sigma^2(1-\rho) \text{ for k=2,3,...,MN.} \tag{3.84}$$

(3.83) can be simplified to

$$\Phi_{\gamma_s}(s)=\frac{1}{(1+\lambda_1\overline{\gamma}_c s)(1+\lambda_k\overline{\gamma}_c s)^{MN-1}}. \tag{3.85}$$

Using partial fraction expansion, we perform an inverse Laplace transform on (3.85) to

obtain the pdf of γ_s for correlated balanced Rayleigh fading as

$$p(\gamma_s)=\frac{\left(1+(MN-1)\rho\right)^{MN-2}}{\bar{\gamma}_c(MN\rho)^{MN-1}}\exp\left(-\frac{\gamma_s}{\bar{\gamma}_c\left(1+(MN-1)\rho\right)}\right) -\sum_{i=0}^{MN-2}\frac{\left(1+(MN-1)\rho\right)^{MN-2-i}}{(MN\rho)^{MN-1-i}(1-\rho)^i\Gamma(i+1)\bar{\gamma}_c^{i+1}}\gamma_s^i\exp\left(-\frac{\gamma_s}{\bar{\gamma}_c(1-\rho)}\right) \quad (3.86)$$

Resorting to (3.27) and following the same approach as in Section 3.4, the derivation of the error probability for OSTBC with constant correlated balanced Rayleigh fading is straightforward.

Note that by letting $\rho=0$, (3.86) coincides with (3.7), and by letting MN=2, (3.86) coincides with (3.77).

3.7.3 Numerical Results

In this section, the impact of correlation on the capacity and performance will be illustrated by simulations.

Fig. 3.21 shows the 98% outage Shannon capacity of OSTBC **G2** over correlated Rayleigh fading channels with one receive antenna. As discussed in [103][104][105], in case of an equally spaced linear antenna array, if we assume a Gaussian model for the power correlation among the channels, the correlation coefficient is

$$\rho=\exp\left[-\frac{k}{2}(i-j)^2\left(\frac{d}{\chi}\right)^2\right],\ i,j=1,\ldots,MN, \quad (3.87)$$

where d is the physical distance between the two adjacent antenna, and χ is the

wavelength of the carrier frequency. The coefficient k = 21.4 is chosen to give the same -3 dB point of the Bessel correlation model as in [103][104][105] for the case of Rayleigh fading. This correlation model is applied to the simulations in this section. Fig. 3.22 shows the capacity of OSTBC DS-CDMA with BPSK and one receive antenna over correlated Rayleigh fading channels. It is shown in these figures that as long as the distance between two adjacent antennas is greater than half the carrier wavelength, the system can achieve almost full capacity as the fading is virtually independent. However, when the distance is less than half the carrier wavelength, the loss in capacity is significant.

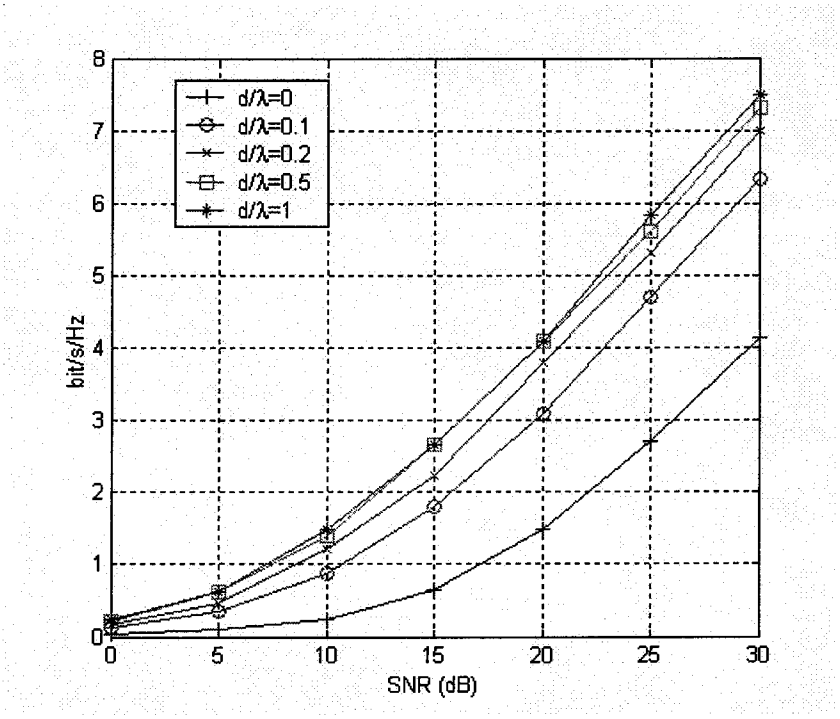

Fig.3.21 98% outage Shannon capacity of OSTBC G2 in correlated Rayleigh fading with one receive antenna.

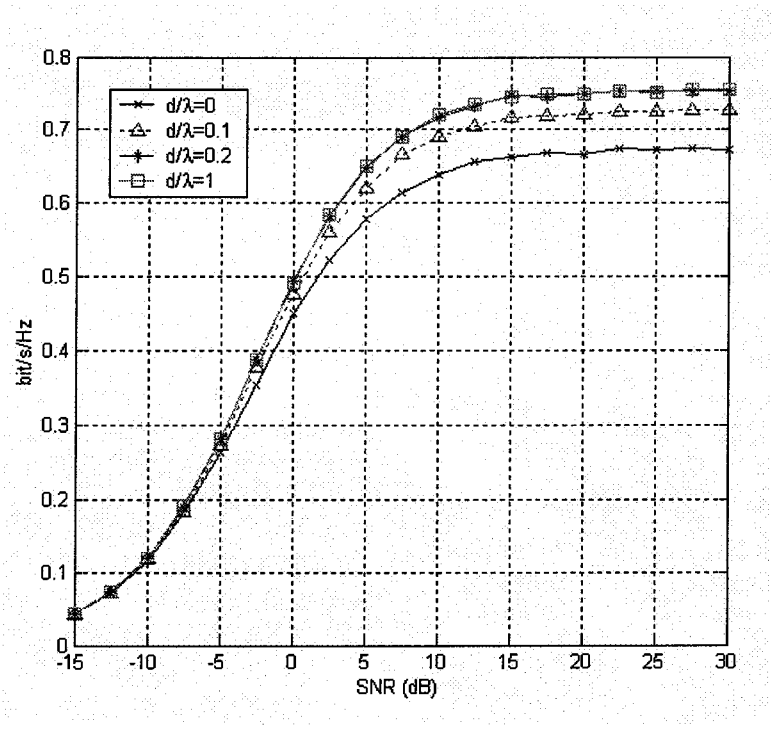

Fig.3.22 Channel capacity of OSTBC G2 with BPSK for OSTBC DS-CDMA in correlated Rayleigh fading with one receive antenna, 30 users and G =32.

Fig. 3.23 and Fig. 3.24 show the analytical and simulation error probabilities for OSTBC G2 OSTBC in balanced correlated Rayleigh fading with one receive antenna and different correlation coefficients, respectively. The results in the two figures are virtually identical. Again, it is shown that as long as the distance between antennas is greater than half the carrier wavelength, the performance difference is negligible.

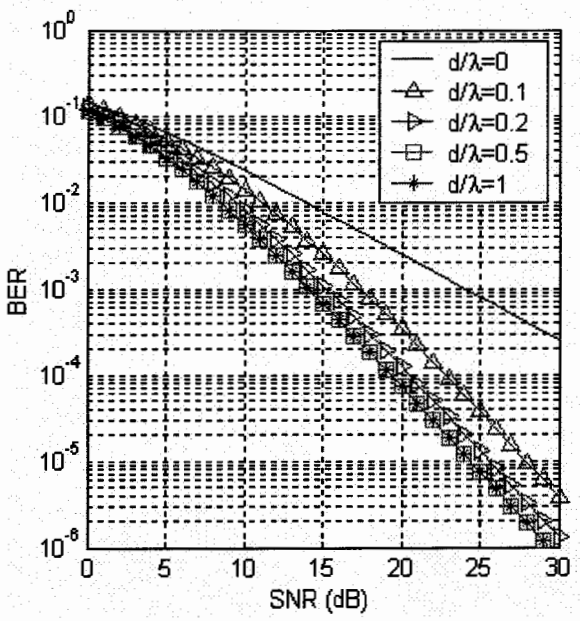

Fig.3.23 Analytical error probability of OSTBC G2 with BPSK over correlated Rayleigh fading with one receive antenna.

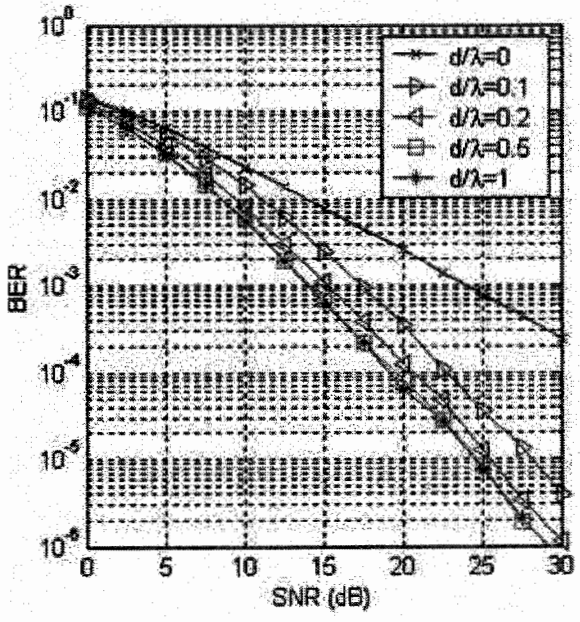

Fig.3.24 Simulation error probability of OSTBC G2 with BPSK over correlated Rayleigh fading with one receive antenna

3.8 Summary

In this chapter, the capacity and error probability of OSTBC were extensively studied with various fading channels and modulation schemes. Both single user and multiple user DS-CDMA systems were studied over flat fading channels. Correlated fading channels were also investigated. Furthermore, as a byproduct of this work, the results of Ricean flat fading channel are applied to MRC multiple channel reception. Compared with existing solutions, the error probabilities derived here are in a simpler form and can be evaluated efficiently with controlled accuracy.

Chapter 4

Capacity and Error Probability of PPAM UWB System

In this chapter, we propose a new modulation scheme called pulse amplitude position modulation (PPAM) for Ultra-Wideband (UWB) communication systems. PPAM combines pulse position modulation (PPM) and pulse amplitude modulation (PAM) to provide good system performance and low computational complexity. A set of MN-ary, $M=2^k$, $N=2^s$, PPAM signals are constructed from N-ary orthogonal PPM signals by including M-ary PAM signals in each dimension. It is shown that MN-ary PPAM has better performance than MN-ary PAM and less complexity than MN-ary PPM for $MN>2$. The channel capacity of PPAM is determined for a time-hopping multiple access UWB communication system. The error probability and performance bounds are derived for a multiuser environment. In particular, it is shown that for $M=2$, $2N$-ary PPAM signals, which are equivalent to a set of $2N$-ary biorthogonal signals, have better

performance than 2*N*-ary PPM with the same throughput and half the computational complexity. The remainder of this chapter is organized as follows. In Section 4.1, the system model and construction of the time-hopping PPAM UWB signal are described. Section 4.2 presents the capacity and error probability analysis of the PPAM UWB system over AWGN channels for a single user. The relationship between the reliable communication distance and channel capacity subject to FCC Part 15 rules is demonstrated. The exact error probability for *MN*-ary PPAM is presented, and a simple upper bound on the probability of error is derived. The multiple access capacity and error probability of a PPAM UWB system are derived in Section 4.3. Section 4.4 presents the numerical results for system performance and capacity, and finally some conclusions are given in Section 4.5.

4.1 Signal Construction And System Model

The *MN*-ary PPAM signal $\mathbf{s}_{mn}$ is defined as an N-dimensional vector with nonzero value in the *n*th dimension

$$\mathbf{s}_{mn} = [0,...,0, A_m\sqrt{E_g},0,...,0] \tag{4.1}$$

where $1 \le n \le N$, $1 \le m \le M$, $M > 1$ and $A_m\sqrt{E_g}$ is one of the M possible PAM amplitudes with $A_m = 2m-1-M$, $E_g = \frac{3E_{av}}{M^2-1}$, and E_{av} is the average energy of the signal.

A typical time hopping format for the signal of the *k*th user in an UWB system is given

by [70]

$$s^{(k)}(t) = \sum_{j=-\infty}^{\infty} A^{(k)}_{d_{\lfloor j/N_s \rfloor}} q\left(t - jT_f - c_j^{(k)} T_c - \delta_{d^{(k)}_{\lfloor j/N_s \rfloor}} \right), \tag{4.2}$$

where $A^{(k)}$ is the signal amplitude, $p(t)$ represents the transmitted impulse waveform that nominally begins at time zero, and the quantities associated with (k) are transmitter dependent. T_f is the frame time, which is typically a hundred to a thousand times the impulse width resulting in a signal with very low duty cycle. Each frame is divided into N_h time slots with duration T_c. The pulse shift pattern $c_j^{(k)}$, $0 <= c_j^{(k)} <= N_h$, (also called time-hopping sequence), is pseudorandom with period T_c. This provides an additional shift in order to avoid catastrophic collisions due to multiple access interference. The sequence d is the MN-ary data stream generated by the kth source after channel coding, and δ is the additional time shift utilized by the N-ary pulse position modulation. If $N_s>1$, a repetition code is introduced, i.e. N_s pulses are used for the transmission of the same information symbol.

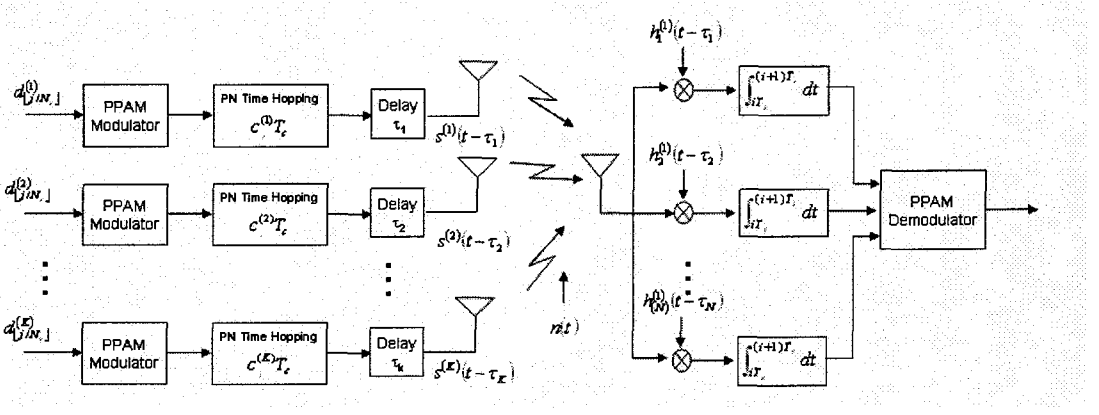

Fig.4.1 System model of a time-hopping multiple-access PPAM UWB system.

The received signal can then be modeled as

$$r(t)=\sum_{k=1}^{K} s^{(k)}(t-\tau_k)+w(t), \tag{4.3}$$

where $w(t)$ is AWGN noise with power density $N_o/2$ and τ_k is the propagation delay for the kth user. If only one user is present, the optimal receiver is an N-ary correlation receiver followed by a detector. When more than one link is active in the multiple-access system, the optimal receiver is a complex structure that takes advantage of all receiver knowledge regarding the characteristics of the multiple-access interference (MAI) [70][64]. However, for simplicity, an N-ary correlation receiver is typically used even when there is more than one active user. Fig. 4.1 shows the structure of the correlation receiver of the proposed PPAM UWB system. Note that for an MN-ary PPAM UWB system, N cross-correlators are required for demodulation. Compared with an MN-ary PPM UWB system, which requires MN cross-correlators for demodulation, the demodulation complexity is much lower.

4.2 Single User Capacity And Error Probability

With a single user active in the system, AWGN is the only source of signal degradation. For simplicity, we further assume that $\delta \geq T_p$, where T_p is the pulse duration, i.e. the MN-ary PPAM signal constellation consists of a set of N-orthogonal signals, not necessarily of equal energy. Then the analysis in [87][92] for the capacity of modulated

channels for PPM and PAM, and the error probability analysis in [45] for PPM, PAM, and biorthogonal signals, can be applied to the proposed PPAM system. Note that the same analysis can be applied to the nonorthogonal case though orthogonal signals are assumed in this chapter.

4.2.1 Channel Capacity for MN-ary PPAM Over AWGN Channels

The Shannon capacity $C = W\log_2(1+SNR)$, where SNR is the signal-to-nose ratio and W is the channel bandwidth, predicts the channel capacity C for an AWGN channel with continuous-valued inputs and outputs. However, a channel with MN-ary PPAM modulation has discrete-valued inputs and continuous-valued outputs, which imposes an additional constraint on the capacity calculation. Let $\mathbf{s}_{mn}$ be the encoded N-dimensional orthogonal PPAM signal vector input to the channel, and $\mathbf{r}$ be the channel output vector corrupted by an AWGN noise vector $\mathbf{w}$, which has zero mean and variance $\sigma^2 = \frac{1}{2}N_0$ in each real dimension, the vector representation of (4.3) with single user is

$$\mathbf{r} = \mathbf{s}_{mn} + \mathbf{w}. \tag{4.4}$$

From chapter 2, the channel capacity with input signals restricted to an equiprobable MN-ary PPAM constellation $\mathbf{C}$, and no restriction on the channel output, is given by

$$C = \log_2(MN) - \frac{1}{MN}\sum_{m=1}^{M}\sum_{n=1}^{N}\iint_{\mathbf{r}} p(\mathbf{r}|\mathbf{s}_{mn})\log_2\left(\frac{\sum_{p=1}^{M}\sum_{q=1}^{N} p(\mathbf{r}|\mathbf{s}_{pq})}{p(\mathbf{r}|\mathbf{s}_{mn})}\right)d\mathbf{y}, \quad (4.5)$$

where $\mathbf{r} = (r_1, \cdots, r_N)$ is the N-dimensional received vector, $r_i = w_i$ for $i \neq n$ and $r_n = A_m\sqrt{E_g} + w_n$. $\mathbf{s}_{mn}$ is the input PPAM signal defined in (4.1). The received signal $\mathbf{r}$ will have a N-dimensional joint Gaussian distribution conditioned on $\mathbf{s}_{mn}$, with PDF

$$p(\mathbf{r}|\mathbf{s}_{mn}) = \left(\frac{1}{2\pi\sigma^2}\right)^{\frac{N}{2}}\left(\prod_{\substack{i=1 \\ i\neq n}}^{N} e^{-\frac{r_i^2}{2\sigma^2}}\right)e^{-\frac{(r_n - A_m\sqrt{E_g})^2}{2\sigma^2}}. \quad (4.6)$$

The channel capacity for an MN-ary PPAM UWB system over an AWGN channel can then be written from (4.5) as

$$C = \log_2(MN) - \frac{1}{MN}\sum_{m=1}^{M}\sum_{n=1}^{N} E_{\mathbf{r}|\mathbf{s}_{mn}}\left[\log_2\left(\sum_{p=1}^{M}\sum_{q=1}^{N}\exp\left(-\frac{r_n^2 - r_q^2 + \left(r_q - A_p\sqrt{E_g}\right)^2 - \left(r_n - A_m\sqrt{E_g}\right)^2}{2\sigma^2}\right)\right)\right]$$

bits/channel use. (4.7)

4.2.2 Capacity of a PPAM UWB System Under FCC Part 15 Rules

Due to the possible interference to other communication systems by the ultra-wideband impulses, UWB is currently only allowed emission on an unlicensed basis subject to FCC part 15 rules which restricts the field strength level to E = 500 *microvolts/meter/MHz* at a distance of 3*m*. This gives the transmitted power constraint for an UWB system with a 1GHz bandwidth as $P_t \leq -11$ dBm. The

following relationship is obtained using a common link budget model [63][64]

$$\frac{\gamma}{G} \le -11dBm - N_{thermal} - F - 10\log\frac{(4\pi d)^n}{\lambda}, \tag{4.8}$$

where $G = N_s T_f W_p$ is the equivalent processing gain, W_p is the bandwidth of the UWB impulse related to the pulse duration T_p, F is the noise figure, $N_{thermal}$ is the thermal noise floor, calculated as the product of the Boltzman's constant, room temperature (typically 300K), noise figure and bandwidth, λ is the wavelength corresponding to the center frequency of the pulse, and n is the path loss exponent. It is easily shown that the maximum reliable communication distance is determined primarily by the signal to noise ratio γ. Based upon (4.7) and (4.8), the maximum distance for reliable transmission can be calculated. The relationship between system capacity and communication range will be demonstrated in Section 4.4.

4.2.3 Error Probability of PPAM Over an AWGN Channel

For N-dimensional orthogonal signals, the receiver has a parallel bank of N cross-correlators as illustrated in Fig. 4.1. Let $\mathbf{h}_j$, $1 \le j \le N$, denotes the nth basis signal vector, which is the vector representation of the basis function $h_j(t)$ shown in Fig. 4.1, defined as

$$\mathbf{h}_j = [0,...,0,1,0,...,0], \tag{4.9}$$

where the nonzero value is in the *i*th dimension. Assuming $\mathbf{s}_{mn}$ was sent, the optimum detector makes a decision on $\mathbf{s}_{mn}$ in favour of the signal corresponding to the crosscorrelator with the minimum Euclidean distance

$$C(\mathbf{r},\mathbf{h}_j)=\mathbf{r}\cdot\mathbf{h}_j=\sum_{k=1}^{N} r_k h_{jk}\ ,j=1,2,...,N, \tag{4.10}$$

where

$$\begin{aligned} C(\mathrm{r},\mathrm{h}_j)&=w_j\ , \quad j\neq n \\ C(\mathrm{r},\mathrm{h}_n)&=A_m\sqrt{E_g}+w_n \end{aligned}\ . \tag{4.11}$$

Thus with the optimum detector, the demodulated signal $\hat{\mathbf{s}}$ is

$$\hat{\mathbf{s}}=\underset{\mathbf{s}_{ij}}{\arg\min}\left\|C(\mathbf{r},\mathbf{h}_j)-A_i\sqrt{E_g}\right\|,\quad i=1,2,...,M \text{ and } j=1,2,...,N. \tag{4.12}$$

The receiver structure can be simplified to facilitate the error probability and union bound analysis. Assuming $\mathbf{s}_{mn}$ was sent, the optimum detector decides the nonzero dimension of $\mathbf{s}_{mn}$, i.e. n, in favour of the dimension corresponding to the largest magnitude of the crosscorrelators given in (4.10), and this largest magnitude is used to decide which of the M possible amplitudes, i.e. m, has been transmitted. According to this decision rule, the average probability of a correct decision is given by

$$P_c=\frac{1}{M}\left(\begin{aligned}&\sum_{m=2}^{M-1}\int_{(A_m-1)\sqrt{E_g}}^{(A_m+1)\sqrt{E_g}}\left(\frac{1}{\sqrt{2\pi}}\int_{-\left|r_m/\sqrt{N_0/2}\right|}^{\left|r_m/\sqrt{N_0/2}\right|}e^{-x^2/2}dx\right)^{N-1}p(r_m)dr_m+\int_{-\infty}^{(A_m+1)\sqrt{E_g}}\left(\frac{1}{\sqrt{2\pi}}\int_{-\left|r_m/\sqrt{N_0/2}\right|}^{\left|r_m/\sqrt{N_0/2}\right|}e^{-x^2/2}dx\right)^{N-1}p(r_m)dr_m\Bigg|_{m=1}\\ &+\int_{(A_m-1)\sqrt{E_g}}^{\infty}\left(\frac{1}{\sqrt{2\pi}}\int_{-\left|r_m/\sqrt{N_0/2}\right|}^{\left|r_m/\sqrt{N_0/2}\right|}e^{-x^2/2}dx\right)^{N-1}p(r_m)dr_m\Bigg|_{m=M}\end{aligned}\right),$$

(4.13)

where

$$p(r_m) = \frac{1}{\sqrt{\pi N_0}} \exp\left(-\frac{\left(r_m - A_m\sqrt{E_g}\right)^2}{N_0} \right). \tag{4.14}$$

Finally, the probability of a symbol error for *MN*-ary PPAM is

$$P_{MN} = 1 - P_c. \tag{4.15}$$

4.2.4 A Union Bound On The Probability Of Error

Since the probability of error expressions given by (4.13) and (4.15) are complex, and must be evaluated via numerical integration, we now derive a simple upper bound on the probability of a symbol error. The error probability of a PPAM signal over an AWGN channel can be upper bounded by using the simplified receiver structure from Section 4.2.3

$$P_{MN|s_{mn}} \le P\left(\left(\bigcup_{\substack{j=1 \\ j \ne n}}^{N} \left|C(\mathbf{r},\mathbf{h}_j)\right| > \left|C(\mathbf{r},\mathbf{h}_n)\right| \right) \bigcup \left(\left|C(\mathbf{r},\mathbf{h}_n) - A_m\sqrt{E_g}\right| > \sqrt{E_g} \right) \right). \tag{4.16}$$

The right term of (4.16) can be upper-bounded by the union bound of the *N* events, i.e.

$$P_{MN|s_{mn}} \le P\left(\left(\bigcup_{\substack{j=1 \\ j\neq n}}^{N}\left|C(\mathbf{r},\mathbf{h}_j)\right| > \left|C(\mathbf{r},\mathbf{h}_n)\right|\right) \bigcup \left(\left|r_n - A_m\sqrt{E_g}\right| > \sqrt{E_g}\right)\right)$$
$$\le \sum_{\substack{j=1 \\ j\neq n}}^{N} P\left(\left|C(\mathbf{r},\mathbf{h}_j)\right| > \left|C(\mathbf{r},\mathbf{h}_n)\right|\right) + P\left(\left|r_n - A_m\sqrt{E_g}\right| > \sqrt{E_g}\right) \quad . \quad (4.17)$$
$$= \left[(N-1)P\left(\left|C(\mathbf{r},\mathbf{h}_j)\right| > \left|C(\mathbf{r},\mathbf{h}_n)\right|\right) + P\left(\left|r_n - A_m\sqrt{E_g}\right| > \sqrt{E_g}\right)\right]_{\forall j\neq n}$$

Given $C(\mathbf{r},\mathbf{h}_j)$, $j=1,\ldots,N$, as in (4.11), we can show that

$$P\left(\left|C(\mathbf{r},\mathbf{h}_j)\right| > \left|C(\mathbf{r},\mathbf{h}_n)\right|\right)\Big|_{s_{mn},j\neq n} < \frac{\sqrt{2}}{2} e^{-\frac{A_m^2 E_g}{2N_0}}, \quad (4.18)$$

and

$$P\left(\left|r_n - A_m\sqrt{E_g}\right| > \sqrt{E_g}\right)\Big|_{s_{mn}} = 2Q\left(\sqrt{\frac{2E_g}{N_0}}\right). \quad (4.19)$$

Assume all PPAM signals are equally likely a priori, the average probability of a symbol error for *MN*-ary PPAM is upper-bounded by

$$P_{MN} < \frac{N-1}{M}\sum_{m=1}^{M}\frac{\sqrt{2}}{2} e^{-\frac{A_m^2 E_g}{2N_0}} + 2Q\left(\sqrt{\frac{2E_g}{N_0}}\right). \quad (4.20)$$

Since an error can only occur in one direction when either one of the *±(M-1)* is transmitted, a tighter bound is given by

$$P_{MN} \le \frac{N-1}{M}\sum_{m=1}^{M}\frac{\sqrt{2}}{2} e^{-\frac{A_m^2 E_g}{2N_0}} + \frac{2(M-1)}{M} Q\left(\sqrt{\frac{2E_g}{N_0}}\right). \quad (4.21)$$

Using $Q(x) < e^{-\frac{x^2}{2}}$, this bound can be further simplified to

$$P_{MN} < \frac{N-1}{M}\sum_{m=1}^{M}\frac{\sqrt{2}}{2}e^{-\frac{A_m^2 E_g}{2N_0}} + \frac{2(M-1)}{M}e^{-\frac{E_g}{2N_0}}. \qquad (4.22)$$

4.2.5 Relationship with PAM, PPM and Biorthogonal Signals

From the definition of the proposed *MN*-ary PPAM signal constellation, both PAM and PPM signals can be viewed as special cases of PPAM with M=1 or N=1. By letting N=1, it can be easily shown that the system capacity given in (4.7), the error probability given in (4.13) and the union bounds given in (4.21) and (4.22) have the same form as those in [45] for M-ary PAM. However, the capacity and performance for M-ary PAM cannot be obtained from the above analysis simply by letting M=1 since these results assume M>1, i.e. more than one amplitude level. If M=2, the 2*N*-ary PPAM signals become 2*N*-ary biorthogonal PPM signals, and the performance given by (4.13) is the same as that given in [45] for biorthogonal signals.

Although increasing the product *MN* can increase the system throughput, the computational complexity will also increase. Since M-ary PAM is a bandwidth efficient modulation scheme rather than power efficient, a small M is suitable in the case of an UWB system where bandwidth efficiency plays a much less important role than in a conventional communication system. In particular, we investigate a special case of the proposed PPAM system for M=2, when the *MN*-ary PPAM signals become 2*N*-ary biorthogonal signals.

For M=2, the union bound for biothogonal signals is

$$P_{2N} < \left(\frac{\sqrt{2}}{2}(N-1)+1 \right) e^{-\frac{Es}{2N_0}} \leq Ne^{-\frac{Es}{2N_0}}. \tag{4.23}$$

From [45], the N-ary PPM signals are mutually equidistant, i.e. geometrically the distance between any pair of signal vectors is $\sqrt{2E_s}$, while for biorthogonal signals, the distance between any pair of signal vector is either $\sqrt{2E_s}$ or $2\sqrt{E_s}$. Hence from the signal space perspective, $2N$-ary biorthogonal signals have better performance than $2N$-ary PPM signals. Using the union bound given in [45] for PPM, we obtain another upper bound for $2N$-ary PPAM

$$P_{2N} < P_{2N,PPM} < (2N-1)Q\left(\sqrt{\frac{E_s}{N_0}} \right). \tag{4.24}$$

It will be shown in Section 4.4 that (4.24) is a tighter upper bound than (4.23). Note that for the same throughput, biorthogonal signalling only requires half the number of cross-correlators required by PPM, and thus has only about half the computational complexity. Therefore, $2N$-ary PPAM, i.e. biorthogonal signalling, is an attractive choice for UWB communication systems.

4.3 Multiple Access Capacity and Error Probability

With more than one user active in the system, multiple-access interference (MAI) is a factor limiting performance and capacity, especially for a large number of users. As

shown in [70][81][82][64], the net effect of the multiple-access interference produced by the undesired users at the output of the desired user's correlation receiver can be modeled as a zero-mean Gaussian random variable, if the number of users is large [45]. Assuming that $\delta \geq T_p$, , i.e. the MN-ary PPAM signal is an orthogonal signal with N dimensions, the capacity and error probability analysis given in Section 4.2 for a single user can be extended to multiple-access systems.

4.3.1 Multiple Access Interference Model

As given in (4.3), the received signal is modeled as

$$r(t) = \sum_{k=1}^{K} s^{(k)}(t - \tau_k) + n(t).$$

To evaluate the average SNR, we make the following assumptions:

a) $s^{(k)}(t-\tau_k)$, for $k=1,2,...,K$, where K is the number of active users, and the noise $n(t)$ are assumed to be independent.

b) The time-hopping sequences $c_j^{(k)}$ are assumed to be independent, identically distributed (i.i.d) random variables uniformly distributed over time interval [0, N_h].

c) For simplicity, and without loss of generality, we assume that each information symbol only uses a single UWB pulse, i.e. $N_s=1$.

d) All MN-ary PPAM signals are equally likely *a priori*.

e) The time delay τ_k is assumed to be i.i.d and uniformly distributed over [0, T_f].

f) Perfect synchronization is assumed at the receiver, i.e. τ_k is known at the receiver.

Without loss of generality, we assume the desired user is k=1. The basis functions of the N cross-correlators of the correlation receiver for user 1 are given as

$$h_i^{(1)}(t) = p(t - \delta_i - \tau_1),\ i=1,...,N. \tag{4.25}$$

The output of each cross-correlator at sample time $t=jT_f$ is

$$\hat{r}_i = \int_{(j-1)T_f}^{jT_f} r(t) h_i^{(1)}\left(t - jT_f - c_j^{(k)} T_c\right) dt \qquad i = 1,...,N. \tag{4.26}$$

Assuming PPAM signal $\mathbf{s_{mn}}$ is transmitted by user 1, (4.26) can be written as

$$\hat{r}_i = \begin{cases} A_m^{(1)} + W_{MAI} + W & i = n \\ W_{MAI} + W & i \neq n \end{cases}, \tag{4.27}$$

where

$$W_{MAI} = \sum_{k=2}^{K} \int_{(j-1)T_f}^{jT_f} A^{(k)} p\left(t - jT_f - c_j^{(k)} T_c - \delta d_j^{(k)} - \tau_k\right) p\left(t - \delta_j - \tau_1 - jT_f - c_j^{(k)} T_c\right) dt \tag{4.28}$$

is the MAI component and

$$W = \int_{(j-1)T_f}^{jT_f} w(t) p\left(t - \delta_j - \tau_1 - jT_f - c_j^{(k)} T_c\right) dt \tag{4.29}$$

is the AWGN component. By defining the autocorrelation function of $w(t)$ as

$$\gamma(\Delta) = \int_0^{T_f} p(t)p(t-\Delta)dt\,, \tag{4.30}$$

(4.28) can be written as

$$W_{MAI} = \sum_{k=2}^{K} A^{(k)}\gamma(\Delta), \tag{4.31}$$

where ? = $\left(c_j^{(1)} - c_j^{(k)}\right)T_c - \left(\delta_{i_j}^{(1)} - \delta_j^{(k)}\right) - (\tau_1 - \tau_k)$, is the time difference between user 1 and user k. Under the assumptions listed above, ? can be modeled as a random variable uniformly distributed over [$-T_f$, T_f]. With the Gaussian approximation, we require the mean and variance of (4.27) to characterize the output of the cross-correlators.

It is easy to show that the AWGN component has mean zero and variance $N_o/2$. However, the mean and variance of the MAI component are determined by the specific pulse waveform. In this chapter, we consider signalling by differentiated Gaussian pulses and Manchester pulses. Note that both of these pulses satisfy the relation $\int_{-\infty}^{\infty} p(t)dt = 0$, i.e. no DC value appears in the power spectrum of the pulse. As in [69], the differentiated Gaussian pulse is defined as

$$w_{DGaussian}(t) = \begin{cases} \dfrac{\sqrt{8}}{\sqrt[4]{2\pi\lambda^3 T_p^6}} te^{-\frac{t^2}{\lambda T_p^2}}, & -\dfrac{T_p}{2} \le t \le \dfrac{T_p}{2} \\ 0, & otherwise \end{cases}, \tag{4.32}$$

where λ=0.0815 is a bandwidth normalization parameter such that 99% of the pulse

energy is contained in the range $-\frac{T_p}{2} \le t \le \frac{T_p}{2}$; the Manchester pulse is defined as

$$w_{Manchester}(t) = \begin{cases} -\sqrt{\frac{1}{T_p}}, & 0 < t < \frac{T_p}{2} \\ \sqrt{\frac{1}{T_p}}, & \frac{T_p}{2} < t < T_p \\ 0, & otherwise \end{cases}. \tag{4.33}$$

The autocorrelation functions of the differentiated Gaussian pulse and the Manchester pulse are then given as

$$\gamma_{DGaussian}(\Delta) = \begin{cases} \left(1 - \frac{\Delta^2}{\lambda T_p^2}\right) e^{-\frac{\Delta^2}{2\lambda T_p^2}}, & 0 \le |t| \le T_p \\ 0, & otherwise \end{cases}, \tag{4.34}$$

and

$$\gamma_{Manchester}(\Delta) = \begin{cases} \left(1 - \frac{3|\Delta|}{T_p}\right), & 0 \le |t| \le \frac{T_p}{2} \\ \left(-1 + \frac{3|\Delta|}{T_p}\right), & \frac{T_p}{2} \le |t| \le T_p \\ 0, & otherwise \end{cases}, \tag{4.35}$$

respectively. Given (4.34) and (4.35), we have

$$E[\gamma(\Delta)] = \frac{1}{2T_f}\int_{-T_f}^{T_f} \gamma(\Delta) d\Delta = 0. \tag{4.36}$$

The mean of W_{MAI} can then be calculated as

$$\begin{aligned} E[W_{MAI}] &= E\left[\sum_{k=2}^{K} A^{(k)}\gamma(\Delta)\right] \\ &= E\left[\sum_{k=2}^{K} A^{(k)}\right]E[\gamma(\Delta)]. \\ &= 0 \end{aligned} \tag{4.37}$$

The variance of W_{MAI} for differentiated Gaussian pulses and Manchester pulses is

$$\begin{aligned} Var[W_{MAI}] &= Var\left[\sum_{k=2}^{K} A^{(k)}\gamma(\Delta)\right] \\ &= \sum_{k=2}^{K} E\left[\left(A^{(k)}\right)^2\right]E\left[\gamma^2(\Delta)\right] \end{aligned} \tag{4.38}$$

On the basis that all PPAM signals are equally likely *a priori*, we have

$$\begin{aligned} Var[W_{MAI,DGaussian}] &= Var\left[\sum_{k=2}^{K} A^{(k)}\gamma_{DGaussian}(\Delta)\right] \\ &= \sum_{k=2}^{K} E\left[\left(A^{(k)}\right)^2\right]E\left[\gamma^2_{DGaussian}(\Delta)\right] \quad , \\ &= \frac{3\sqrt{\pi\lambda}T_p(K-1)}{8T_f}E_{av} \end{aligned} \tag{4.39}$$

for differentiated Gaussian pulses and

$$\begin{aligned} Var[W_{MAI,Manchester}] &= Var\left[\sum_{k=2}^{K} A^{(k)}\gamma_{Manchester}(\Delta)\right] \\ &= \sum_{k=2}^{K} E\left[\left(A^{(k)}\right)^2\right]E\left[\gamma^2_{Manchester}(\Delta)\right] \quad , \\ &= \frac{(K-1)T_p}{6T_f}E_{av} \end{aligned} \tag{4.40}$$

for Manchester pulses. By defining the spread ratio $\rho = \frac{T_f}{T_p}$, (4.39) and (4.40) can be written as

$$Var[W_{MAI,DGaussian}] = \frac{3\sqrt{\pi\lambda}(K-1)}{8\rho}E_{av} \tag{4.41}$$

and

$$Var[W_{MAI,Manchester}] = \frac{(K-1)}{6\rho}E_{av}, \tag{4.42}$$

respectively. Hence the outputs of the cross-correlators for the receiver of user 1 can be modeled as independent Gaussian random variables with distribution

$$\begin{cases} \hat{r}_j \sim N\left(A_m\sqrt{E_g}^{(1)}, \sigma^2_{MAI} + \frac{N_0}{2}\right) & j = n \\ \hat{r}_j \sim N\left(0, \sigma^2_{MAI} + \frac{N_0}{2}\right) & j \neq n \end{cases}, \tag{4.43}$$

where $\sigma^2_{MAI} = \frac{3\sqrt{\pi\lambda}(K-1)}{8\rho}E_{av}$ for differentiated Gaussian pulses and $\sigma^2_{MAI} = \frac{(K-1)}{6\rho}E_{av}$ for Manchester pulses.

4.3.2 Multiple-Access Capacity

From (4.43), we conclude that the multiple-access PPAM UWB system has the same received vector representation as given in (4.4) for a single user PPAM UWB system

$$\mathbf{r} = \mathbf{s}_{mn} + \mathbf{w}, \tag{4.44}$$

where $\mathbf{w}$ has zero mean and variance $\sigma^2 = \sigma^2_{MAI} + \frac{1}{2}N_0$ in each real dimension. Thus the information theoretic capacity for a PPAM UWB system over AWGN with a single

user given in (4.7) can be directly extended to multiple-access system by substituting $\sigma_{MAI}^2 + \frac{N_0}{2}$ for σ^2, which gives

$$C = \log_2(MN) - \frac{1}{MN}\sum_{m=1}^{M}\sum_{n=1}^{N} E_{\mathbf{r}|s_{mn}}\left[\log_2\left(\exp\left(-\frac{r_n^2 - r_q^2 + \left(r_q - A_p\sqrt{E_g}\right)^2 - \left(r_n - A_m\sqrt{E_g}\right)^2}{2\left(\sigma_{MAI2}^2 + \frac{N_0}{2}\right)}\right)\right)\right]. \quad (4.45)$$

Applying the link budget model given in (4.8) under FCC Part 15 rules, tradeoffs between number of users, reliable distance, system performance and channel capacity can be demonstrated. Numerical results will be presented in Section 4.4.

4.3.3 Multiple-Access Error Probability

Given the vector representation of the time-hopping multiple-access PPAM UWB system in (4.44), the error probability can be obtained from (4.13) by substituting $\sigma_{MAI}^2 + \frac{N_0}{2}$ for σ^2, giving

$$P_{MN} = 1 - P_c, \quad (4.46)$$

where

$$P_c = \frac{1}{M}\left[\begin{array}{l} \displaystyle\sum_{m=2}^{M-1}\int_{(A_m-1)\sqrt{E_g}}^{(A_m+1)\sqrt{E_g}}\left(\frac{1}{\sqrt{2\pi}}\int_{-\frac{r_m}{\sqrt{\sigma_{MAI}^2+\frac{N_0}{2}}}}^{\frac{r_m}{\sqrt{\sigma_{MAI}^2+\frac{N_0}{2}}}} e^{-x^2/2}dx\right)^{N-1} p(r_m)\,dr_m \\ \displaystyle+\int_{-\infty}^{(A_m+1)\sqrt{E_g}}\left(\frac{1}{\sqrt{2\pi}}\int_{-\frac{r_m}{\sqrt{\sigma_{MAI}^2+\frac{N_0}{2}}}}^{\frac{r_m}{\sqrt{\sigma_{MAI}^2+\frac{N_0}{2}}}} e^{-x^2/2}dx\right)^{N-1} p(r_m)\,dr_m\Bigg|_{m=1} \\ \displaystyle+\int_{(A_m-1)\sqrt{E_g}}^{\infty}\left(\frac{1}{\sqrt{2\pi}}\int_{-\frac{r_m}{\sqrt{\sigma_{MAI}^2+\frac{N_0}{2}}}}^{\frac{r_m}{\sqrt{\sigma_{MAI}^2+\frac{N_0}{2}}}} e^{-x^2/2}dx\right)^{N-1} p(r_m)\,dr_m\Bigg|_{m=M} \end{array}\right], \quad (4.47)$$

and

$$p(r_m) = \frac{1}{\sqrt{2\pi\left(\sigma_{MAI}^2+\frac{N_0}{2}\right)}}\exp\left(-\frac{\left(r_m - A_m\sqrt{E_g}\right)^2}{2\left(\sigma_{MAI}^2+\frac{N_0}{2}\right)}\right). \quad (4.48)$$

The upper bound for a single user PPAM system given in (4.22) can then be applied to (4.45) to obtain

$$P_{MN} < \frac{N-1}{M}\sum_{m=1}^{M}\frac{\sqrt{2}}{2}\exp\left(-\frac{A_m^2 E_g}{4\left(\sigma_{MAI}^2+\frac{N_0}{2}\right)}\right)+\frac{2(M-1)}{M}Q\left(\sqrt{\frac{2E_g}{2\left(\sigma_{MAI}^2+\frac{N_0}{2}\right)}}\right). \quad (4.49)$$

$$< \frac{N-1}{M}\sum_{m=1}^{M}\frac{\sqrt{2}}{2}e^{-\frac{A_m^2 E_g}{4\left(\sigma_{MAI}^2+\frac{N_0}{2}\right)}}+\frac{2(M-1)}{M}e^{-\frac{E_g}{2\left(\sigma_{MAI}^2+\frac{N_0}{2}\right)}}$$

By letting M=2, we obtain an upper bound for time-hopping biorthogonal PPAM

$$P_{MN} < \left(\frac{\sqrt{2}}{2}(N-1)+1\right)e^{-\frac{A_m^2 E_g}{4\left(\sigma_{MAI}^2+\frac{N_0}{2}\right)}} < Ne^{-\frac{A_m^2 E_g}{2\left(\sigma_{MAI}^2+\frac{N_0}{2}\right)}}, \quad (4.50)$$

and similarly, (4.24) can be applied to give

$$P_{MN} < (2N-1)Q\left(\sqrt{\frac{E_s}{2\left(\sigma_{MAI}^2+\frac{N_0}{2}\right)}}\right). \quad (4.51)$$

4.4 Numerical Results

In this section, some numerical results are presented to illustrate and verify the capacity and error probability expressions obtained previously.

Fig. 4.2 shows the channel capacity for a 2N-ary PPAM system over an AWGN channel. This shows that 2N-ary PPAM has the same capacity as 2N-ary PPM and 2N-ary PAM for large SNR. PPAM has a smaller SNR threshold to achieve capacity than PAM and PPM for the same throughput. However, the advantage over PPM decreases as SNR

and N increase. This will also be shown by the performance of $2N$-ary PPAM and $2N$-ary PPM given later.

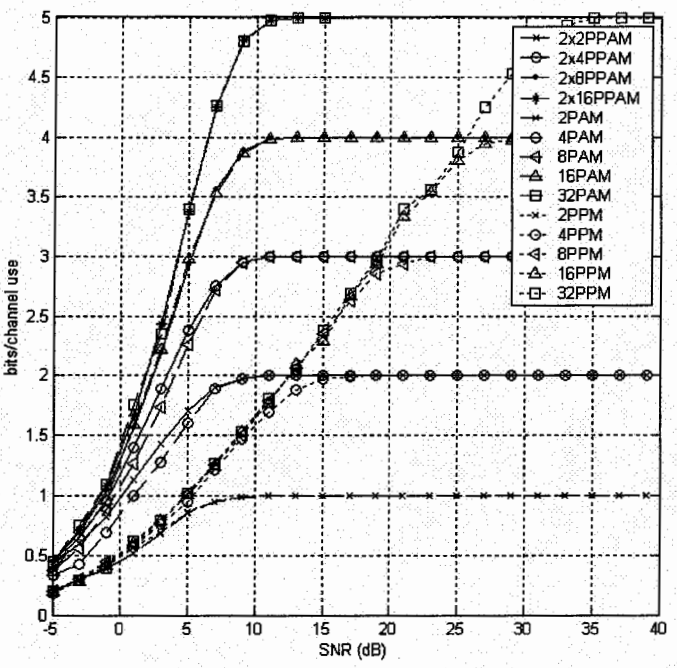

Fig.4.2 Channel capacity with $2N$-ary PPAM over an AWGN channel.

Fig. 4.3 shows the channel capacity for $4N$-ary PPAM over an AWGN channel. This shows that the SNR threshold of $4N$-ary PPAM is larger than PPM, while smaller than PAM for the same throughput. This justifies our design initiative of PPAM to provide a compromise between complexity and system performance. Note that $2N$-ary PPAM is a special case which has better performance than PPM with the same throughput. In general, MN-ary PPAM provides a compromise between complexity and performance.

Fig. 4.4 demonstrates the relationship between reliable channel capacity and communication range subject to FCC Part 15 rules. The link budget model in (4.8) was

applied and a free space propagation transmission model was assumed, i.e. n=2. The equivalent processing gain G was set to 100. This figure shows that 2N-ary PPAM can provide full capacity within 100m in most cases, and approximately half of capacity when the communication distance is extended to 400m for 2x2 PPAM. In general, an UWB system is only capable of reliable transmission over small to medium ranges under the restriction of FCC Part 15 rules.

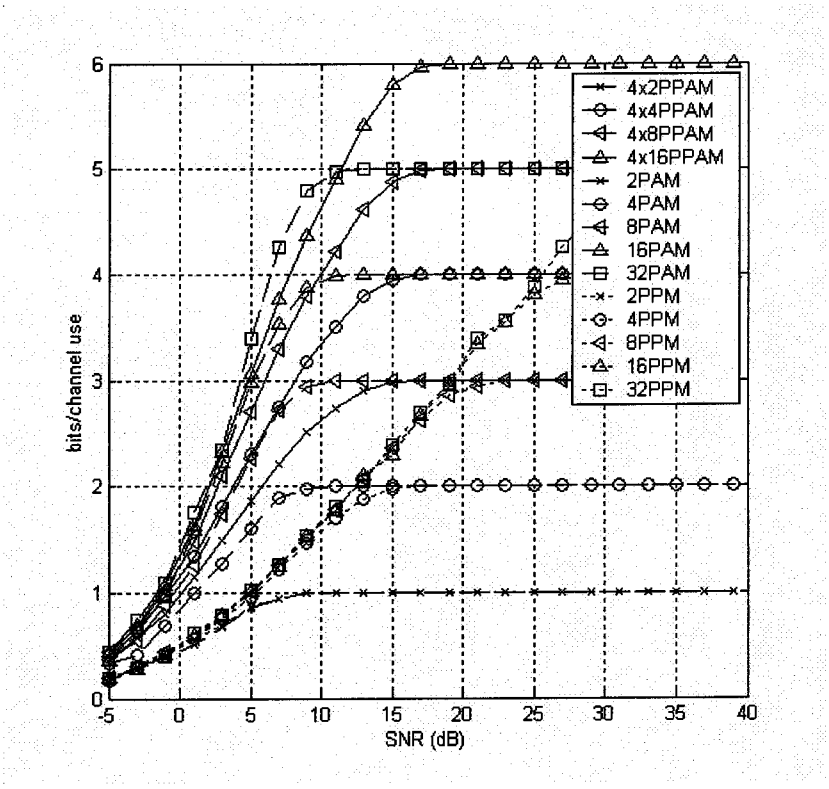

Fig.4.3 Channel capacity with 4N-ary PPAM over an AWGN channel.

The performance of 2x2 PPAM (biorthogonal), is shown in Fig. 4.5 for Gaussian first derivative pulses and Manchester pulses. Both the pulse width T_p and the modulation index δ were set to 0.6 ns in both cases. The upper bounds given by (4.23) and (4.24) are also shown for comparison. The two pulse types have similar performance, and

(4.24) is a better bound than (4.23), and is sufficiently tight for large SNR.

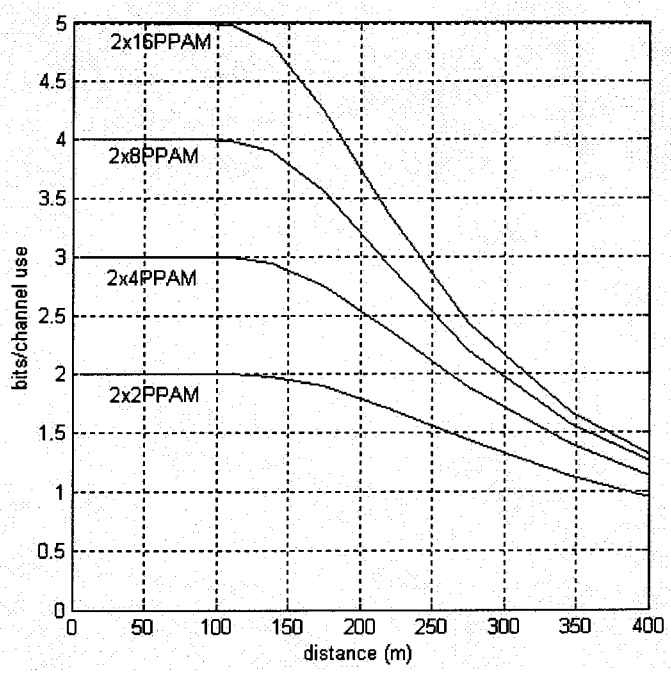

Fig.4.4 UWB spectral efficiency as a function of range for n=2, G=100 and 2N-ary PPAM.

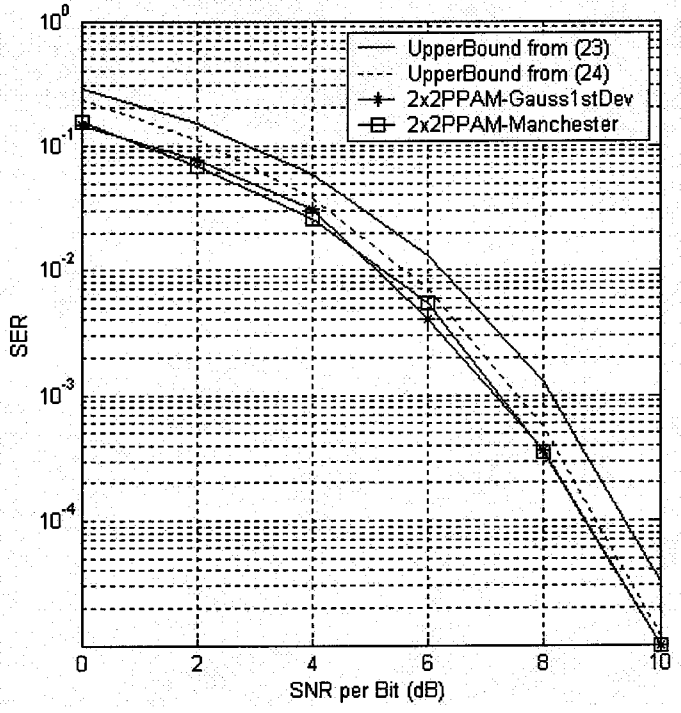

Fig.4.5 Performance of a 2x2PPAM UWB system with Gaussian first derivative pulses and Manchester pulses.

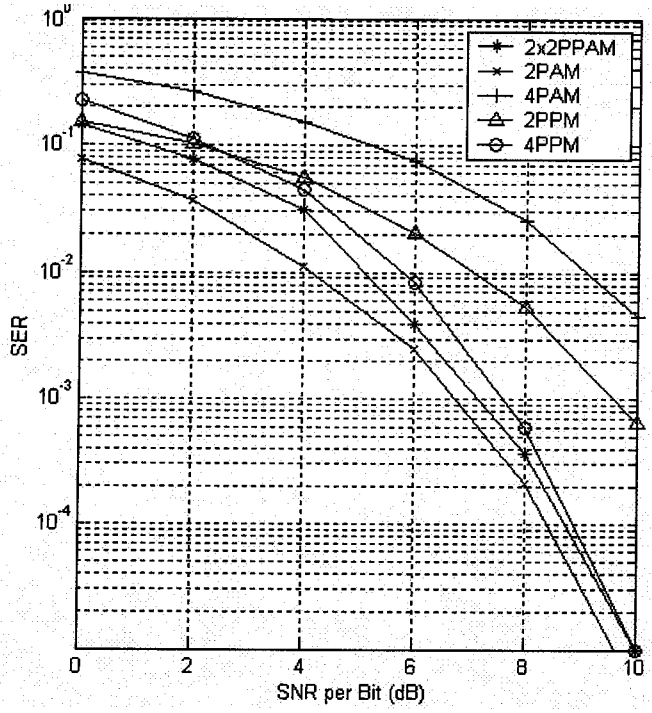

Fig.4.6 Performance comparison between PAM, PPM and PPAM with Gaussian first derivative pulses.

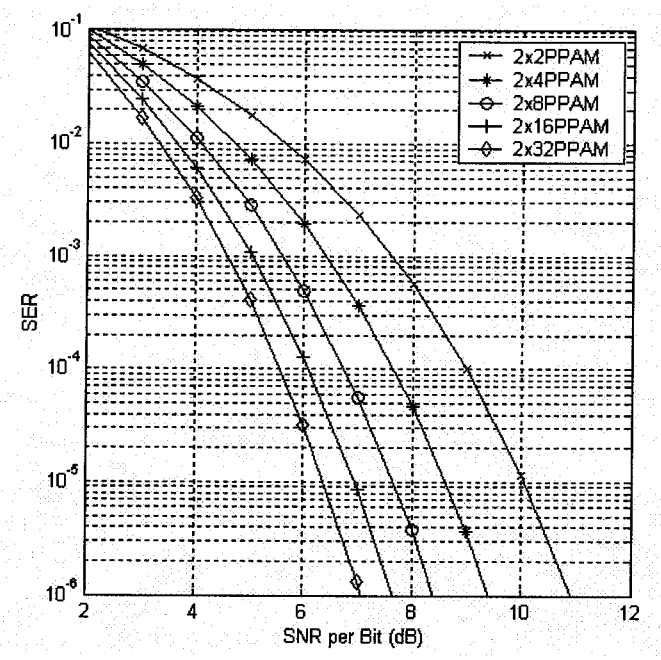

Fig.4.7. The upper bound on error probability (24) for a 2N-ary PPAM UWB system.

Fig. 4.6 compares the performance of PPAM, PAM and PPM using Gaussian first

derivative pulses. This shows that 2x2 PPAM has better performance than 2PPM and 4PPM, however, the advantage over 4PPM is small, particularly for large SNR, which follows from the similar SNR capacity thresholds shown in Fig. 4.2. Note that 2x2 PPAM has computational complexity similar to 2PPM with twice the capacity and better performance, while 2x2 PPAM has only about half of the computational complexity of 4PPM with better performance. Given this fact, 2x2-PPAM is an attractive choice for UWB communications. As shown in the figure, 2-PAM has better performance than both PPAM and PPM, however the performance decreases dramatically for 4-PAM. Performance upper bounds are given in Fig. 4.7 for $2N$-ary PPAM. This shows that better performance is achieved as N increases. However, the computational complexity doubles each time N increases, but the performance improvement diminishes.

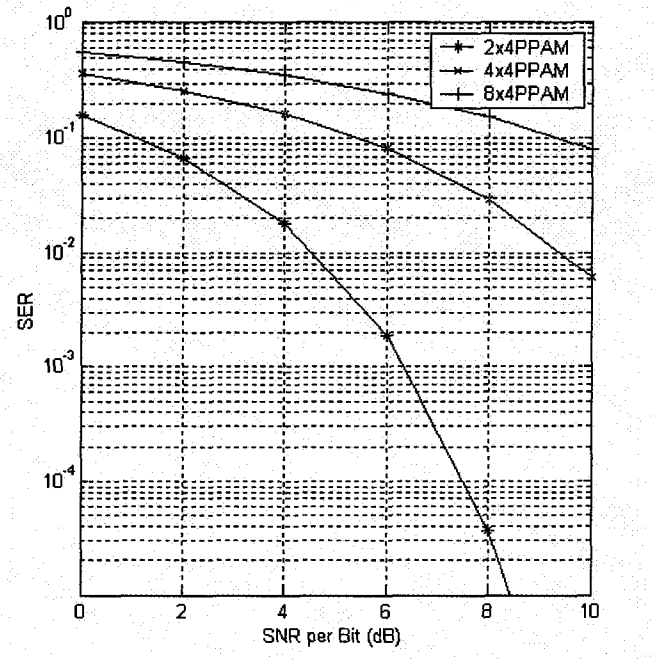

Fig.4.8 Performance of a $M4$-ary PPAM UWB system over AWGN channel with M=2,4, and 8

The performance of $M4$-ary PPAM is presented for M=2, 4 and 8 in Fig. 4.8. As shown in the figure, the error probability increases dramatically as M increases. The performance penalty for 4 amplitude levels over 2 amplitude levels is almost 5 dB. However, the decoding complexity is only about half that with 2 amplitude levels. Note that a comparison with Fig. 4.7 shows that the performance bound given by (4.24) is very tight for 2x4 PPAM.

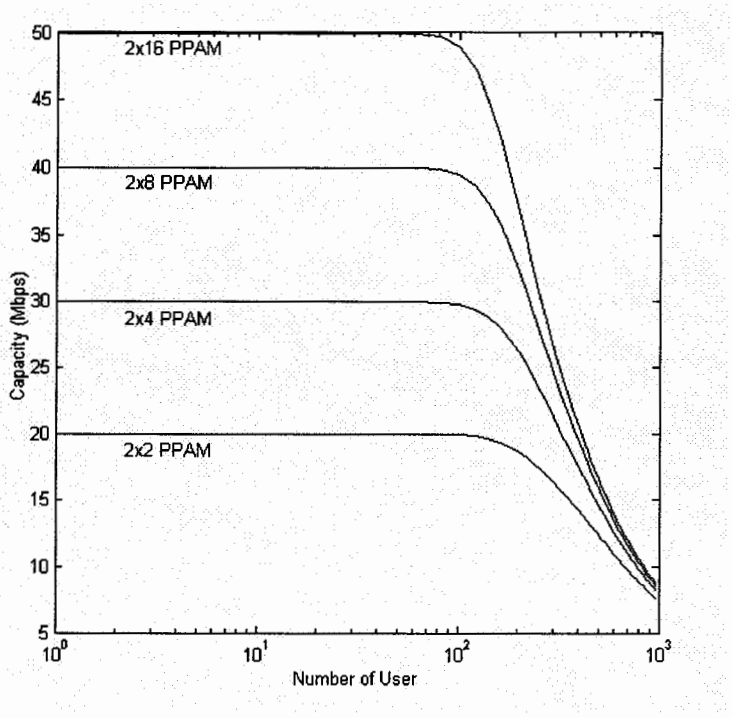

Fig.4.9 Capacity of a 2N-ary PPAM UWB system with ?=100, SNR=15 dB, Manchester pulses and Tp=1 ns.

User capacity in *Mbps* is shown in Fig. 4.9 for *SNR*=10dB, spread ratio ?=100, and Gaussian first derivative pulses with the pulse width set to 1*ns*. The transmission rate

R_s is given by $1/(?T_p)$. This shows that the system can accommodate approximately 100 simultaneous active users for full capacity. Only half of the capacity can be achieved when the number of users is increased to 500 for 2x2-PPAM. This shows that 50 *Mbps* can be achieved with 15 users for 2x16-PPAM, while with 50 users, the achievable capacity is only 20 *Mbps*.

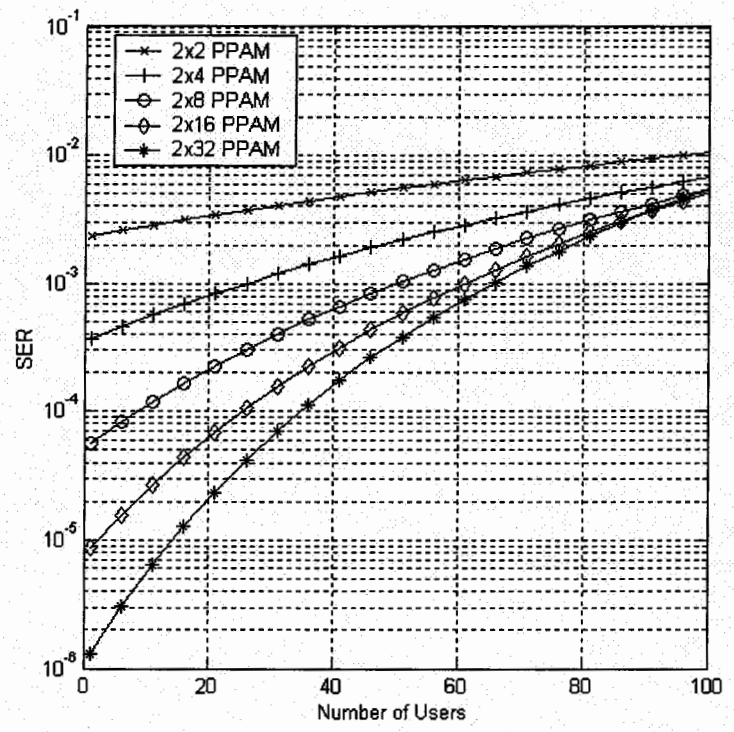

Fig.4.10 Capacity of a 2N-ary PPAM UWB system with ?=500, SNR/bit=7 dB and Gaussian first derivative pulses.

Fig. 4.10 presents the user capacity from the perspective of error probability for a multiple-access time-hopping UWB system. Again 2*N*-ary PPAM is considered with an *SNR* per bit of 7 dB and a spread ratio of 500. This shows that the error probability

increases as the number of users increases, as expected.

4.5 Conclusions

A new modulation scheme, pulse position amplitude modulation, has been proposed for time-hopping UWB systems. The channel capacity and error probability have been analyzed over AWGN channels for both single and multiple user environments. It was shown that the proposed PPAM UWB system provides a compromise between system performance and computational complexity. In particular, a $2N$-ary PPAM UWB system provides better performance than a $2N$-ary PPM system with only half the computational complexity. Thus $2N$-ary PPAM is an attractive alternative to $2N$-ary PPM modulation for time-hopping UWB systems.

It should be noted that the use of the ultra short impulse enhances the system capability to resolve multipath replicas. This significantly reduces the fading effects in indoor environments if a proper diversity reception technique, such as a Rake receiver, is used.

It should also be noted that the multiple access interference of an UWB system is not Gaussian. Although a Gaussian approximation for MAI was used in this work, as well as in most of the literature [59][61][62][64][70], the non-validity of the Gaussian approximation to characterize the MAI in TH PPM system has been demonstrated in

[106], especially for a non-repetition code and a small number of users. However, using with repetition code, i.e. Ns>1, and a large number synchronously active user will make the Gaussian approximation more reasonable. However, a more accurate model for multiple access interference is still needed for better understanding of the behaviour of multiuser TH UWB systems. This will be one of the major items in the future works.

Chapter 5

Conclusions and Future Work

This chapter provides conclusions and comments on the results presented in this thesis and a few guidelines for future work.

5.1 Conclusion

Space-time block coding is a remarkable technique which can provide full diversity gain with very low computational complexity. As a part of the 3G UTRA (Universal Terrestrial Radio Access) FDD (Frequency Division Duplex) standard, OSTBC has been proposed for use in the downlink of Direct Sequence Code Division Multiple Access (DS-CDMA) systems to provide transmit diversity. The first part of this work has contributed to better understand the behavior of space time block codes over various fading channels and modulation schemes from the perspective of capacity and performance. Channel capacities for OSTBCs over fading channels were illustrated in various forms. Closed form error probability expressions were derived for flat

Rayleigh/Ricean/Nakagami-*m* fading with q-ary PAM/PSK/QAM OSTBC. Both uncorrelated and correlated channels were considered. Finally the analysis was extended to a practical DS-CDMA downlink. The system information capacity and user capacity for a practical DS-CDMA system employing OSTBC in the downlink was derived and demonstrated over fading channels.

The second part of this work proposed a new modulation scheme, pulse position amplitude modulation for UWB communication systems. The capacity and error probability of the proposed PPAM UWB system were obtained for both single user and multiple user situations. It was shown that the proposed PPAM UWB systems provide a compromise between performance and computational complexity. In particular, 2N-ary PPAM, i.e. biorthogonal signaling, emerges as an attractive choice for an UWB system which can provide better performance than PPM with the same thoughput and only about half the computational complexity.

5.2 Future Work

In relation with this research work, it would be worthwhile to study the following issues.

- In this analysis we assumed a quasi static flat fading channel. It would be interesting and attractive to study the impact of using a frequency selective

fading channel for OSTBC.

- In this analysis we assumed a balanced MIMO channel, i.e. each fading channel has the same average SNR. The capacity and error probability of OSTBC over unbalanced MIMO fading channel would be another possible research direction.
- The error probability over correlated Ricean and Nakagami fading still remain an open form, research effort could be spent on this subject to find more elegant solutions.
- Non-orthogonal PPAM is a definite future research subject for UWB.
- Proper model to characterize the multiple access interference of Time Hopping PPM/PPAM UWB systems.

Appendix I

Using integration by parts, the proof of (29) is as follows

$$
\begin{aligned}
f(L) &= \int_0^\infty Q\left(\sqrt{ax}\right) x^{L-1} e^{-x/u} dx \\
&= -\int_0^\infty Q\left(\sqrt{ax}\right) x^{L-1} u de^{-x/u} \\
&= -Q\left(\sqrt{ax}\right) x^{L-1} u e^{-x/u}\Big|_0^\infty + \int_0^\infty e^{-x/u} u \left(Q\left(\sqrt{ax}\right) x^{L-1}\right)' dx \\
&= u(L-1)\int_0^\infty Q\left(\sqrt{ax}\right) x^{L-2} e^{-x/u} dx - u\sqrt{\frac{a}{8\pi}} \int_0^\infty x^{L-\frac{3}{2}} e^{-x/u} e^{-ax/2} dx \qquad \text{(I.1)} \\
&= u(L-1)\int_0^\infty Q\left(\sqrt{ax}\right) x^{L-2} e^{-x/u} dx - u\sqrt{\frac{a}{8\pi}} \int_0^\infty x^{L-\frac{3}{2}} e^{-x/u} e^{-ax/2} dx \\
&= u(L-1) f(L-1) - \frac{1}{2} u^L \mu \left(\frac{1-\mu^2}{4}\right)^{L-1} \frac{(2L-2)!}{(L-1)!}
\end{aligned}
$$

where $\mu = \sqrt{\dfrac{au}{2+au}}$. Repeating the process, we have

$$
f(L) = u^{L-1}\Gamma(L) f(1) - \frac{1}{2} u^L \Gamma(L) \sum_{k=2}^{L} \mu \left(\frac{1-\mu^2}{4}\right)^{k-1} \binom{2k-2}{k-1}. \qquad \text{(I.2)}
$$

Now using the fact that

$$
f(1) = \int_0^\infty Q\left(\sqrt{ax}\right) e^{-x/u} dx = \frac{1}{2} u(1-\mu), \qquad \text{(I.3)}
$$

we obtain (3.27)

$$
f(L) = \frac{1}{2} u^L \Gamma(L) \left[1 - \sum_{k=0}^{L-1} \mu \left(\frac{1-\mu^2}{4}\right)^k \binom{2k}{k}\right]. \qquad \text{(I.4)}
$$

Appendix II

The truncation of (3.68) to the first N terms will introduce an error of

$$\lambda\sum_{i=N}^{\infty}\mu\left(\frac{1-\mu^2}{4}\right)^{L+i}\binom{2(L+i)}{L+i}\left[1-\sum_{n=0}^{i}\frac{(LK)^n e^{-LK}}{\Gamma(n+1)}\right]. \qquad \text{(II.1)}$$

Given the fact that $\left(\frac{1}{4}\right)^{L+i}\binom{2(L+i)}{L+i}<1$ for all i, we have

$$\lambda\sum_{i=N}^{\infty}\mu\left(\frac{1-\mu^2}{4}\right)^{L+i}\binom{2(L+i)}{L+i}\left[1-\sum_{n=0}^{i}\frac{(LK)^n e^{-LK}}{\Gamma(n+1)}\right]<\lambda\mu\left[1-\sum_{n=0}^{N}\frac{(LK)^n e^{-LK}}{\Gamma(n+1)}\right]\sum_{i=N}^{\infty}\left(1-\mu^2\right)^{L+i}. \qquad \text{(II.2)}$$

The right hand side of inequality (II.2) can be simplified to

$$\lambda\mu\left[1-\sum_{n=0}^{N}\frac{(LK)^n e^{-LK}}{\Gamma(n+1)}\right]\sum_{i=N}^{\infty}\left(1-\mu^2\right)^{L+i}=\lambda\mu\left[1-\sum_{n=0}^{N}\frac{(LK)^n e^{-LK}}{\Gamma(n+1)}\right]\left(1-\mu^2\right)^{L+N}\sum_{i=0}^{\infty}\left(1-\mu^2\right)^{i}. \qquad \text{(II.3)}$$

Given that $\sum_{i=0}^{\infty}q^i=\frac{1}{1-q}$, for $-1\le q\le 1$, (II.2) can be written as

$$\lambda\sum_{i=N}^{\infty}\mu\left(\frac{1-\mu^2}{4}\right)^{L+i}\binom{2(L+i)}{L+i}\left[1-\sum_{n=0}^{i}\frac{(LK)^n e^{-LK}}{\Gamma(n+1)}\right]<\lambda\frac{\left(1-\mu^2\right)^{L+N}}{\mu}\left[1-\sum_{n=0}^{N}\frac{(LK)^n e^{-LK}}{\Gamma(n+1)}\right]. \qquad \text{(II.4)}$$

Thus, truncation of (3.68) to the first N terms will introduce an error of at most

$\lambda\mu\frac{\left(1-\mu^2\right)^{L+N}}{\mu}\left[1-\sum_{n=0}^{N}\frac{(LK)^n e^{-LK}}{\Gamma(n+1)}\right]$ in the error probability.

References

[1] P. Chaudhury, "The 3GPP proposal for IMT-2000," *IEEE Communication Magazine*, vol.37, pp.72-81, Dec. 1999.

[2] G.J. Foschini and M.J. Gans, "On limits of wireless communications in a fading environment when using multiple antennas," *Wireless Personal Communications*, vol. 6, pp. 311-335, 1998.

[3] E.Telatar, "Capacity of multi-antenna Gaussian channels," *Technical memo.*, AT&T Bell Labs, June 1995

[4] S. M. Alamouti, "A simple transmit diversity technique for wireless communications," *IEEE Journal on Selected Areas in Communications*, vol. 16, no 8, pp.1452-1458, Oct. 1998.

[5] V. Tarokh, H. Jafarkhani and A. R. Calderbank, "Space-time block codes from orthogonal designs," *IEEE Transactions on Information Theory*, vol. 45, pp.1456-1467, July 1999.

[6] V. Tarokh, H. Jafarkhani and A. R. Calderbank, "Space-time block coding for wireless communications: performance results," *IEEE Journal on Selected Areas in Communications*, vol. 17, no. 3, pp. 451-460, Mar. 1999

[7] R.A. Scholtz and M.Z. Win, "Impulse radio," *Proceeding of PIRMC*, Sept. 1997.

[8] D.J. Goodman, "Trends in cellular and cordless communications," *IEEE Communication Magazine*, vol.29, pp.31-40, June 1991.

[9] J.H. Winters, "Optimum combining in digital mobile radio with cochannel interference," *IEEE Journal on Selected Areas in Communications*, vol. SAC-2, pp.528-539, July 1984.

[10] J.H. Winters, "On the capacity of radio communication systems with diversity in a rayleigh fading environment," *IEEE Journal on Selected Areas in Communications*, vol. SAC-2, pp.871-878, June 1987

[11] P. Balaban and J. Salz, "Optimum diversity combining and equalization in digital data transmission with application to cellular mobile radio," *IEEE Transactions on Vehicle Technology*. vol. 40, pp.342-354, May 1991.

[12] P. Balaban and J. Salz, "Optimum diversity combining and equalization in data transmission with application to cellular mobile radio," *IEEE Transactions on Communications*, vol. 40, pp.885-907, May 1992.

[13] J.G. Proakis, "Adaptive equalization technique for multipath channels," *IEEE Transactions on Vehicle Technology*, vol. 40, pp.333-341, May 1991.

[14] P. Rice and J.P.E. Green, "A communication technique for multipath channels," in *Proceeding. IRE*, vol. 46, pp. 555-570, Mar. 1958.

[15] G. Turin, "Introduction to spread-spectrum antimultipath techniques and their applcation to urban digital radio," *Proceeding IEEE*, vol. 68, pp. 328-353, Mar. 1980.

[16] B. Glance and L. Greestein, "Frequency-selective fading effects in digital mobile radio with diversity combining," *IEEE Transactions on Communications*, vol. COM-31, pp.1085-1094, Sept. 1983.

[17] F. Adachi and K. Ohno, "BER performance of QDPSK with postdetection diversity reception in mobile radio channels," *IEEE Transactions on Vehicular Technology.*, vol. 40, pp. 237-249, Feb. 1991.

[18] H. Zhou, R. Deng, and T. Tjhung, "Performance of combined diversity reception and convolutional coding for QDPSK land mobile radio," *IEEE Transactions on Vehicle Technology*, vol. 43, pp. 499-508, Aug. 1994.

[19] F. Lotse, J.E. Berg, U. Forssen, and P. Idhal, "Base station polarization diversity reception in marcocelluar systems at 1800 MHz," in *Proceeding Vehicular Technology Conference*, 1996, vol. 3, pp. 1643-1646, May 1996.

[20] J. Winters, "Switched diversity with feedback for DPSK mobile radio systems," *IEEE Transactions on Information Theory*, vol. IT-32, pp. 134-150, Feb. 1983.

[21] G. Raleigh and J. Cioffi, "Spatio-temporal coding for wireless communications," in *Proc. IEEE Global Telecommunications Conference.*, London, U.K., pp. 533-537, Nov. 1996.

[22] A.Wittneben, "Base station modulation diversity for digital SIMULCAST," in *Proceeding IEEE Vehicular Technology Conf.*, pp.505–511, May 1993.

[23] N. Seshadri and J. Winters, "Two signalling schemes for improving the error performance of frequency-division-duplex (FDD) transmission systems using transmitter antenna diversity," *Intel Journal on Wireless Information Network*, vol. 1, pp. 49–60, Jan. 1994.

[24] J. Winters, "The diversity gain of transmit diversity in wireless systems with Rayleigh fading," *IEEE Transactions on Vehicular Technology*, vol. 47, pp. 119–123, Feb. 1998.

[25] T. Hattori and K. Hirade, "Multitransmitter simulcast digital signal transmission by using frequency offset strategy in land mobile radio-telephone system," *IEEE Transactions on Vehicular Technology*, vol. VT-27, pp. 231–238,

Nov. 1978.

[26] A. Hiroike, F. Adachi, and N. Nakajima, "Combined effects of phase sweeping transmitter diversity and channel coding," *IEEE Transactions on Vehicular. Technology*, vol. 41, pp. 170–176, May 1992.

[27] V. Tarokh, N. Seshadri, and A. Calderbank, "Space–time codes for high data rate wireless communication: Performance criterion and code construction," *IEEE Transactions on Information Theory*, vol. 44, pp. 744–765, Mar. 1998.

[28] N. Seshadri, V. Tarokh, and A. Calderbank, "Space–time codes for high data rate wireless communications: Code construction," in *Proceeding IEEE Vehicular Technology Conference*, Phoenix, AZ, pp. 637–641, 1997.

[29] V. Tarokh, N. Seshadri, and A. Calderbank, "Space–time codes for high data rate wireless communications: Performance criterion and code construction," in *Proc. IEEE International Conference on Communications*, Montreal, QB, Canada, pp. 299–303, 1997.

[30] V. Tarokh, A. Naguib, N. Seshadri, and A. Calderbank, "Space–time codes for high data rate wireless communications: Mismatch analysis," in *Proc. IEEE Int. Conf. Communications*, Montreal, QB, Canada, pp. 309–313, 1997.

[31] A. Naguib, V. Tarokh, N. Seshadri, and A. Calderbank, "A space–time coding modem for high-data-rate wireless communications," *IEEE Journal on Selected Areas in Communications*, vol. 16, pp. 1459–1478, Oct. 1998.

[32] V. Tarokh, A. Naguib, N. Seshadri, and A. Calderbank, "Space–time codes for high data rate wireless communication: Performance criteria in the presence of channel estimation errors, mobility, and multiple paths," *IEEE Transactions on. Communications,* vol. 47, pp. 199–207, Feb. 1999.

[33] V. Tarokh, A. Naguib, N. Seshadri, and A. Calderbank, "Combined array processing and space–time coding," *IEEE Transactions on Information Theory*, vol. 45, pp. 1121–1128, May 1999.

[34] S. Alamouti, "A simple transmit diversity technique for wireless communications," *IEEE Journal on Selected Areas in Communications,* vol. 16, pp. 1451–1458, Oct. 1998.

[35] V. Tarokh, H. Jafarkhani, and A. Calderbank, "Space–time block codes from orthogonal designs," *IEEE Transactions on Information Theory*, vol. 45, pp. 1456–1467, July 1999.

[36] V. Tarokh, H. Jafarkhani, and A. Calderbank, "Space–time block coding for wireless communications: Performance results," *IEEE Journal on Selected Areas in Communications*, vol. 17, pp. 451–460, Mar. 1999.

[37] T.H. Liew, and L. Hanzo, "Space-time codes and concatenated channel codes for wireless communications," *Proceedings of the IEEE* 90(2):187-219.

[38] G. Ganesan and P. Stoica, "Space–time block codes: A maximum SNR approach," *IEEE Transactions on Information Theory*, vol. 47, pp. 1650–1656, May 2001.

[39] B. M. Hochwald, T. L. Marzetta, and C. B. Papadias, "A transmitter diversity scheme for wideband CDMA systems based on space–time spreading," *IEEE Journal on Selected Areas in Communication*, vol. 19, pp. 48–60, Jan. 2001.

[40] O. Tirkkonen and A. Hottinen, "Square-matrix embeddable space–time block codes for complex signal constellations," *IEEE Transactions on Information Theory*, vol. 48, pp. 1122–1126, Feb. 2002.

[41] W. Su and X.G Xia, "Two generalized complex orthogonal space-time block codes of rates 7/11 and 3/5 for 5 and 6 transmit antennas," *IEEE Transactions on Information Theory*, vol. 49, pp. 313 -316, Jan. 2003

[42] S. Sandhu and A. Paulraj, "Space-time block codes: A capacity perspective," *IEEE Communications Letters*, vol.4, no. 12, pp.384-386, Dec. 2000.

[43] H. C. Espinosa, J.R. Fonollosa and J. A. Delgado Penin, "Channel capacity of space-time block coding," *IST mobile communications summit*, sitges Spain, 9-12 Sept. 2001.

[44] C. Gao and A.M. Haimovich, "Bit error probability for space-time block code with coherent and differential detection," Proc. *IEEE Vehic. Tech. Conf.,* pp. 410-414, Sep.2002.

[45] J.G. Proakis, "*Digital Communications,*" 4th Ed., McGraw-Hill, 2001.

[46] X. Li, T. Luo, G. Yue and C. Yin, "A squaring method to simplify the decoding of orthogonal space-time block codes," *IEEE Transactions on Communications,* vol.49, pp.1700-1703, Oct. 2001.

[47] G. Taricco and E. Biglieri, "Exact pairwise error probability of space-time codes," *IEEE Transactions on Information Theory*, vol 48, no.2, pp. 510-514, Feb. 2002.

[48] Sang-Hyo Kim, Ik-Seon Kang, and Jong-Seon No, "Exact bit error probability of orthogonal space-time block codes with quadrature amplitude modulation," *IEEE International Symposium on Information Theory*, p.63, June 29-July 4, 2003

[49] M.-S.Alouini and A.J. Goldsmith, "A unified approach for calculating error rates of linearly-moudlated signals over generalized fading channels," *IEEE. Transactions on Commun.*, vol.47, no.9, pp.1324-1334, Sep. 1999.

[50] H. B¨olcskei and A. J. Paulraj, "Performance analysis of space-time codes in correlated Rayleigh fading environments," in *Proc. of Asilomar Conf. Signals, Systems, and Computers*, Pacific Grove, CA, pp. 687–693, Nov. 2000.

[51] P. Lombardo, F. Fedele, M. M. Rao, "MRC Performance for Binary Signals in Nakagami Fading with General Branch Correlation," *IEEE Transactions on Communications,* Vol. 47, No. 1, pp.44-50, January 1999.

[52] L. Fang, G. Bi, and A. C. Kot, "New Method of Performance Analysis for Diversity Reception with Correlated Rayleigh-fading Signals," *IEEE Transactions on Vehicular Technology,* Vol. 49, No. 5, pp.1807-1812, Sept. 2000.

[53] R.U. Nabar, H. Bolcskei, and A.J. Paulraj, "Outage properties of space-time block codes in correlated Rayleigh or Rician fading environments," *IEEE International Conference on Communications*, vol.3, 13-17, pp. 2381-2384, May 2002.

[54] Z.Zhang, G.Li and J.Zhu, "A novel decoding algorithm of OSTBC for CDMA receiver in multipath fading environments," Proc. *IEEE Vehic. Tech. Conf.*, pp.1956-1959 ,2001.

[55] N. Morinaga, M. Nakagawa and. R. Kohono, "New Concepts and Technologies for Achieving Highly Reliable and High-Capacity Multimedia Wireless Communications Systems," *IEEE Communications magazine*, pp. 28-33, Jan. 1997.

[56] H. Hashemi, "The Indoor Radio Propagation Channel," *Proceedings IEEE* vol. 81, No. 7, July 1993.

[57] P. Withington II and L. W. Fullerton. "An Impulse Radio Communications System in Ultra-Wideband Short-Pulse Electromagnetics," Plenum Press, 1993.

[58] J. Schandle, "Impulse Radio System bid for PCS Communications Role," *Electronic Design*, February 4, 1993, pp. 32-34.

[59] R. A. Scholtz, "Multiple Access with Time Hopping Impulse Modulation," invited paper, *Proceedings of IEEE MILCOM conference*, Dec. 1993.

[60] L. B. Milstein and M. K. Simon, "Spread Spectrum Communications," *Mobile Communications Handbook, IEEE press,* 1996.

[61] Ramirez-Mireles and R.A. Scholtz, "System performance analysis of impulse radio modulation," *Proc. IEEE RAWCON*, pp. 67-70, Aug. 1998.

[62] Ramirez-Mireles and R.A. Scholtz, "Multiple-access performance limits with time hopping and pulse position modulation," *Proc. IEEE Military Commun.*

Conf., pp. 529-533, Oct. 1998.

[63] L. Zhao and A.M. Haimovich, "Capacity of M-ary PPM ultra-wideband communications over AWGN channels," *Proc. IEEE Vehic. Tech. Conf.*, pp. 1191-1195, Oct. 2001.

[64] L. Zhao and A.M. Haimovich, "The capacity of an UWB multiple-access communications system," Proc. *IEEE Int. Commun. Conf.*, pp. 1964-1968, 2002.

[65] J.R. Foerster, "The effects of multipath interference on the performance of UWB systems in an indoor wireless channel," *Proc. IEEE Vehic. Tech. Conf.*, pp. 1176-1180, May 2001.

[66] C.J. Le Marter and G.B.Giannakis, "All-digital PAM impulse radio for multiple-access through frequency-selective multipath," *Proc. IEEE Global Telecommun. Conf.*, pp. 77 –81, 2000.

[67] J.R. Foerster, "Ultra-Wideband Technology for Short- or Medium-Range Wireless Communications," *Intel Technical Journal*, Q2, 2001.

[68] F.Ramirez-Mireles and R.A. Scholtz, "N-orthogonal time-shift-modulated codes for impulse radio", *IEEE Int. Commun. Conf*, Nov.1997.

[69] O. Wintzell and D.K. Zigangirov, "On the capacity of a pulse-position-hopped CDMA system," *IEEE Transactions on Information Theory*, vol.47, pp. 2639-2644, Sep. 2001.

[70] M.Z. Win and R.A. Scholtz, "Ultra-wide bandwidth time-hopping spread-spectrum impulse radio for wireless multiple-access communications," *IEEE Transactions on Communications*, vol 48, pp.679-691, Apr. 2000.

[71] R. A. Scholtz and M. Z. Win, "Impulse Radio," invited paper, *Proceedings of IEEE PIMRC conference*, September 1997. Printed in Wireless Communications: TDMA versus CDMA, S. G. Glisic and P. A. Lepp anen, eds., Kluwer Academic Publishers, 1997.

[72] M. Z. Win and R. A. Scholtz, "Impulse Radio: How It Works," in *IEEE Communications Letters*, vol. 2, no. 2, February 1998.

[73] Moe Z. Win and Robert A. Scholtz, "Characterization of Ultra-Wide Bandwidth Wireless Indoor Channels: A Communication-Theoritic View" *IEEE Journal on Selected Areas in Communications*, Vol. 20,No. 9, Dec 2002.

[74] R. J. M. Cramer, R. A. Scholtz, and M. Z. Win, "Evaluation of an Ultra-Wide Band Propagation Channel" *IEEE Transactions on Antennas and Propagation*, May 2002.

[75] M. Z. Win and R. A. Scholtz, "Ultra-Wide Bandwidth (UWB) Signal Propagation for Indoor Wireless Communications," in *Proceedings IEEE ICC'97*, June 1997.

[76] M. Z. Win, F. Ramrez-Mireles, R. A. Scholtz and M. A. Barnes, "Ultra-WideBandwidth (UWB) Signal Propagation for Outdoor Wireless Communications," in *Proceedings IEEE VTC conference,* May 1997.

[77] R. Jean-Mark Cramer, M. Z. Win and R. A. Scholtz, "Impulse Radio MultipathCharacteristics and Diversity Reception," in *Proceedings IEEE ICC conference*, June 1998.

[78] R. Jean-Mark Cramer, M. Z. Win and R. A. Scholtz, "Evaluation of the Multipath Characteristics of the Impulse Radio Channel," *IEEE PIMRC'98*.

[79] M. Z. Win and R. A. Scholtz, "Statistical Characterization of Ultra Wide Bandwidth Wireless Communications Channels," in *Proceedings IEEE ASILOMARconference*, November 1997.

[80] F. Ramrez-Mireles, M. Z. Win and R. A. Scholtz, "Signal Selection for the Indoor Impulse Radio Channel," in *Proceedings IEEE VTC conference*, May 1997.

[81] F. Ramrez-Mireles and R. A. Scholtz, "Performance of Equicorrelated Ultra Wideband Pulse-Position-Modulated Signals in the Indoor Wireless Impulse Radio Channel," in *Proceedings IEEE PACRIM conference*, August 1997.

[82] F. Ramrez-Mireles, R. A. Scholtz and M. Z. Win, "Performance of Ultra Wideband Time-Shift-Modulated Signals in the Indoor Wireless Impulse Radio Channel," in *Proceedings 31st Asilomar conference*, November 1997.

[83] M. Z. Win and R. A. Scholtz, "On the Robustness of Ultra-Wide Bandwidth Signals in Dense Multipath Environments," in *IEEE Communications Letters*, vol. 2, no. 2, February 1998.

[84] G.W. Wornell and M.D. Trott, "Signal processing techniques for efficient use of transmit diversity in wireless communications," *IEEE ICASSP* '96, pp. 1057-1064, 1996.

[85] G.G. Raleigh and J.M. Cioffi, "Spatio-temporal coding for wireless communications," *IEEE Globecom '96*, vol. 3, pp. 1809-1814, 1996.

[86] P.V. Rooyen, M. L otter, and D.V. Wyk, "Space-time processing for CDMA Mobile Communications," Kluwer Academic Publishers, Boston, MA, 2000.

[87] G. Ungerboeck, "Channel coding with multilevel/phase signals," *IEEE Transaction on Information Theory*, vol. 28, no. 1, pp.55-67, Jan. 1982.

[88] T.L. Marzetta and B.M. Hochwald, "Capacity of a mobile multiple-antenna communication link in Rayleigh at fading," *IEEE Transactions on Information*

Theory, vol. 45, pp. 139-157, Jan. 1999.

[89] S. G. Wilson, "Digital modulation and coding," Englewood Cliffs, NJ: Prentice-Hall, 1996

[90] L. H. Ozarow, S. Shamai, and A.D. Wyner, "Information theoretic considerations for cellular mobile radio," *IEEE Transactions on Vehicular Technology*, vol.43, pp. 359-378, May 1994

[91] E.Baccarelli, "Evaluation of the reliable data rates supported by multiple-antenna coded wireless links for QAM transmissions," *IEEE Journal on Selected Areas in Communications*, vol. 19, no. 2, pp. 295-304, Feb. 2001.

[92] S. Dolinar, D. Divsalar, J. Hamkins and F. Pollara, "Capacity of pulse-position modulation (PPM) on Gaussian and Webb channels," *JPL TMO Progress Report*, vol. 42-142, pp. 1-31, Apr.-June 2000.

[93] F. R. Farrokhi, G. J. Foschini, A. Lozano, R. A. Valenzuela, "Link-Optimal Space-Time Processing with Multiple Transmit and Receive Antennas", *IEEE Communications Letters*, vol. 5, N°.3, March 2001.

[94] M. Shayesteh and A. Aghamohammadi, "On the error probability of linearly modulated signals on frequency-flat Ricean, Rayleigh, and AWGN channels," *IEEE Transactions on Communications*, vol. 43, pp.1454-1466, Feb. 1995.

[95] S.X. Wei, "An alternative derivation for the signal-to-noise ratio of a SSMA system," *IEEE Transactions on Communications*, pp. 2224-2226, vol. 42, June 1994.

[96] T.S. Rappaport, *"Wireless communications principles and practice,"* Prentice-Hall, 1996.

[97] T. Staley, R. North, J. Luo, W. Ku and J. Zeidler, "Performance evaluation for multichannel reception of coherent MPSK over slowly fading frequency selective fading channels," *IEEE Transactions on Vehicular. Technology*, vol. 50, pp. 877-894, July 2001.

[98] T. Staley, R. North, J. Luo, W. Ku and J. Zeidler, "Error probability performance prediction for multichannel reception of linearly modulated coherent systems on fading channels," *IEEE Transaction on Communications*, vol.50, pp.1423-1428, Sept. 2002.

[99] W.C. Yee, "Mobile Communications Engineering," New York: McGraw-Hill, 1982.

[100] P. Lombardo, G. Fedele, and M. M. Rao, "MRC performance for binary signals in Nakagami fading with general branch correlation," *IEEE Transactions on Communications*, vol. 47, no.1, Jan. 1999

[101] J. N. Pierce and S. Stein, "Multiple diversity with nonindependent fading," *Proc. IRE*, vol. 48, pp.89-104, Jan. 1960.

[102] M. Schwartz, W.R. Bennett, and S. Stein, "Communication Systems and Techniques," New York: McGraw-Hill, 1979.

[103] W. R. Braun and U. Dersch, "A physical mobile radio channel model," *IEEE Transactions on Vehicular Technology*, vol. 40, pp. 472–482, May 1991.

[104] J. Salz and J. H. Winters, "Effect of fading correlation on adaptive arrays in digital mobile radio," *IEEE Transactions on Vehicular Technology*, vol. 43, pp.1049–1057, Nov. 1994.

[105] W. C. Y. Lee, "Effects on correlation between two mobile radio base station antennas," *IEEE Transactions on Communications*, vol. COM-21, pp. 1214–1224, Nov. 1973.

[106] G. Durisi and G. Romano, "On the Validity of Gaussian Approximation to Characterize the Multiuser Capacity of UWB TH PPM," *IEEE Conference on Ultra Wideband Systems and Technologies,* 2002.